


Summer 2018

Thermosetting Polymers via Azide Alkyne Cycloaddition

Richard H. Cooke III
University of Southern Mississippi

Follow this and additional works at: <https://aquila.usm.edu/dissertations>

 Part of the [Materials Chemistry Commons](#), [Organic Chemistry Commons](#), [Physical Chemistry Commons](#), and the [Polymer Chemistry Commons](#)

Recommended Citation

Cooke III, Richard H., "Thermosetting Polymers via Azide Alkyne Cycloaddition" (2018). *Dissertations*. 1558.
<https://aquila.usm.edu/dissertations/1558>

This Dissertation is brought to you for free and open access by The Aquila Digital Community. It has been accepted for inclusion in Dissertations by an authorized administrator of The Aquila Digital Community. For more information, please contact Joshua.Cromwell@usm.edu.

THERMOSETTING POLYMERS VIA AZIDE-ALKYNE
CYCLOADDITION

by

Richard Hunter Cooke III

A Dissertation
Submitted to the Graduate School,
the College of Science and Technology
and the School of Polymer Science and Engineering
at The University of Southern Mississippi
in Partial Fulfillment of the Requirements
for the Degree of Doctor of Philosophy

Approved by:

Dr. Robson F. Storey, Committee Chair
Dr. Jeffrey S. Wiggins
Dr. Derek L. Patton
Dr. Sergei I. Nazarenko
Dr. Xiaodan Gu

Dr. Robson F. Storey
Committee Chair

Dr. Jeffrey S. Wiggins
Department Chair

Dr. Karen S. Coats
Dean of the Graduate School

August 2018

COPYRIGHT BY

Richard Hunter Cooke III

2018

Published by the Graduate School



ABSTRACT

This dissertation exploits properties inherent to azide-alkyne cycloaddition and applies practical solutions to difficult problems. Chapter II addresses structure-property relationships in glassy azido-alkyne matrices by varying the identity of the central linkage within tetrapropargyl *bis*-aniline-type crosslinkers, and by the addition or omission of Cu(I) catalyst. This systematic study showed that an ether or methylene linkage yielded lower melting tetrapropargyl crosslinkers that were soluble in, and produced homogeneous, networks when cured with, a standard azido resin, di(3-azido-2-hydroxypropyl) ether of bisphenol-A; in contrast, a sulfone linkage yielded a relatively insoluble crosslinker and poorly dispersed, heterogeneous networks when reacted with the same resin. The study also showed that the presence of Cu(I) and the concomitant network regularity afforded by a single triazole regioisomer increased compression modulus and T_g . However, due to increased kinetics of reaction the catalyzed system was much harder to process.

Chapter III introduces the use of azide-alkyne cycloaddition as an alternative curing mechanism in non-isocyanate polyurethanes (NIPU). Several commercial polyisocyanate resins derived from hexamethylene diisocyanate were converted to propargyl carbamates by reaction with propargyl alcohol; azidated co-reactants were synthesized from several different commercial polyols including polyether, polyester, and polyacrylic types. Each resin/coreactant combination was rendered into a two-component coating system and cured in the presence and absence of Cu(I) catalyst. Coating properties were compared to the precursor polyisocyanate/polyol coating systems, and the best-performing NIPU coating was found to result from a propargylated

allophanate resin, XP2580, and an azidated polyacrylic resin, Setalux DA870. The latter coatings met or exceeded the properties of the precursor polyurethane coatings except for uncatalyzed rate of cure at ambient temperature.

Chapter IV focused on increasing the sluggish curing kinetics observed for the azide-propargyl systems. In Chapter III, this was overcome by the addition of Cu(I). However, this also caused discoloration to the coating. This chapter focused on making an aesthetically pleasing coating that cured similarly to the as received material. This was achieved by the synthesis of 2-hydroxyethyl propiolate (2-HEP) and its subsequent reaction with XP2580 to form a propiolate modified polyurethane resin. Incorporation of the propiolate functionality increased the rate of reaction with the azidated Setalux DA870, such that the observed curing kinetics were approximately the same as that of the as-received resin pairs.

Chapter V, the final chapter, addressed problem that plagued the carbamates synthesized in the previous two chapters. Upon propargylation, the viscosity increased dramatically, making the resins difficult to work with unless diluted by an appreciable amount of organic solvents. This was overcome by sacrificing a fraction of the isocyanate functionality to attach internal plasticizing moieties consisting of a monoalkyl ether of either ethylene glycol (EG) or diethylene glycol (DEG). This approach was successful in reducing coating system viscosity, and created a softer and more flexible coating with a lower glass transition. This study showed that the length of alkyl chain, rather than the choice of EG or DEG, produced the larger effect on viscosity and coating properties, i.e., butyl provided a much greater plasticizing effect than ethyl.

ACKNOWLEDGMENTS

First, I would like to thank God for being a constant especially in the times of chaos. Next my advisor, Dr. Robson Storey, who has pushed me further than I ever thought I could go. Doc, from the beginning you saw things in me that I did not realize and had way of cultivating these traits into passions. Thank you. Secondly, I would like to thank my committee, Dr. Wiggins, Dr. Patton, Dr. Nazarenko, and Dr. Gu. All of you have played an active role in my development and for that I am grateful. Dr. Wiggins, thank you for taking a special interest in me and my work. All of our discussions on leadership and life have meant a lot. Thank you for your time and I look forward to our continued collaboration! President Bennett, I would also like to thank you for mentoring me during my last year as a graduate student. Our conversations on leadership and more specifically leading a university have been life changing. The knowledge I have gained through our discussions will be utilized throughout my career.

I would also like to thank present and past members of the Storey Research Group: Dr. Mark Brei, Morgan Heskett, Dr. Bin Yang, Dr. Garrett Campbell, Dr. Corey Parada, Travis Holbrook, Tom Wu, Logan Dugas, Danny Hanson, and Savannah Steadman. Thank you to all of you for making the daily grind of graduate school enjoyable. I will look back fondly of my days as a Storey group member and as they say “You only Storey Group once!”

To my team of undergrads, words cannot express how grateful I am to all of you. To my REUs, Christina Gray and Daniel Van DeWalle, thank you for spending your summer with me in sweltering Hattiesburg, MS. I hope that your experience was both fun and challenging. Good luck on your future endeavors! To my Covestro Team,

Grace Parker and Tom Wu, thank you for your time and effort. Thank you for giving me your weekends and evenings. Thank you for always working with the same infectious positive attitude no matter if research was going our way or not. These traits will serve you well in your future careers. To my Composite Team, Nathaniel Prine, thank you for your inquisitive nature and your drive to push science further. Keep that up and you will have a bright graduate school career. Last but not least, to my right-hand man, Harrison Livingston, who may have been my greatest teacher. Thank you for not only your nights, weekends, and holiday breaks but also thank you for being one of my biggest supporters and teaching me what it means to be an effective leader. You have developed so much since we first started working together three years ago. You have a bright future ahead and I cannot wait to see where life takes you!

I would also like to thank the past and present Wiggins Research Group, specifically Dr. Brian Greenhoe, Dr. Andrew Frazee, Dr. Kyler Knowles, Dr. John Misasi, Dr. Jeremy Moskowitz, Andrew Janisse, Matt Hartline, Matt Patterson, Travis Palmer, and Jeremy Weigand, for their collaboration and comradery. We have spent a lot of time together in an out of lab and I must say nearly all of my greatest memories of graduate school involve hanging out with at least a few members of WRG. I would also like to thank the Thames-Rawlins Research Group, specifically Jessica Davison , Austin Maples, Dr. Dwaine Braasch and David Delatte for offering their lab, equipment and expertise. In addition I would like to thank the Patton Research Group and the Morgan Research Group for allowing use of their equipment and specifically April Fogel of the Morgan Research Group for her help with rheometric studies.

To my first year class, I realize that I am biased but I truly believe that I was part of the greatest first year class ever. Despite first year being a pain the majority of the time, I look back with only the best memories. I love all of you. Please keep in touch.

I would also like to thank friends outside of the department who were paramount in keeping things in perspective: Samantha Hughes, Bobby Wehrle, Alisha Sink, and all of Group Chat.

Lastly, I would like to thank my funding sources, the NSF-NRT Fellowship as well as Covestro for financing my research.

DEDICATION

I would like to dedicate this dissertation to my parents, Richard and Bonnetta Cooke, my sister, Ashley Cooke, and my aunt, Shirley Willis. Your love and continuous support are among the biggest reasons I have been able to achieve this dream. Thank you!

I would also like to dedicate this dissertation to any future nieces and nephews as well as my many young cousins, which there are too many to name. I hope that one day many of you will become scientists.

TABLE OF CONTENTS

ABSTRACT	ii
ACKNOWLEDGMENTS	iv
DEDICATION	vii
LIST OF TABLES	xiii
LIST OF ILLUSTRATIONS	xv
LIST OF SCHEMES.....	xxiii
CHAPTER I - INTRODUCTION	1
1.1 Motivation of Research.....	1
1.2 Background.....	6
1.2.1 Thermosetting Composite Matrices	6
1.2.2 Non-Isocyanate Polyurethane Coatings.....	6
1.2.3 Azide-Alkyne Cycloaddition	8
CHAPTER II – THE EFFECT OF MICROSTRUCTURE ON THERMAL AND MECHANICAL PROPERTIES IN AZIDE-ALKYNE MATRICES	11
2.1 Introduction.....	11
2.2 Experimental	14
2.2.1 Materials	14
2.2.2 Instrumentation	15
2.2.3 Synthesis of Azidated Resin	18

2.2.4 Preparation of Tetrafunctional Alkyne Crosslinkers	18
2.2.5 Synthesis of CuCl ₂ [PMDETA] complex	21
2.2.6 Mechanical Testing	21
2.3 Results and Discussion	22
2.3.1 Dissolution of Crosslinkers.....	22
2.3.2 Kinetics of Cure for both Catalyzed and Uncatalyzed Systems	26
2.3.3 Rheological Measurements	32
2.3.4 Dynamic Mechanical Analyses.....	35
2.3.5 Uniaxial Compression Testing.....	40
2.3.6 Thermogravimetric Analyses.....	42
2.4 Conclusions and Future Work	44
CHAPTER III – NON-ISOCYANATE CURED POLYURETHANES VIA AZIDE-	
ALKYNE CYCLOADDITION	47
3.1 Introduction.....	47
3.2 Experimental	50
3.2.1 Materials	50
3.2.2 Instrumentation	51
3.2.3 Preparation of Polyazides	53
3.2.4 Preparation of Polypropargyl Carbamates	54
3.2.5 Synthesis of CuCl ₂ [PMDETA] complex	55

3.2.6 Real-Time Cure Kinetics as a Function of Catalyst Concentration	56
3.2.7 Preparation of Coated Substrates	56
3.2.8 Coatings Testing	57
3.3 Results and Discussion	58
3.3.1 Polyazide Synthesis	58
3.3.2 Polyalkyne Synthesis	70
3.3.3 Coating Formulation and Curing	73
3.3.4 Physical Properties of Neat and Modified Resins.....	78
3.4 Conclusions and Future Work	81
 CHAPTER IV – REDUCED TEMPERATURE NON-ISOCYANATE POLYURETHANE COATINGS VIA CATALYST-FREE AZIDO-ALKYNE CYCLOADDITION	
	83
4.1 Introduction.....	83
4.2 Experimental.....	84
4.2.1 Materials	84
4.2.2 Instrumentation	85
4.2.3 Synthesis of Azidated Setalux DA 870.....	86
4.2.4 Direct Amidation of Desmodur XP2580	88
4.2.5 Synthesis of 2-HEP via Ethoxylation	88
4.2.6 Synthesis of 2-HEP via Fischer Esterification using H ₂ SO ₄ catalyst	89

4.2.7 Synthesis of 2-HEP via Fischer Esterification using <i>p</i> -Toluenesulfonic Acid	
Catalyst	90
4.2.8 FTIR Kinetic Study.....	91
4.2.9 Coating Curing.....	92
4.2.10 Coating Physical Testing	92
4.3 Results and Discussion	93
4.3.1 Direct Amidation of Desmodur N3200A.....	94
4.3.2 Synthesis of 2-HEP via Ring-Opening of Ethylene Oxide.....	94
4.3.3 Synthesis and Characterization of 2-HEP via Fischer Esterification.....	97
4.3.4 Synthesis of Desmodur XP2580-2HEPC.....	105
4.3.5 Synthesis of azidated Setalux DA 870.....	106
4.3.6 Kinetic Studies	108
4.3.7 Physical Properties of Neat and Modified Resins.....	113
4.4 Conclusions and Future Work	114
 CHAPTER V - LOW VISCOSITY NON-ISOCYANATE POLYURETHANE COATINGS VIA AZIDO-ALKYNE CYCLOADDITION USING MONO- HYDROXYETHYLENE GLYCOL OLIGOMERS	
	117
5.1 Introduction.....	117
5.2 Experimental	119
5.2.1 Materials	119

5.2.2 Instrumentation	119
5.2.3 Synthesis	121
5.2.4 Preparation of Coated Substrates	122
5.2.5 Coatings Testing	122
5.3 Results and Discussion	123
5.3.1 Initial Viscosity Measurements.....	123
5.3.2 ¹³ C and ¹ H NMR Characterization of Low Viscosity Propargyl Carbamates	125
5.3.3 600 MHz ¹ H NMR Characterization of Low Viscosity Propargyl Carbamates	128
5.3.4 Viscosity Analysis of Modified Resins.....	133
5.3.5 Coating Properties.....	135
5.3.6 Conclusions and Future Work	142
CHAPTER VI.....	144
REFERENCES	148

LIST OF TABLES

Table 2.1 Properties of Tetrafunctional Aromatic Crosslinkers	23
Table 2.2 Gel Points Achieved by DAHP-BPA and Tetrafunctional Aromatic Alkynes with and without Catalyst	34
Table 2.3 Activation Energies of Thermal Transitions for Each System	36
Table 2.4 Crosslink Density Calculations from Rubbery Storage Modulus Measured at 1 Hz.....	40
Table 2.5 Uniaxial Compressive Data of all Crosslinkers Studied.....	42
Table 2.6 Degradation Profile of All Matrices	44
Table 3.1 Results from MALD-TOF of Partially Tosylated PPG 1000	62
Table 3.2 Results from MALD-TOF of End-Group Modified PPG 1000.....	65
Table 3.3 Linear Regression of MALDI-TOF Spectra for Both Major and Minor Distributions (Neat and Mesylated).....	69
Table 3.4 Compatibility of Synthesized Azide and Alkyne Resins.....	74
Table 3.5 Performance Properties of Propargylated Desmodur XP2580/azidated Setalux DA 870 Coating Compared to a Control Coating Using As-Received Precursor Resins	79
Table 3.6 Adhesion Properties of Propargylated Desmodur XP2580/azidated Setalux DA 870 Coating Using Various Cleaning Methods Compared to a Control Using As- Received Precursor Resins Cleaned with Acetone	80
Table 4.1 Calculated Rate Constants (k) for Each Resin Pair at Specified Temperatures	110
Table 4.2 Activation Energy (E_a) Calculated by the Arrhenius Relationship of Each Resin Pair	111

Table 4.3 Performance Properties of Desmodur XP2580-2HEPC/azidated Setalux DA 870 Coating Compared to Desmodur XP2580-PC and As-Received Precursor Resins.	114
Table 5.1 Viscosity of Various Modified Resins.....	123
Table 5.2 Propargylation Results of Ethylene Glycol Modified Resins.....	132
Table 5.3 Properties of Azidated Setalux DA 870 Cured with EGME-Modified Desmodur XP2580 Compared to Desmodur XP2580-PC and Unmodified Resins.....	136
Table 5.4 Properties of Azidated Setalux DA 870 Cured with DEGME-Modified Desmodur XP2580 Compared to Desmodur XP2580-PC and Unmodified Resins	137
Table 5.5 Properties of Azidated Setalux DA 870 Cured with DEGBE-Modified Desmodur XP2580 Compared to Desmodur XP2580-PC and Unmodified Resins	138
Table 5.6 Crosslink Density Calculations from Rubbery Storage Modulus Measured at 1 Hz.....	142

LIST OF ILLUSTRATIONS

Figure 1.1 General Structure of Crosslinkers used in Chapter II.....	3
Figure 2.1 Difunctional azidated resin, tetrafunctional aromatic alkynes, and catalyst used in this work.	14
Figure 2.2 Light microscopy images of DAHP-BPA/TP44DDS. Heating prescription 70 °C to 150 °C at 3 °C/min.	24
Figure 2.3 DAHP-BPA/TP44DDS held isothermally at 90 °C (top) and 100 °C (bottom).	25
Figure 2.4 Non-dissolved crosslinker in cured azide-alkyne matrix. Formulation consisted of BPA:TP44DDS:TPDPE at 1:0.1:0.9 (mol:mol:mol) and was cured using the uncatalyzed cure profile.	26
Figure 2.5 Isothermal cure progression at 70 °C of DAHP-BPA with TPDPE (triangles) or TPMDA (circles). The filled data markers refer to systems containing 0.2 mol% CuCl ₂ [PMDETA]; whereas the open data markers refer to uncatalyzed systems.....	27
Figure 2.6 Dynamic DSC curves of uncatalyzed DAHP-BPA/TPDPE at 2 (solid), 5 (dash) or 10 (dash-dot) °C/min (first heat), with their respective user-defined baselines.	28
Figure 2.7 Conversion vs. temperature for various heating rates as well as the model predicted by the software for uncatalyzed DAHP-BPA/TPDPE.....	29
Figure 2.8 Activation Energy (E_a) as a function of conversion for DAHP-BPA cured with neat TPDPE (green solid), TPDPE with CuCl ₂ [PMDETA] (green dash), TPDPE with CuCl ₂ [PMDETA] and reducing agent (green dot dash), neat TPMDA (red solid), TPMDA with CuCl ₂ [PMDETA] (red dash).	31

Figure 2.9 Arrhenius Pre-factor as a function of conversion for DAHP-BPA cured with neat TPDPE (green solid), TPDPE with CuCl ₂ [PMDETA] (green dash), TPDPE with CuCl ₂ [PMDETA] and reducing agent (green dot dash), neat TPMDA (red solid), TPMDA with CuCl ₂ [PMDETA] (red dash).	32
Figure 2.10 Rheological cure progression of DAHP-BPA and TPDPE performed isothermally at 70 °C (uncatalyzed – left; catalyzed – right).....	33
Figure 2.11 Rheological cure progression of DAHP-BPA and TPMDA performed isothermally at 70 °C (uncatalyzed – left; catalyzed – right).....	34
Figure 2.12 Generic structure of crosslinked matrix with both 1,4- and 1,5-regioisomer present. Green structures represent probable ring flips; whereas red structures represent unlikely ring flips. Dashed lines represent hydrogen bonding between triazole linkage and hydroxyl from hydroxy propyl ether linkage.	37
Figure 2.13 Tan delta vs. temperature curve recorded at 1 Hz of DAHP-BPA cured with neat TPDPE (black solid), catalyzed TPDPE (black dashed), neat TPMDA (red solid), and catalyzed TPMDA (red dashed). Inset shows sub-T _g relaxations.....	38
Figure 2.14 Storage modulus vs. temperature curve recorded at 1 Hz of DAHP-BPA cured with neat TPDPE (black solid), catalyzed TPDPE (black dashed), neat TPMDA (red solid), and catalyzed TPMDA (red dashed). Inset shows curved in rubbery region and was used to calculate v _e and M _c	40
Figure 2.15 Compressive stress-strain data of the four matrices under investigation: neat TPDPE (black solid), catalyzed TPDPE (black dashed), neat TPMDA (red solid), and catalyzed TPMDA (red dashed).....	42

Figure 2.16 Thermal decomposition of all matrices cured with DAHP-BPA: neat TPDPE (black solid), catalyzed TPDPE (black dashed), neat TPMDA (red solid), and catalyzed TPMDA (red dashed). Inset shows the differences in degradation onset.....	43
Figure 3.1 MALDI-TOF mass spectrum of chlorinated PPG 1000.....	60
Figure 3.2 Linear regression of MALDI-TOF spectrum of chlorinated PPG 1000.....	60
Figure 3.3 MALDI-TOF mass spectrum of partially tosylated PPG 1000 showing three sets of end group functionalities.	61
Figure 3.4 Linear regression of each MALDI-TOF spectrum of Figure 3: HO-PPG1000-OH (circle), TosO-PPG1000-OH (triangle), and TosO-PPG1000-OTos (square).	62
Figure 3.5 MALDI-TOF spectra of PPG 1000 (bottom), its methanesulfonyl intermediate (middle), and its final, azidated derivative (top).....	64
Figure 3.6 Linear Regression of MALDI-TOF spectra for neat (circle), mesylated (square) and azidated (triangle) PPG 1000.	65
Figure 3.7 ¹³ C NMR spectrum (150 MHz, CDCl ₃ , 23 °C) of PPG 1000 (bottom), its methanesulfonyl intermediate (middle), and its final, azidated derivative (top).	66
Figure 3.8 MALDI-TOF spectra of neat (lower) and mesylated (upper) Desmophen 650A.....	67
Figure 3.9 Linear regression of neat and mesylated Desmophen 650A. Minor distributions, defined as the less intense peaks in Figure 3.8, are open circles; major distributions are closed circles.	68
Figure 3.10 FTIR of neat (a), mesylated (b), and azidated polyester (c).....	70
Figure 3.11 Propargylation of Desmodur N3300A: initial process (left) and water-free process (right).	72

Figure 3.12 FTIR of as received (top) and propargylated Desmodur XP2580 (bottom)..	72
Figure 3.13 Curing kinetics at 80 °C of Desmodur XP2580 cured with Setalux DA 870 (open circle), Desmophen 650A (open square), and PPG 1000 (open triangle), and Desmodur XP2580-PC cured with: azidated Setalux DA 870 (solid circle), azidated Desmophen 650A (solid square), and azidated PPG 1000 (solid triangle).....	75
Figure 3.14 Curing kinetics at 80 °C of Setalux DA 870 cured with Desmodur XP2580 (open circle), Desmodur N3200A (open square), and Desmodur N3300A (open triangle), and azidated Setalux DA 870 cured with: Desmodur XP2580-PC (solid circle), Desmodur N3200A-PC (solid square), and Desmodur N3300A-PC (solid triangle).....	76
Figure 3.15 RT-FTIR isothermal cure kinetics (80 °C) of azidated Setalux DA 870 and Desmodur XP2580-PC with various Cu(II)[PMDETA] loadings: 0 (closed circle), 0.2 (closed down triangle), 0.4, (closed square), 1.0 (closed star), and 2.0% (w/w) (closed up triangle). Two drops of stannous octanoate were added to 1 g of these formulations immediately prior to analysis. In addition two controls are present: 2% (w/w) Cu(II)[PMDETA without stannous octanoate (open down triangle) and as received resin (open circle) Weight % values are relative to polyazide.	78
Figure 3.16 Coatings prepared from propargylated Desmodur XP2580 and azidated Setalux DA 870 (right) compared to as-received precursor resins (left), drawn down on steel panels and cured at 80 °C for 4 h.....	79
Figure 4.1 ¹ H NMR spectrum (300 MHz, CDCl ₃ , 23 °C) of 2-HEP synthesized by ring-opening of ethylene oxide using propiolic acid. Peaks labeled with (*) and EG are indicative of diethylether solvent.....	96

Figure 4.2 ¹ H NMR spectrum (300 MHz, CDCl ₃ , 23 °C) of 2-HEP synthesized by Fischer Esterification using 5:1:0.02 (ethylene glycol:propionic acid:H ₂ SO ₄).	98
Figure 4.3 of 2-HEP synthesized by Fischer Esterification using 5:1:0.007 (ethylene glycol:propionic acid:H ₂ SO ₄).	99
Figure 4.4 ¹ H NMR spectrum (600 MHz, CDCl ₃ , 23 °C) of 2-HEP. Inset shows splitting of peaks b and c.....	100
Figure 4.5 ¹³ C NMR spectrum (150 MHz, CDCl ₃ , 23 °C) of 2-HEP.	101
Figure 4.6 HSQC NMR spectrum (CDCl ₃ , 23 °C) of 2-HEP.....	102
Figure 4.7 Gas chromatograph of 2-HEP.	102
Figure 4.8 Mass spectrum of peak in Figure 4.7.....	103
Figure 4.9 FTIR spectrum of 2-HEP.....	104
Figure 4.10 ¹ H NMR spectrum (600 MHz, CDCl ₃ , 23 °C) of 2-HEP synthesized by Fischer Esterification using 5:1:0.02 (ethylene glycol:propionic acid:p-toluenesulfonic acid monohydrate) after purification.	105
Figure 4.11 ¹³ C NMR spectrum (150 MHz, CDCl ₃ , 23 °C) of Desmodur XP2580 as received and after propiolation.	106
Figure 4.12 FTIR spectra of as-received Setalux DA 870 (bottom), mesylated Setalux DA 870 (middle), and azidated Setalux DA 870 (top).	107
Figure 4.13 Isothermal curing kinetics at various temperatures of: as received Setalux DA 870 and Desmodur XP2580 (○), Az-Setalux DA 870 and Desmodur XP2580-PC (+), and Az-Setalux DA 870 and Desmodur XP2580-2HEPC (×).....	109
Figure 4.14 Determination of k for Az-Setalux DA870 and Desmodur XP2580-2HEPC at 70 °C.	110

Figure 4.15 Arrhenius relationship of Az-Setalux DA870 and Desmodur XP2580-2HEPC.	111
Figure 4.16 MEK double rubs, after pre-determined time points during the standard cure profile, of: Setalux DA870 and Desmodur XP2580 (horizontal lines), Az-Setalux DA870 and Desmodur XP2580-PC (forward slash), and Az-Setalux DA870 and Desmodur XP2580-2HEPC (backward slash).....	113
Figure 5.1 Isothermal viscosity of Desmodur N3200-PC with various amounts of 1-propanol: 0 wt% (empty), 2 wt% (forward slash), 5 wt% (back slash), and 10 wt% (horizontal slash). All systems additionally contained approximately 20 wt% n-butyl acetate.	124
Figure 5.2 N3200-PC with various amounts of isopropanol: 0 wt% (empty), 2 wt% (forward slash), 5 wt% (back slash), and 10 wt% (horizontal slash). All systems contained approximately 20 wt% n-butyl acetate.	125
Figure 5.3 ¹³ C NMR spectrum (150 MHz, CDCl ₃ , 23 °C) of EGME-modified propargyl carbamates as well as the Desmodur XP2580 precursor and Desmodur XP2580-PC. ..	126
Figure 5.4 ¹³ C NMR spectrum (150 MHz, CDCl ₃ , 23 °C) of DEGBE-modified propargyl carbamates as well as the Desmodur XP2580 precursor and Desmodur XP2580-PC. ..	127
Figure 5.5 ¹³ C NMR spectrum (150 MHz, CDCl ₃ , 23 °C) of DEGBE modified propargyl carbamates as well as neat Desmodur XP2580 and Desmodur XP2580-PC.....	128
Figure 5.6 ¹ H NMR spectrum (600 MHz, CDCl ₃ , 23 °C) of 33EGME-XP2580-PC. Inset shows region used to verify %propargyl.	130
Figure 5.7 ¹ H NMR spectrum (600 MHz, CDCl ₃ , 23 °C) of 33DEGME-XP2580-PC. Inset shows region used to verify %propargyl.....	131

Figure 5.8 ¹H NMR spectrum (600 MHz, CDCl₃, 23 °C) of 33DEGBE-XP2580-PC.
 Inset shows region used to verify %propargyl..... 132

Figure 5.9 Room temperature isothermal viscosity of Desmodur XP2580 (vertical slash),
 Desmodur XP2580-PC (open), and various loadings of monohydroxyethylene glycols.
 Loadings are 10% (forward slash), 25% (backward slash), and 33% (horizontal slash).
 The type of monohydroxyethylene glycol is depicted in each plot. Percentages are
 normalized to 100% propargylated system..... 135

Figure 5.10 Crosshatch adhesion of as-received Setalux DA 870 cured with Desmodur
 XP2580 (open) and Azidated Setalux DA 870 cured with Desmodur XP2580-PC
 (forward slash). The final three bars are formulations containing various loadings of
 monohydroxyethylene glycols. Loadings are 10% (backward slash), 25% (horizontal
 slash), and 33% (vertical slash). The type of ethylene glycol is depicted in each plot.. 138

Figure 5.11 Pencil Hardness of as received Setalux DA 870 cured with Desmodur
 XP2580 (open) and Azidated Setalux DA 870 cured with Desmodur XP2580-PC
 (forward slash). The final three bars are formulations containing various loadings of
 monohydroxyethylene glycols. Loadings are 10% (backward slash), 25% (horizontal
 slash), and 33% (vertical slash). The type of ethylene glycol is depicted in each plot.. 139

Figure 5.12 Glass transition temperature (T_g) as determined by DSC of as received
 Setalux DA 870 cured with Desmodur XP2580 (open) and Azidated Setalux DA 870
 cured with Desmodur XP2580-PC (forward slash). The final three are formulations
 containing various loadings of monohydroxyethylene glycols. Loadings are 10%
 (backward slash), 25% (horizontal slash), and 33% (vertical slash). The type of ethylene

glycol is depicted in each plot. The percentages are normalized to the as-received samples..... 140

Figure 5.13 Representative storage modulus vs. temperature plots of cured coatings comprised of ether alcohol modified propargyl carbamates at three loading levels: 10% (solid), 25% (dash), and 33% (dash-dot). The type of ether alcohol is displayed in the plot. 141

LIST OF SCHEMES

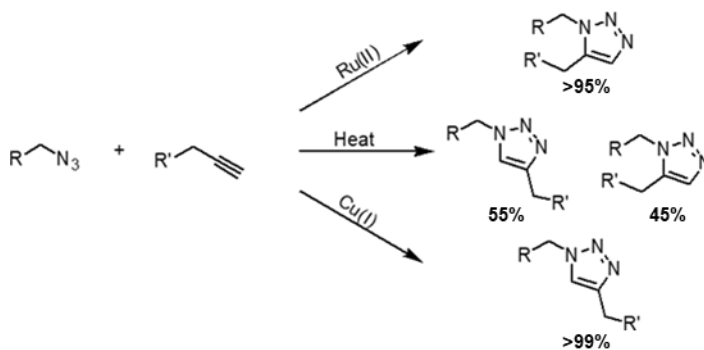
Scheme 1.1 Regioisomers formed via catalyzed or uncatalyzed azide-alkyne cycloadditions.	1
Scheme 2.1 Synthesis of Tetrapropargyl Aromatic Diamines	19
Scheme 3.1 Two synthetic strategies for achieving polyazide component. Route A: direct azidation using diphenyl phosphoryl azide (DPPA). Route B: two-step method involving 1) conversion of alcohol moieties to a mesylate leaving group, and 2) nucleophilic substitution using NaN ₃	59
Scheme 3.2 Propargylation of an isocyanurate-based polyisocyanate	71
Scheme 4.1 Two Routes to yield propiolate HDI-based resin. Route 1 involves the direct reaction of propiolic acid with an isocyanate to produce an amide linkage and CO ₂ . Route 2 involves first synthesizing 2-HEP and subsequent reaction with an isocyanate in the presence of DBTDL catalyst to produce a carbamate linkage.....	93
Scheme 4.2 Synthesis of 2-HEP via ring-opening of ethylene oxide using propiolic acid.	95
Scheme 4.3 Fischer esterification of 2-HEP.	97
Scheme 5.1 Synthesis of low-viscosity resins.	122

CHAPTER I - INTRODUCTION

1.1 Motivation of Research

The focus of this dissertation lies in modifying commercially-available two-component systems with azide and alkyne functionalities. Once modified, the reaction rate can be increased dramatically by the addition of catalyst¹ or by utilizing an electron deficient alkyne.² In addition, the relative abundance of regioisomers can easily be controlled by the addition or omission of catalysts. Shown in Scheme 1.1 are the possible regioisomers formed by curing in the presence or absence of specific catalysts along with the relative abundance of regioisomers. In the absence of catalyst both the 1,4- and 1,5-regioisomers are present with a slight excess favoring the 1,4-regioisomer.³ When catalyzed with Cu(I) the reaction greatly favors the 1,4-regioisomer,¹ and when catalyzed with Ru(II) catalyst the reaction favors the 1,5-regioisomer.⁴

Scheme 1.1 Regioisomers formed via catalyzed or uncatalyzed azide-alkyne cycloadditions.



The following chapters exploit these characteristics of the azide-alkyne cycloaddition to probe fundamental properties such as reaction rate or structure-property

relationships in crosslinked polytriazole networks while offering practical polymer solutions to unmet areas of need within material science.

This dissertation can be divided into two overall projects. The goal of the first project was to create an out of autoclave resin with a triggered cure via azido-alkyne cycloaddition. Brei *et al.*⁵ were able to show approximately 80% conversion of these azido-alkyne networks within 30 s at room temperature when incorporating Cu(II) into the matrix and using UV light to reduce Cu(II) into Cu(I). However, in no instance were they able to exceed approximately 80-90% conversion without an external heat source, which was later ascribed to vitrification.^{5,6} This issue led to a paradigm shift in which the focus redirected heavily toward the structure-property relationships inherent to these fully cured networks. As shown in Scheme 1.1, the relative abundance of regioisomers can be controlled by the addition or omission of catalyst. This was well-known in solution but was relatively unexplored in bulk polymerizations. Furthermore, it was virtually unknown how the relative abundance of these regioisomers affected network properties. This curiosity led to a project that was designed by Brei and Cooke⁷ to prove regioisomers control in thermoplastic polytriazoles performed in bulk and to give general parameters for achieving regioisomer control in fully cured polymeric networks. Ultimately it was found that the desired control could be achieved by the addition or omission of catalyst. However, in order to reach adequate conversion with the Ru(II) catalyzed system a large amount of catalyst was needed along with solvent. Both of these constraints made polymer network development impractical and Ru(II) was removed from further studies.

Previous research in the Storey Research Group by Gorman *et al.*² demonstrated the synthesis of di(3-azido-2-hydroxypropyl)ether of bisphenol-A (DAHP-BPA) from commercially available EPON 825 and evaluated a library of alkyne curatives to conclude that propargyl amine family of curatives showed the most promise for composite fabrication. Brei and Cooke⁵ furthered this research by synthesizing a library of tetrapropargyl aromatic amines and found that the thermal and mechanical properties increased relative to Gorman's study which was comprised of aliphatic crosslinkers. Chapter II drives this research even further by understanding structure-property relationships in Cu(I) and uncatalyzed azido-alkyne systems. This molecular architecture control was performed by strategically using three bis-aniline crosslinkers that only varied by the central linkage denoted as 'R' in Figure 1.1 where R = -O-, -CH₂-, or -SO₂-. This strategic design allowed for the understanding the role that the central linkage and relative abundance of regioisomer has in these glassy azido-alkyne networks.

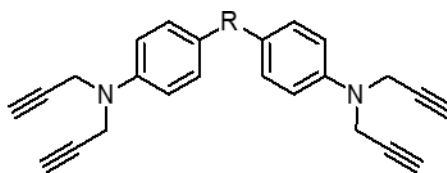


Figure 1.1 General Structure of Crosslinkers used in Chapter II.

A problem inherent to these polytriazole networks first described by Gorman *et al.*² and carrying through to current research is the proclivity for the reaction to auto-accelerate. Although empirical data has attributed this tendency to the material's surface area-to-volume ratio, only loose rules of thumb have been developed to contain this issue. Over time, this process requirement naturally led to the adaptation of these systems to

polymeric coatings, which have a much more favorable ratio than thick composite matrices.

The goal of the second project was to develop non-isocyanate polyurethanes (NIPUs) that cure by azide-alkyne cycloaddition. Most typically, polyurethanes are synthesized by the addition reaction of a polyisocyanate and a polyol.⁸ The former is well-known for many health hazards,^{9,10} which has led to legislation requiring to phase it out over the next few years.¹¹ Due to these concerns, it became apparent that a new material was needed that could retain the desired properties of polyurethanes while not exposing end users to free isocyanates in the final curing step. This was achieved by converting the isocyanate and alcohol groups of commercially available polyisocyanates and polyols to propargyl and azide functionalities, respectively. Chapters III-V address different aspects of developing these NIPU coatings. Chapter III demonstrates the synthesis of each component of the 2K coating, presents the curing of these systems and displays the properties of the cured coatings. *It was hypothesized that converting isocyanate and alcohol functionalities to alkyne and azide will cause only minor difference in final coating properties, but will, in the absence of catalysis, reduce curing kinetics.* In the absence of Cu(I) these components result in aesthetically pleasing coatings that meet and in some cases exceed the properties of the unmodified commercially available coating. However, the kinetics of the azide-alkyne cycloaddition are too sluggish to be a practical alternative to the traditional method for making polyurethanes. When catalyzed with Cu(I), the kinetics can be tailored to increase reactivity even beyond that of the unmodified isocyanate and alcohol reaction. However, the addition of copper, even in small amounts, results in discoloration of the coatings.

Chapter IV introduces a method to increase the kinetics of the reaction without using a copper catalyst and instead incorporating an electron deficient alkyne functionality. This idea was originally inspired by Gorman *et al.*² who developed propiolate functional crosslinkers for out of autoclave processes but found that these were too reactive and tended to auto-accelerate making them impractical for their intended goal. The increase in reactivity that proved to be problematic for Gorman's thick composite samples proved to be ideal for the thin coating samples as the coatings containing this functionality had similar curing kinetics to commercially available unmodified samples. *The principle hypothesis for Chapter IV was that by incorporating the electron-deficient alkyne, the kinetics would increase to be similar to the as received material.*

Chapter V sought to overcome a problem inherent to all carbamates synthesized from commercially available isocyanates, which is a dramatic viscosity increase. This increase was attributed to an increase in polymer-polymer hydrogen bonding resulting from the urethane linkage and makes it impractical to achieve aesthetically pleasing coatings without diluting the resin with an organic solvent. *It was hypothesized that by incorporating ethylene glycol oligomers into the network then the viscosity could be considerably reduced without having detrimental effects on the cured coating properties.* Three ether alcohols were strategically chosen: ethylene glycol monoethyl ether (EGME), diethylene glycol monoethyl ether (DEGME), and diethylene glycol butyl ether (DEGBE). The purposeful utilization of these three ether alcohols allowed for the systematic study the effect ethylene glycol concentration (EGME vs. DEGME) and chain end (DEGME vs. DEGBE) had on viscosity as well as the coating properties.

1.2 Background

1.2.1 Thermosetting Composite Matrices

Carbon fiber reinforced polymers (CFRPs) are strong and light weight composite materials comprised of high tensile strength fibers and a matrix to hold the fibers in place. They have gained popularity since their inception in the 20th century due to their impressive properties such as light weight, high strength, high stiffness, and good corrosion resistance.¹² CFRPs are currently utilized in a variety of markets, including aerospace, defense, sporting goods, and a number of niche applications, and in 2013 they reached a world market value of over \$16 billion.¹³

Traditional CFRPs are cured within an autoclave, *i.e.*, a controlled-temperature, pressure chamber, under conditions of elevated temperature and pressure. Part size is effectively limited by the autoclave capacity and use of an autoclave increases production costs due to increased capital expenditure and higher energy consumption. This research seeks to overcome the limitations of autoclave processing by developing a resin system that can cure out of autoclave (OOA) using a well-known “click” reaction, Cu(I) catalyzed azide-alkyne cycloaddition (CuAAC). Specifically we propose to utilize an azido-modified epoxy resin (DGEBA-based) as reported by Gorman *et al.*,² along with various aromatic polyalkyne crosslinkers.

1.2.2 Non-Isocyanate Polyurethane Coatings

Otto Bayer first demonstrated the addition of polyols to polyisocyanates to yield polyurethanes in 1947.⁸ Since then, polyurethanes have become important and often dominant in a variety of industries including elastomers,¹⁴ foams,¹⁵ and coatings.¹⁶ The widespread use of polyurethanes has resulted in part from the large variety of materials

that can be produced from a relatively small number of simple precursors, a broad range of reactivity,¹⁷ facile tunability of mechanical properties,¹⁸ excellent solvent resistance, and good weather stability.¹⁹ The aforementioned reaction with an alcohol to form a urethane linkage is just one example of the utility of the isocyanate functional group. It can also react with an amine to form a urea linkage, and in the case of flexible foams, isocyanates are sometimes purposefully reacted with water to produce a primary amine and carbon dioxide, which works as an *in situ* blowing agent.²⁰ The propensity for isocyanates to react with these common nucleophiles can sometimes be problematic. For instance, isocyanates can react with ambient moisture, as mentioned above, which can dramatically reduce shelf-life.²¹ In addition, isocyanates pose multiple health risks, and in 1994 OSHA named them as one of the main causes of occupational asthma and other respiratory illnesses.⁹ More recently, a review by Redlich *et al.*¹⁰ discussed the risk of skin exposure to isocyanates. These concerns have resulted in specific legislation in Europe along with the European Regulation on Registration, Evaluation, Authorisation, and Restriction of Chemicals (REACH) to phase-out many isocyanates.¹¹

The desirable properties of polyurethanes are an inherent result of the unique primary and secondary structure of the urethane linkage. The linkage itself is naturally resistant to chemicals such as acids, bases, and solvents, and its capacity to serve as both a hydrogen bond donor and acceptor promotes organization of the polyurethane chains into microdomains that increase the bulk properties of the material.¹⁹ The desirability of the urethane linkage, combined with the health concerns associated with isocyanates, has generated an interest in non-isocyanate polyurethanes (NIPU), defined herein as a polyurethane produced without the presence of free isocyanate groups in the final curing

step. Thus, NIPUs possess urethane linkages, but workers such as painters are not at risk of exposure to free isocyanate groups. One method to produce a NIPU is to incorporate functional groups for an alternative curing mechanism into the polymer via urethane linkages. An example is the capping of isocyanate-terminated oligomers with 2-hydroxyethyl acrylate or 2-hydroxyethyl methacrylate. The result is consumption of free isocyanates and creation of urethane linkages, with their attendant desirable properties, and at the same time, providing an alternative curing pathway, in this case UV-induced radical chain polymerization of acrylate groups.^{14,22-24}

1.2.3 Azide-Alkyne Cycloaddition

In 2001, Sharpless *et al.*¹ identified a set of very facile chemical reactions, dubbed collectively “click chemistry,” which meet the following criteria: “The reaction must be modular, wide in scope, give very high yields, generate only inoffensive byproducts that can be removed by nonchromatographic methods, and be stereospecific (but not necessarily enantioselective).” According to Sharpless *et al.*, the Huisgen dipolar cycloaddition of an azide with an alkyne is the “cream of the crop” of click chemistry. . Several attributes of the Huisgen cycloaddition reaction are expected to make it particularly advantageous toward both processes: it is tolerant to a wide range of impurities; it is high yielding; no small molecule is evolved, and most notably, the reaction is highly exothermic, with a ΔH between -210 and -270 kJ/mol. When uncatalyzed, this reaction is capable of reaching high conversion, but heat is necessary to activate and sustain the reaction, and as a result the resulting triazole product is non-regiospecific.^{3,25} For example, it was found that the reaction produces nearly equivalent amounts of 1,4 and 1,5 isomers (activation barriers, E_a , were found to be 25.7 and 26.0

kcal/mol, respectively²⁶) as shown in Scheme 1.1 from a variety of azides and alkynes. The activation energy for the reaction is lessened dramatically when the alkyne contains electron withdrawing groups or catalyzed by transition metals.¹

In the early 2000s, the research groups of Sharpless¹ and Meldal²⁷ reported that Cu(I) was able to catalyze the Huisgen 1,3-dipolar cycloaddition of an azide with an alkyne and produce almost exclusively the 1,4 isomer (Scheme 1.1 bottom). This discovery created great interest in the polymer community, and the catalyzed reaction has since been used in a variety of fields, including medicinal chemistry,^{1,28} material science,^{29,30} and organic chemistry.^{31,32}

As compared to the uncatalyzed reaction, CuAAC offers not only the benefit of regioselectivity, but also a rate acceleration on the order of 10^7 or 10^8 times without additional heating.¹ When Cu(I) is added, the reaction is no longer concerted, but instead involves a number of discrete steps.³³

After observing that CuAAC is one of the more robust catalytic processes (*i.e.* the cycloaddition can be performed with a breadth of azides and alkynes and in a variety of solvents), Fokin *et al.*³³ set out to determine the mechanism of both the uncatalyzed (Scheme 1.1 middle) and Cu(I) catalyzed cycloadditions (Scheme 1.1 bottom) using Density Functional Theory (DFT) calculations. The E_a for the uncatalyzed reaction was found to be 25.7 kcal/mol for the 1,4-isomer and 26.0 kcal/mol for the 1,5-isomer and for the CuAAC reaction, the E_a was around 11 kcal/mol lower.

The original DFT calculations by Fokin *et al.*³³ were based on mononuclear Cu(I) as the catalytic source, but a related kinetic study by Rodionov *et al.*³⁴ showed a second-order dependency on Cu(I) concentration. The dinuclear mechanism was later adopted

because DFT calculations showed a drop in E_a from 17 kcal/mol for the mononuclear mechanism to 10-13 kcal/mol for the dinuclear mechanism and agreed with the kinetic study.³⁵

Cu(I) can be introduced by direct addition^{27,36-38} or it can be created *in-situ* from Cu(II) by a number of ways, including the use of a reducing agent,^{33,39,40} UV light,⁴¹⁻⁴³ or ultrasound.⁴⁴ In this work, the *in-situ* reduction of Cu(II) to Cu(I) was utilized in Chapters II and III. In Chapter II, the amine crosslinkers were capable of reducing Cu(II) to Cu(I) whereas in Chapter III the addition of tin(II) 2-ethylhexanoate was needed as a reducing agent. In the final two chapters, Chapter IV and Chapter V, still other methods were used to cure the polytriazole where Chapter IV used an electron-withdrawing group conjugated to the alkyne and Chapter V focused on the uncatalyzed cure.

CHAPTER II – THE EFFECT OF MICROSTRUCTURE ON THERMAL AND MECHANICAL PROPERTIES IN AZIDE-ALKYNE MATRICES

2.1 Introduction

The reaction between an azide and an alkyne to produce a 1,2,3-triazole ring (sometimes called 1,3-dipolar cycloaddition) is a thermodynamically favorable, high conversion process that produces no small molecule condensate and under appropriate conditions is regioselective (Scheme 1.1; bottom). These are very desirable features for a reaction used to produce a composite matrix.^{2,45} However, in the absence of a catalyst, an external heat source is required to activate and sustain the reaction.^{3,25} In addition, the uncatalyzed process is non-regioselective, i.e., it results in a mixture of two regioisomeric triazoles (Scheme 1.1; middle). Azide-alkyne cycloaddition responds well to catalysis, and the copper(I)-catalyzed process (CuAAC) is nearly universally regarded as the “cream of the crop” of the so-called “click” reaction family, defined by Sharpless *et al.* as a group of reactions characterized as modular, wide in scope, high yielding, and stereospecific.¹ The CuACC reaction is a relatively recent development, first reported in the early 2000s by the research groups of Sharpless¹ and Meldal,²⁷ and has greatly expanded the value of this reaction in chemistry^{1,28,31,32} and material science,^{29,30} in part due to dramatically faster reaction rates under ambient temperature conditions but also to the aforementioned regiospecificity.

Relatively, bulk step-growth CuAAC polymerizations are not as well established as their solution analogs. Likely the earliest example of CuAAC in bulk was reported by Finn *et al.*⁴⁶ who developed a series of multi-functional azide and alkyne monomers that were used as thermoset adhesives on copper substrates. Wan *et al.*⁴⁵ used the uncatalyzed

1,3-dipolar cycloaddition of *p*-xylene diazide and N,N,N',N'-tetrapropargyl-4,4'-methylenedianiline to demonstrate the efficacy of a polytriazole resin as a composite matrix. Furthermore, Wang and coworkers⁴⁷ set out to establish the relationship between the crosslinked structure of polytriazole resins and thermal properties by systematically varying the ratio between a difunctional azide, trifunctional azide, and difunctional alkyne in the absence of catalyst. In all of these examples, the authors chose to survey matrices created using either the catalyzed or the uncatalyzed reaction, but in no case was the presence/absence of catalyst treated as an experimental variable. The manner by which the presence or absence of catalyst affects thermal and mechanical properties of the resulting polytriazole matrix remains a largely unanswered question.

The goal of this chapter is to determine the effect of the mechanism of network formation as well as crosslinker identity on network properties in triazole networks. The former will be studied by exploiting chemistry inherent to these cycloadditions. As shown in Scheme 1.1, one can easily manipulate the regioisomer composition of the triazole linkages by the addition or omission of a catalyst and by the catalyst type. Although Ru(II) may be used to produce predominately the 1,5-regioisomer (Scheme 1.1; top), we have previously shown⁷ that this reaction is impractical in the bulk due to insolubility of the catalyst. Therefore, networks containing high 1,5-regioisomer contents produced using Ru(II) have been excluded from this study. However, a usefully broad range of regioisomers can be achieved simply through addition or omission of Cu(I); adding Cu(I) to the matrix results in nearly 100% 1,4-regioisomer, while its omission yields approximately a 45:55 mixture favoring the 1,4-regioisomer.^{4,7,33} The reaction kinetics of the catalyzed and uncatalyzed system as a function of conversion can be

followed using the Ozawa method.⁴⁸ Kessler and coworkers⁴⁹ sought to establish kinetics of the bulk CuAAC polymerization in linear systems, admittedly a difficult task, but ultimately showed that a decrease in E_a occurs with increasing catalyst concentration and the polymerization follows nth order reaction kinetics.

Network architecture, in terms of flexibility of chains between crosslinks⁵⁰ or in terms of geometric isomers produced by incorporation of 3,3'-diaminodiphenyl sulfone vs. 4,4'-diaminodiphenyl sulfone into epoxy matrices,⁵¹ has been shown to greatly effect thermal and mechanical properties. In addition, small changes in the molecular architecture of a system can greatly affect the sub- T_g relaxations. The effect of these relaxations on bulk mechanical properties such as Young's modulus has been reported.⁵⁰ Owing to the fact that polytriazole networks are a relatively new type of network, there appears to be little, if any, research on their sub- T_g relaxations (γ and β relaxations) or how controlling the network architecture can affect bulk properties.

The effect of regioisomer content on network properties will be directly compared using three crosslinkers, TPDPE, TPMDA, and TP44DDS, (Figure 2.1) which differ only with regard to the central linkage within each molecule. It is expected that by systematically varying both the presence of catalyst as well as crosslinker type, several network properties can be explored, including T_g , crosslinking density, degree of cure, and mechanical properties. *It is hypothesized that the Cu(I)-catalyzed networks will have higher T_g 's as well as higher compressive modulus due to more favorable molecular motions predicted for the 1,4-regioisomer.*

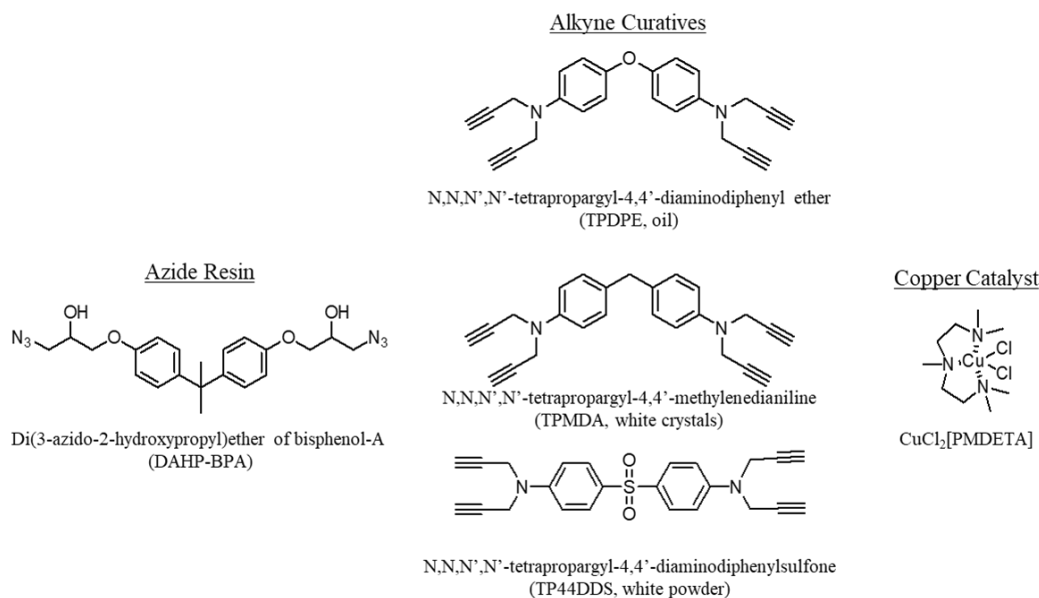


Figure 2.1 Difunctional azidated resin, tetrafunctional aromatic alkynes, and catalyst used in this work.

2.2 Experimental

2.2.1 Materials

N,N-dimethylformamide (DMF) (Certified ACS), dichloromethane (DCM) (Certified ACS), acetonitrile (Optima®), and magnesium sulfate (MgSO₄) were purchased from Fisher Scientific. Deuterated dimethyl sulfoxide (DMSO-*d*₆; 1 v/v% TMS; 99.9 atom %D), deuterated chloroform (CDCl₃ 99.8+ atom % D, 0.03 v/v% TMS) and 4,4'-methylenedianiline (MDA; 97%) were purchased from Acros Organics. 4,4'-Diaminodiphenyl ether was purchased from Wakayama Seika Kogyo Co. Propargyl bromide (80 wt% in toluene, 0.3% magnesium oxide stabilizer), ammonium chloride (ACS reagent, ≥ 99.5%), potassium carbonate (K₂CO₃; ReagentPlus®, 99%), sodium azide (NaN₃; ReagentPlus®, ≥ 99.5%), silica gel (high purity grade, pore size 60 Å, 70-230 mesh, 63-200 μm), N,N,N',N'',N''-pentamethyldiethylenetriamine (99%), and

copper(II) chloride (97%) were all purchased from Sigma-Aldrich. EPON 825 was generously donated by Hexion. All materials were used as received.

2.2.2 Instrumentation

Proton nuclear magnetic resonance (^1H NMR) spectra were obtained using a 600.13 MHz Bruker Ascend (TopSpin 3.5) NMR spectrometer. Typical acquisition parameters were 10 s recycle delay, 7.8 μs pulse corresponding to a 45 degree flip angle, and an acquisition time of 1.998 s. The number of scans acquired for each sample was 32. All ^1H chemical shifts were referenced to TMS (0 ppm). Sample solutions were prepared at a concentration of approximately 1 wt% in either CDCl_3 or $\text{DMSO-}d_6$ containing 1% TMS as an internal reference, and the resulting solution was charged to a 5 mm NMR tube. Carbon nuclear magnetic resonance (^{13}C NMR) spectra were obtained using a 600.13 MHz Bruker Ascend (TopSpin 3.5) NMR spectrometer. Typical acquisition parameters were 1 sec recycle delay, 11 ms pulse corresponding to a 45 degree flip angle, and an acquisition time of 0.908 s. The number of scans acquired for each sample was 1024. All ^{13}C chemical shifts were referenced to residual chloroform (77.16 ppm) or residual DMSO (128.06 ppm). Sample solutions were prepared at a concentration of approximately 5 wt% in CDCl_3 containing 1% TMS as an internal reference, and the resulting solution was charged to a 5 mm NMR tube.

Isothermal real-time Fourier transform infrared spectroscopy (RT-FTIR) was measured using a Thermo Fisher Scientific Nicolet 6700 FTIR equipped with a mid-IR beam splitter and integrated with a Simplex Scientific HT-32 heated transmission cell. The Simplex software was paired to the OMNIC FTIR software native to the Nicolet 6700. Approximately 1.5 g of sample was hand mixed at 1:1 azide:alkyne stoichiometry

for 2 min. A small aliquot was taken from the mixture and squished between two polished NaCl plates. The plates were then inserted in the transmission cell and subsequently placed in the chamber for FTIR analysis. The sample was rapidly heated from room temperature to 70 °C, and spectra were immediately obtained in 1 min intervals (32 scans; 4 cm⁻¹ resolution) for the duration of the run (60 min). Conversion was monitored as the disappearance of the coincident peaks attributed to azide (N=N=N stretching) and alkyne (C≡C stretching) at centered approximately 2100 cm⁻¹. Aliphatic C-H stretching (centered at 2755 cm⁻¹) was used as an internal standard. Baselines were taken as a two-point straight line between ~1950 and 2300 cm⁻¹ for the azide/alkyne peak and between ~2750 and 3000 cm⁻¹ for the alkane internal standard.

Dynamic mechanical analysis (DMA) was performed on a TA Instruments Q800 in tension mode at a strain of 0.05% and at a frequency of 1 Hz unless otherwise stated. Specimens were degassed and then cast in a silicon mold (*vide infra*). After curing, the samples were polished using 600 grit sandpaper to final dimensions of approximately 11.00 mm length, 5.00 mm width, and 1.15 mm thickness. The temperature was ramped at 3 °C/min from -120 °C to 250 °C in an inert environment at a frequency of 1 Hz. To determine the E_a of sub-T_g relaxations three additional frequencies were utilized: 0.1 Hz, 10 Hz, and 100 Hz. The data were exported to TA Universal Analysis Software which was used for calculation of the glass transition temperature (T_g) and various sub-T_g relaxations associated with relative maxima of the tan δ curve.

Thermogravimetric analysis (TGA) was performed using a TA Instruments Q500. Samples (approximately 20 mg) were loaded into pre-tared platinum sample pans and heated from room temperature to 600 °C at a heating rate of 10 °C/min in a N₂

environment. Data were exported to TA Universal analysis to determine T_{d95} , T_{d90} , and char yield.

Differential scanning calorimetry (DSC) was performed using a TA Instruments Q200. Approximately 1-2.5 mg of premixed (1:1 azide-alkyne) uncured sample was loaded into a hermetically sealed pan. A method by Friedman *et al.*⁵² was utilized to find activation energy (E_a) and the Arrhenius pre-exponential factor (A'). Heating ramps of 2, 5, and 10 °C/min were performed on all samples starting at room temperature and ending approximately 30 °C below the T_{d95} (~200 – 250 °C). A heat/cool/heat cycle was performed on the sample ramped at 10 °C/min, to verify that complete cure was being achieved during the first heating cycle. A MATLAB program developed by Anders and coworkers⁵³ and modified by Patterson⁵⁴ was used to calculate E_a and A' with 1000 point resolution. In addition, cured DMA bars (~5 mg) were subjected to a heat/cool/heat cycle to determine degree of cure. In all samples, no residual exotherm was present in the first or second heating cycle.

Rheometric cure profiles were determined using an ARES (TA Instruments) rheometer equipped with a heating oven set to 70 °C. Samples were mixed at 1:1 stoichiometry (azide/alkyne), and approximately 1 mL of the uncured mixture was loaded directly onto 25.0 mm disposable aluminum parallel plates with the gap set to 1 mm. Dynamic time sweeps were performed at a frequency of 6.28 rad/s and 10% strain. The experiments were stopped well after vitrification. Gel time (t_{gel}) was defined as the time corresponding to G'/G'' crossover point and was calculated using TA Orchestrator software.

Compression testing was performed on a MTS Insight equipped with a 10 kN load cell and 1" diameter compression sub-press in accordance with ASTM D695 using cubical specimens (approximately 6 mm x 6 mm x 6 mm). The platen separation was 6 mm, data acquisition rate was 10 Hz and the test speed was 1.27 mm/min.

Dissolution videos were made using a Nikon OPTIPHOT2-POL polarizing light microscope operating in transmission mode and integrated with a Mettler FP82 HT hot stage that was used to bring the sample to prescribed temperatures. DAHP-BPA and TP44DDS were mixed at 1:1 stoichiometry (azide/alkyne) and initially were heated from 70 °C to 150 °C at 3 °C/min. Later samples were isothermally cured at various temperatures within this range. Crosslinker dissolution was measured by image analysis of photographs taken by an Olympus UC50 during the entire heating prescription; images were processed using OLYMPUS Stream Essentials [Version 1.7] imaging software.

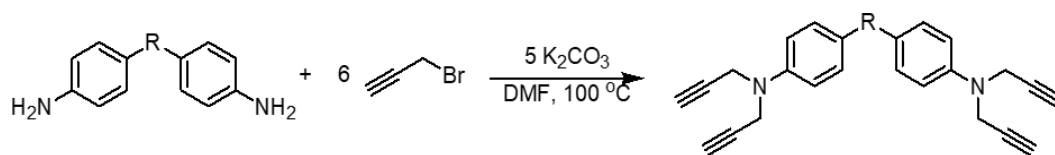
2.2.3 Synthesis of Azidated Resin

The azidated resin, di(3-azido-2-hydroxypropyl) ether of bisphenol-A (DAHP-BPA, Figure 2.1 left), was synthesized using a method developed by Gorman *et al.*² ¹H NMR (600 MHz, CDCl₃): δ = 1.62 (s, 6H, CH₃), 2.82 (bs, 2H, OH), 3.51 (m, 4H, CH₂-N₃), 3.98 (d, 4H, O-CH₂), 4.13 (m, 2H, CH-OH), 6.80 (d, 4H, Ar-C_{2,6}-H), 7.13 (d, 4H, Ar-C_{3,5}-H) ppm. ¹³C NMR (150 MHz, CDCl₃): δ = 30.95 (CH₃), 41.71 (C-CH₃), 53.41 (CH₂-N₃), 66.52 (CH-OH), 69.24 (O-CH₂), 113.93 (Ar-C_{3,5}), 127.78 (Ar-C_{2,6}), 143.80 (Ar-C₁), 156.04 (Ar-C₄) ppm.

2.2.4 Preparation of Tetrafunctional Alkyne Crosslinkers

The aromatic tetrapropargyl crosslinkers were synthesized from commercially available aromatic diamines following the same general procedure (Scheme 2.1). The

synthesis of N,N,N',N'-tetrapropargyl-4,4'-diaminodiphenyl ether (TPDPE, Figure 2.1, top alkyne curative) is representative. Into a 250 mL three-neck round-bottom flask equipped with overhead stirrer, condenser, and nitrogen bubbler, were charged 4,4'-oxydianiline (DPE) (10.0 g; 50 mmol), K₂CO₃ (34.55 g; 250 mmol), and 150 mL of DMF. The resulting mixture was heated at 40 °C until complete dissolution of DPE was observed using a thermostatic oil bath. A solution of 80% propargyl bromide in toluene (44.6 g, 300 mmol propargyl bromide) was then slowly added to the flask. The reaction temperature was gradually increased to 100 °C over a 30-min period and allowed to react at 100 °C overnight



Scheme 2.1 Synthesis of Tetrapropargyl Aromatic Diamines

The reaction mixture was then cooled to room temperature. The cooled reaction mixture, containing the desired product, toluene, DMF, unreacted propargyl bromide, and salts, was filtered to remove the salts and transferred to a 500 mL separatory funnel, using a DCM wash to ensure quantitative transfer. DI H₂O (100 mL) was added to the separatory funnel to aid in the separation of DMF. The resulting mixture was extracted with DCM (50 mL x 3), and the extracts were combined, washed with brine (100 mL x 4), chemically dried with MgSO₄ and concentrated *in vacuo*. The resulting black solid was further purified by redissolving in DCM and passing through a silica gel plug. Again, the solvent was removed *in vacuo* to yield 14.54 g (82.6 % yield) of the desired product as a burnt orange oil. ¹H NMR (600 MHz, CDCl₃): δ = 6.933 (s, 4H, Ar-C_{2,6}-H), 6.929 (s, 4H, Ar-C_{3,5}-H), 4.06 (d, *J* = 0.004 Hz, 8H, -CH₂-C≡), 2.25 (t, *J* = 0.004 Hz, 4H,

C≡C-H). ¹³C NMR (150 MHz, CDCl₃): δ = 41.14 (N-CH₂), 72.86 (≡C-H), 79.13 (CH₂-C≡), 118.07 (Ar-C_{3,5}), 119.27 (Ar-C_{2,6}), 143.76 (Ar-C₄), 151.50 (Ar-C₁) ppm.

Synthesis of N,N,N',N'-tetrapropargyl-4,4'-methylenedianiline (TPMDA, Figure 2.1, middle alkyne curative) from 4,4'-methylenedianiline was conducted similarly. However, the resulting product was crystalline, so rather than using column chromatography in the final purification step, recrystallization from hexanes was performed, resulting in white needle-like crystals (63.4% yield; m.p. = 53.1 °C, taken as DSC peak maximum). ¹H NMR (600 MHz, CDCl₃): δ = 2.22 (t, *J* = 0.004 Hz, 4H, ≡C-H), 3.83 (s, 2H, Ar-CH₂-Ar), 4.07 (d, *J* = 0.004 Hz, 8H, CH₂-C≡), 6.88 (d, *J* = 0.015 Hz, 4H, Ar-C_{3,5}-H), 7.09 (d, *J* = 0.015 Hz, 4H, Ar-C_{2,6}-H). ¹³C NMR (150 MHz, CDCl₃): δ = 40.07 (Ar-CH₂-Ar), 40.59 (CH₂-C≡), 72.64 (≡C-H), 79.29 (CH₂-C≡), 116.16 (Ar-C_{3,5}), 129.50 (Ar-C_{2,6}), 133.05 (Ar-C₁), 146.03 (Ar-C₄) ppm.

Synthesis of N,N,N',N'-tetrapropargyl-4,4'-diaminodiphenylsulfone (TP44DDS, Figure 2.1, bottom alkyne curative) from 4,4'-diaminodiphenylsulfone was conducted similarly. The crude product, a brown oil, was passed through a silica gel plug as a 25% solution in DCM. Evaporation of DCM yielded a solid that was recrystallized using toluene (49.6% yield; m.p. = 178.8°C, taken as DSC peak maximum). ¹H NMR (600 MHz, DMSO-*d*₆): δ = 3.16 (t, *J* = 0.004 Hz, 4H, ≡C-H), 4.25 (d, *J* = 0.004 Hz, 8H, CH₂-C≡), 6.98 (d, *J* = 0.008 Hz, 4H, Ar-C_{3,5}-H), 7.72 (d, *J* = 0.008 Hz, 4H, Ar-C_{2,6}-H). ¹³C NMR (150 MHz, CDCl₃): δ = 39.77 (CH₂-C≡), 75.16 (≡C-H), 79.27 (CH₂-C≡), 113.53 (Ar-C_{3,5}), 128.27 (Ar-C_{2,6}), 113.53 (Ar-C₁), 149.93 (Ar-C₄) ppm.

2.2.5 Synthesis of CuCl₂[PMDETA] complex

The preparation of CuCl₂[PMDETA] (Figure 2.1 right) followed a procedure reported by Song *et al.*⁴¹ To a 100 mL single neck round-bottom flask, CuCl₂ (0.993 g; 7.39 mmol) and acetonitrile (7.5 mL) were charged. PMDETA (1.283 g; 7.40 mmol) was added dropwise to the stirred solution. Upon the addition, the reaction turned from brown to turquoise. After reacting at room temperature for 24 h, the acetonitrile was removed *in vacuo* resulting in a blue powder, CuCl₂[PMDETA].

2.2.6 Mechanical Testing

All networks were formulated using a 1:1 stoichiometric ratio of azide to alkyne functionalities. Catalyzed systems were formulated with 0.2 mol% CuCl₂[PMDETA] catalyst relative to azide functionality. The reaction of DAHP-BPA with TPDPE is representative. DAHP-BPA (13.781 g; 32.33 mmol) was charged to a 50 mL side arm flask equipped with magnetic stirring. In the case of a catalyzed system, 36.8 mg (0.129 mmol) CuCl₂[PMDETA] was additionally added to the flask. DCM (~2 mL) was used to solubilize the catalyst in the resin and was removed using a vacuum oven set to 50 °C. The complete removal of DCM was measured using ¹H NMR spectroscopy. The flask was stoppered, and the resin was degassed under vacuum at 70 °C until bubbles were no longer forming in the bulk material or approximately 2 h, whichever came first. Typically bubbles formed from agitation caused by the stir bar throughout the degas period but were ignored. The de-gassed mixture was removed from the heat and brought to atmospheric pressure. TPDPE (5.712 g; 16.22 mmol) was charged to the flask using a syringe and allowed to mix *in vacuo* at 70 °C for an additional 30 min. For catalyzed systems, the reaction was cooled to 50 °C before adding the alkyne crosslinker to

mitigate auto-acceleration potential; mixing was then carried out *in vacuo* at 50°C for 10 min.

The homogenous mixture was then cast into pre-heated silicon molds (70 °C) and cured to produce compression and DMA (both rectangular) test specimens. For uncatalyzed systems, the following curing prescription (uncatalyzed cure profile), developed for tripropargyl amine (TPA; b.p. = 79-85 °C), was employed: the specimens were isothermally cured at 70 °C for 12 h, then ramped at 1 °C/min to 135 °C, and finally held at 135 °C for an additional 3 h. For the catalyzed specimens, the curing prescription was slightly modified to slowly ramp from 50 °C to 70 °C over the course of the initial 12 h period (catalyzed cure profile). This modification was done to mitigate the chance of gel effect. The subsequent ramp and final isotherm were identical to those used for the uncatalyzed specimens.

After curing, the specimens possessed a convex outer surface (the face not touching the mold). The samples were flattened using 300 grit sandpaper and finally polished using 600 grit sandpaper. The final dimensions for DMA specimens were 10-15 mm length by 5.00 mm width (gage) by 1.15 mm thick.

2.3 Results and Discussion

2.3.1 Dissolution of Crosslinkers

Dramatic differences in physical appearance and properties of the tetrafunctional alkynes, resulting from varying the central linkage (Scheme 2.1; R group), were immediately apparent upon synthesis and are summarized in Table 2.1. TPDPE is a low viscosity oil and TPMDA is a low melting, soft solid at room temperature; while TP44DDS is a high-melting white powder. This same trend is observed with regard

to the melting point for diphenyl sulfone (128-129 °C),⁵¹ which is significantly higher than that of diphenyl ether (28 °C)⁵⁵ or diphenylmethane (24-25 °C).⁵⁶ In commercial applications, these differences would dictate corresponding process differences. For instance, an extruder equipped with a solids feeder might be required to handle TPMDA or TP44DDS; while the low viscosity TPDPE might be desirable for lab-scale processes where hand mixing is more typically utilized. In addition, the identity of the central linkage greatly effects the temperature for onset of cure. For TPDPE and TPMDA, this temperature is nearly the same, and relatively low, likely because these materials are much more soluble in the DAHP-BPA matrix. Whereas, TP44DDS has a much higher cure-onset temperature, around 115 °C, indicating decreased reactivity and/or solubility. The lack of solubility of TP44DDS in the DAHP-BPA resin could be determined visually as well. Mixing DAHP-BPA with either TPDPE or TPMDA at 50 °C resulted in an easily stirred homogenous systems. Whereas mixing DAHP-BPA with TP44DDS resulted in a heterogeneous system that was very difficult to stir by hand.

Table 2.1 Properties of Tetrafunctional Aromatic Crosslinkers

Crosslinker	Appearance	Melting Point (°C)	Cure Onset Temp. ⁱ (°C)
TPDPE	oil	---	99.1
TPMDA	Needle-like crystals	53.2	96.4
TP44DDS	White powder	178.8	115.2

ⁱ Cure onset temperature was measured as the intersection of the baseline and the line tangent to exothermic peak using 10 °C/min heating ramp on DSC.

Due to the limited solubility of TP44DDS, a thorough analysis of cure prescription was performed in hopes that complete solubilization in DAHP-BPA could be achieved with this crosslinker. Figure 2.2 shows light microscopy images of DAHP-BPA/TP44DDS acquired at various temperatures during a heating ramp from 70 °C to

150 °C at 3 °C/min. At the start of the curing profile, the crosslinker was not soluble in the matrix but as the temperature was increased to 95, 110, and 150 °C, the crosslinker steadily dissolved until only a single large chunk remained in the sample heated to 150 °C.

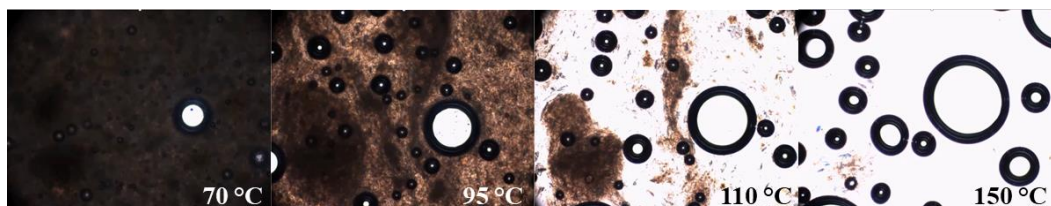


Figure 2.2 Light microscopy images of DAHP-BPA/TP44DDS. Heating prescription 70 °C to 150 °C at 3 °C/min.

After discovering that dissolution began to occur around 90-95 °C, a series of isothermal cures was performed. At 90 °C the dissolution of TP44DDS was relatively slow, but at 100 °C the dissolution was much quicker and still well below the cure onset. This gave credence that 100 °C would be a suitable temperature to properly dissolve the crosslinker and adequately cure the matrix. However, size-scale and more specifically surface area-to-volume ratio proved to be important when curing the matrix. Even most DMA bars, which have a very favorable surface area-to-volume ratio succumbed to gel effect at 100 °C. Of the few bars that did not char, all exhibited small crystals trapped inside the matrix indicating gelation before complete dissolution.

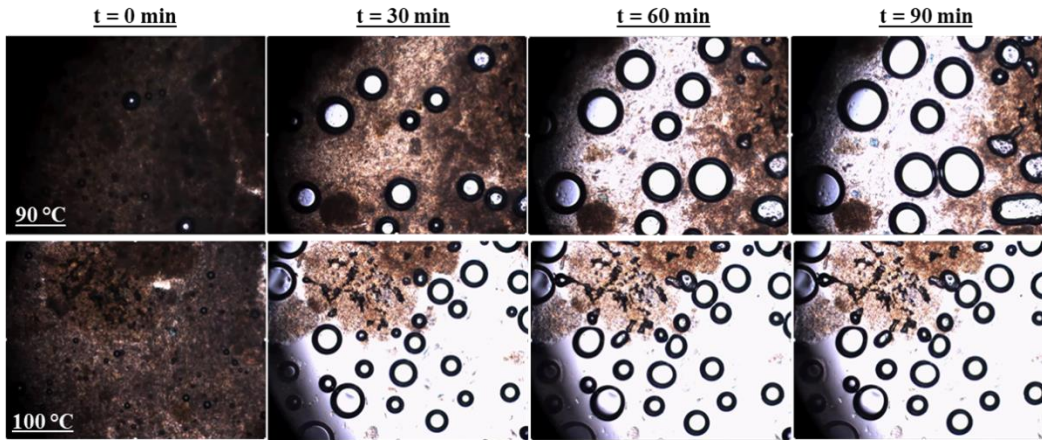


Figure 2.3 DAHP-BPA/TP44DDS held isothermally at 90 °C (top) and 100 °C (bottom).

Solvent processing techniques were utilized to create homogeneous DAHP-BPA/TP44DDS mixtures, but to no avail. The general procedure was to use a solvent capable of dissolving both DAHP-BPA and TP44DDS, and then removing the solvent *in vacuo* before casting. Polar, volatile solvents, including acetone, methanol, and DCM were utilized, but all resulted in either charred material resulting from the extended processing time at elevated temperature required to remove the solvent, or more often, crystallites of TP44DDS that precipitated from the matrix upon solvent removal. Mechanical dispersion techniques including grinding with mortar and pestle or sonication were tried but found to be ineffectual. Recently, Frazee *et al.*⁵⁷ showed that by utilizing a reactive diluent one could easily solubilize previously insoluble components in matrices. Inspired by these findings, a study was conducted in which TPDPE, which is readily soluble in DAHP-BPA, was used as a reactive diluent. Two formulations were examined. The first consisted of DAHP-BPA:TP44DDS:TPDPE at approximately 1:0.49:0.51 and the second at 1:0.1:0.9 (mol:mol:mol). Each formulation was subjected to the uncatalyzed cure profile. Figure 2.4 shows the resulting cured matrix for the 1:0.1:0.9 (mol:mol:mol) formulation, which is representative. In spite of the presence of

TPDPE, undissolved crosslinker was still visible in the cured matrix. Because of this dissolution issue, TP44DDS was removed from the rest of the study.

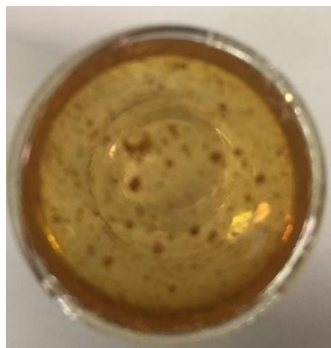


Figure 2.4 Non-dissolved crosslinker in cured azide-alkyne matrix. Formulation consisted of BPA:TP44DDS:TPDPE at 1:0.1:0.9 (mol:mol:mol) and was cured using the uncatalyzed cure profile.

2.3.2 Kinetics of Cure for both Catalyzed and Uncatalyzed Systems

Previous work by the Bowman research group^{41,42} and Yagci *et al.*⁵⁸ indicated that $\text{CuCl}_2[\text{PMDETA}]$ is a suitable source of Cu(I), when combined with a reducing agent or subjected to an external stimulus such as UV irradiation, as it is highly soluble in many organic compounds. In initial experiments, we found that the rate of the bulk azide-alkyne reaction with $\text{CuCl}_2[\text{PMDETA}]$ was substantial at room temperature even in the absence of a reducing agent or other stimulus, and that at temperatures slightly above room temperature, charring could occur. To understand these empirical observations, RT-FTIR was used to monitor the conversion of resin formulations, with and without $\text{CuCl}_2[\text{PMDETA}]$ catalyst, as a function of time; Figure 2.5 shows representative conversion plots of DAHP-BPA cured at 70 °C with either TPDPE or TPMDA. In the absence of catalyst, the reaction was sluggish, reaching approximately 10 and 18% conversion after 1 h for TPDPE and TPMDA, respectively. In the presence of catalyst,

the rate dramatically increased, such that the conversion of the catalyzed systems surpassed the conversion of the uncatalyzed systems in fewer than ten minutes. These results were initially very puzzling because there was no purposeful attempt to reduce Cu(II) to Cu(I). It is noteworthy that in the uncatalyzed system, the kinetics of cure for TPDPE were slower than TPMDA, but when catalyzed, the opposite was true; ultimately however, the conversions were almost identical after 60 min, reaching ~65%.

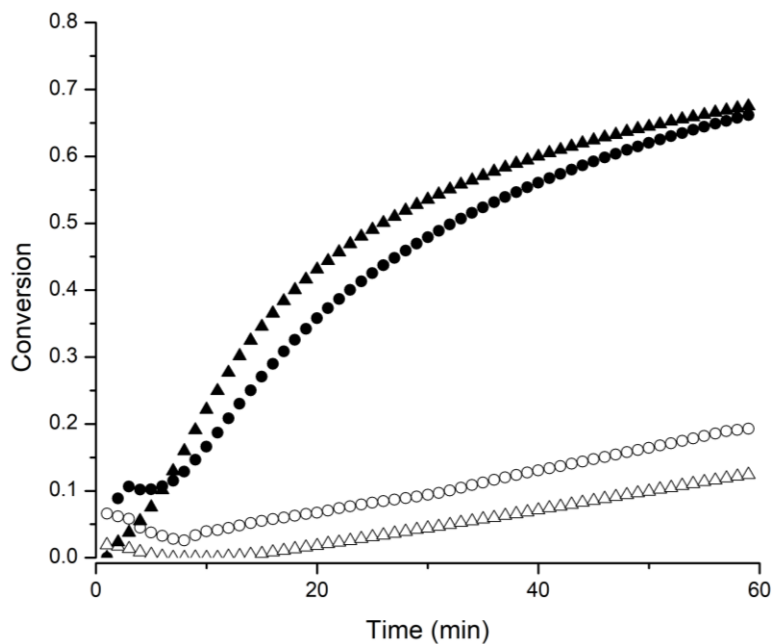


Figure 2.5 Isothermal cure progression at 70 °C of DAHP-BPA with TPDPE (triangles) or TPMDA (circles). The filled data markers refer to systems containing 0.2 mol% CuCl₂[PMDETA]; whereas the open data markers refer to uncatalyzed systems.

To further understand the kinetics of cure, DSC combined with the Flynn-Wall-Ozawa (FWO) method was chosen to model the system.⁴⁸ Isoconversional methods of this type were deemed to be especially appropriate for this work due to their ability to yield activation energy and the Arrhenius Pre-exponential Factor as a function of conversion. This detail was important because it was hypothesized that as conversion

increased, the copper catalyzed reaction mechanism would become less effective due to gelation, allowing the thermal mechanism to become the predominate mode of curing.

The FWO model was used to examine TPDPE and TPMDA with and without catalyst. Application of the method will be described in detail for the uncatalyzed TPDPE system, which is representative. Figure 2.6 shows heat flow vs. temperature for DAHP-BPA cured with TPDPE at three different heating rates. Very typical of these plots, as the heating rate was increased, the temperatures for onset of cure and for peak exotherm also increased. The dashed lines represent the user-defined baselines which were chosen as the temperature at which the local minimum occurred before and after the exothermic peak (typically around 50 °C and 200 °C).

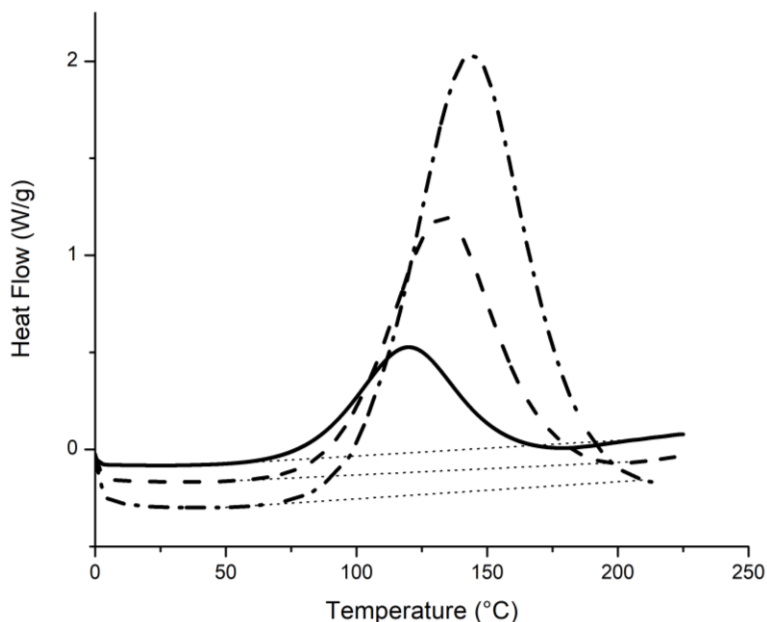


Figure 2.6 Dynamic DSC curves of uncatalyzed DAHP-BPA/TPDPE at 2 (solid), 5 (dash) or 10 (dash-dot) °C/min (first heat), with their respective user-defined baselines.

Figure 2.7 shows the conversion vs. temperature at the various heating rates. As heating rate increased from 2 to 5 and finally to 10 °C/min, the cure-onset temperature of

the reaction also increased from approximately 70 °C to over 90 °C. In addition, the derived model for each temperature ramp showed great correlation with the experimental data ($r^2 > 0.99$).

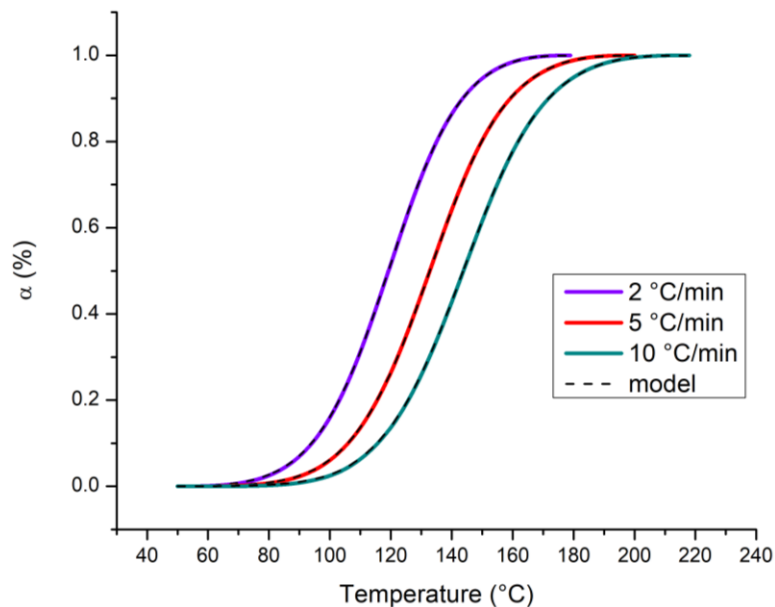


Figure 2.7 Conversion vs. temperature for various heating rates as well as the model predicted by the software for uncatalyzed DAHP-BPA/TPDPE.

As stated, initially four sets of DSC data were used to determine A' and E_a via FWO analyses: data for two crosslinkers, each with and without catalyst. The E_a as a function of conversion (10% to 90%) is shown in Figure 2.8. At very high and very low conversions, the model did not fit the data very well, and these conversion ranges were omitted from Figure 2.8, as they were not important to this study. For the uncatalyzed systems (solid curves), E_a was nearly independent of conversion and possessed nearly the same value for the two curing agents, in the range of 80 to 85 kJ/mol. Constancy of E_a with conversion suggests no change in mechanism with conversion, which is consistent for systems in which only the thermal (uncatalyzed) reaction is possible. The similar E_a 's

of the two crosslinkers reflect their very similar structures; they vary only by a central linkage between two phenyl rings that are located 7 atoms away from the alkyne moieties participating in the reaction, and that central linkage is not conjugated to the alkynes. The presence of copper catalyst resulted in higher energy of activation for both TPDPE and TPMDA, and both reached maximum E_a at 60-70% conversion before rapidly decreasing. Rapid decrease in E_a at high conversion suggests the possibility of an auto-catalytic mechanism; however, this is inconsistent with a report by Kessler *et al.*⁴⁹ who showed that the bulk CuAAC mechanism followed nth order reaction kinetics. The fact that adding $\text{CuCl}_2[\text{PMDETA}]$ increases activation energy suggests that the unknown reduction pathway from Cu(II) to Cu(I) is the reaction whose E_a is actually being measuring. This interpretation is consistent with the study by Gorman.⁵⁹ As an additional experiment, stannous octanoate was included in a reaction formulation containing DAHP-BPA, TPDPE, and $\text{CuCl}_2[\text{PMDETA}]$ to purposefully reduce the Cu(II) to Cu(I). Interestingly, the addition of stannous octanoate greatly changed the energetics of the reaction as can be seen by the green dash-dot line. At low conversion, the E_a was approximately the same as for all TPDPE formulations but as cure progressed, a steep decline in E_a was observed, indicating the presence of an auto-catalytic mechanism, which again is contradictory to what Kessler *et al.*⁴⁹ reported. These great differences in activation energy strongly suggest that different reaction mechanisms occur for neat azide-alkyne cycloaddition, azide-alkyne with Cu(II), and finally azide-alkyne in the presence of Cu(II) and a reducing agent.

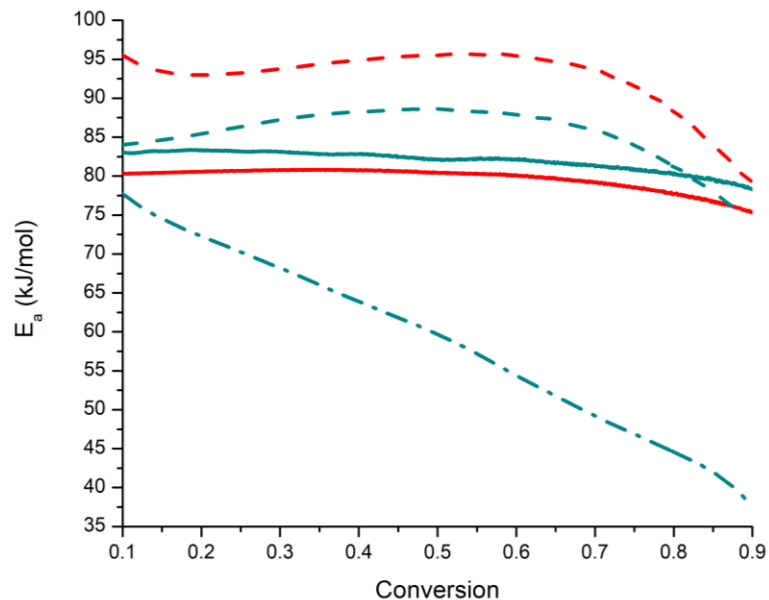


Figure 2.8 Activation Energy (E_a) as a function of conversion for DAHP-BPA cured with neat TPDPE (green solid), TPDPE with $\text{CuCl}_2[\text{PMDETA}]$ (green dash), TPDPE with $\text{CuCl}_2[\text{PMDETA}]$ and reducing agent (green dot dash), neat TPMDA (red solid), TPMDA with $\text{CuCl}_2[\text{PMDETA}]$ (red dash).

The observed higher activation energies for the $\text{CuCl}_2[\text{PMDETA}]$ -catalyzed systems in Figure 2.7 initially appear to contradict the observation that this catalyst greatly increases the rate of cure for the bulk azide-alkyne mechanism. This paradox can be resolved by observing the Arrhenius pre-exponential factor as a function of conversion, which can be seen in Figure 2.9. When Cu(II) was added to the system, the pre-exponential factor increased by over an order of magnitude for TPDPE and by over three orders of magnitude for TPMDA. These large increases in the pre-exponential factor explain the increased rate observed in the system only containing Cu(II).

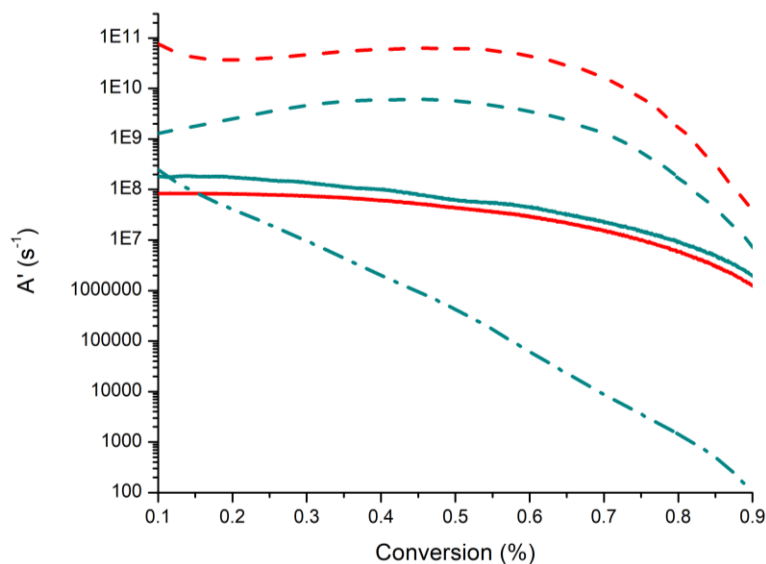


Figure 2.9 Arrhenius Pre-factor as a function of conversion for DAHP-BPA cured with neat TPDPE (green solid), TPDPE with CuCl₂[PMDETA] (green dash), TPDPE with CuCl₂[PMDETA] and reducing agent (green dot dash), neat TPMDA (red solid), TPMDA with CuCl₂[PMDETA] (red dash).

Although our hypothesis that E_a would be lower for the catalyzed system and slowly increase to become equivalent to the uncatalyzed system was incorrect, the data may actually be suggesting a more interesting possibility. More studies need to be performed to confirm mechanistically what is happening but it appears that three different mechanisms are possible, depending on formulation: 1) an uncatalyzed, thermal process 2) a Cu(I)-catalyzed process, in which Cu(I) is generated from Cu(II) by a reducing agent and 3) a Cu(I)-catalyzed process, in which Cu(I) is being generated in situ from an unknown mechanism.

2.3.3 Rheological Measurements

Ultimately, our goal was to understand how the relative abundance of 1,4- and 1,5-triazole regioisomers affects the bulk thermal and mechanical properties of the cured matrices. While the RT-FTIR and DSC experiments are valid and important in

understanding reaction kinetics and mechanism, they are conducted at extremely small scale and may not accurately predict system behavior at larger scales, especially when considering the propensity toward auto-acceleration in these systems. Isothermal rheology was therefore used to determine the gel point of the catalyzed and uncatalyzed species at 1 mm thickness, which was similar to the desired thickness of DMA bars. Figure 2.10 displays the rheological cure profile of DAHP-BPA cured with TPDPE, in the presence (Figure 2.10 right) and absence (Figure 2.10 left) of 0.2 mol% $\text{CuCl}_2[\text{PMDETA}]$; the respective gel points are listed in Table 2.2. The ability of $\text{CuCl}_2[\text{PMDETA}]$ to catalyze the system was once again confirmed. In the uncatalyzed TPDPE system, the gel point did not occur until approximately 5.5 h, but upon addition of the catalyst, the gel point occurred within 2 h.

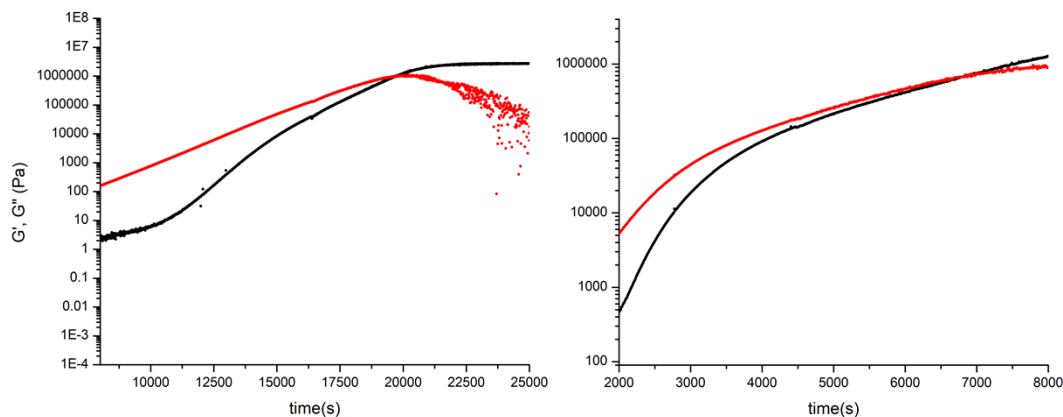


Figure 2.10 Rheological cure progression of DAHP-BPA and TPDPE performed isothermally at 70 °C (uncatalyzed – left; catalyzed – right).

Figure 2.11 compares the catalyzed and uncatalyzed DAHP-BPA cured with TPMDA. Again, the addition of $\text{CuCl}_2[\text{PMDETA}]$ greatly reduced the time to gelation. For the uncatalyzed system cured with TPMDA gelation occurred at about 7.5 h, which was 2 h longer than for uncatalyzed TPDPE. However, adding the catalyst caused the

gelation to occur in just under 2 h which was very similar to the catalyzed TPDPE system. The difference in gel times for the uncatalyzed systems was noteworthy and attributed to the difference in structure between the two crosslinkers. TPDPE is a liquid at room temperature; whereas TPMDA is crystalline (*vide supra*). At 70 °C, both crosslinkers are liquid; therefore the difference in physical state should not matter. However, TPDPE has the central ether linkage which could be treated as a hydrogen bonding acceptor for the secondary alcohol present in DAHP-BPA offering better miscibility, which in turn would lead to a quicker time to gelation.

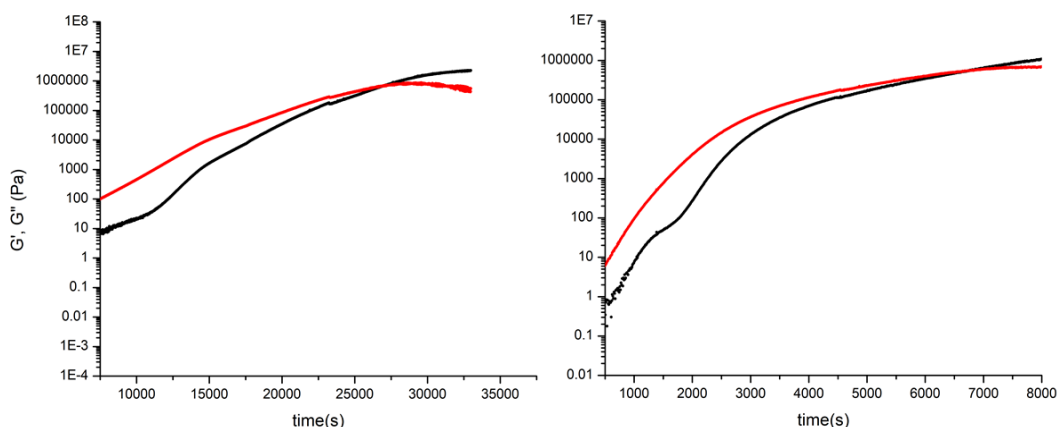


Figure 2.11 Rheological cure progression of DAHP-BPA and TPMDA performed isothermally at 70 °C (uncatalyzed – left; catalyzed – right).

Table 2.2 Gel Points Achieved by DAHP-BPA and Tetrafunctional Aromatic Alkynes with and without Catalyst

Crosslinker	Gel Point (min)
TPDPE	326.83
TPDPE – CuCl ₂ [PMDETA]	113.23
TPMDA	448.33
TPMDA – CuCl ₂ [PMDETA]	110.35

Ultimately, the gelation data were conclusive in determining that CuCl₂[PMDETA] is an effective catalyst for curing DAHP-BPA with the aromatic crosslinkers. This raises the question of whether CuCl₂[PMDETA] catalyzes the reaction

or whether *in situ* reduction to Cu(I) occurs. A possible reduction mechanism is Glaser coupling, or more specifically the Eglinton reaction, which is a modification of Glaser coupling that involves Cu(II) rather than Cu(I).⁶⁰ The Eglinton reaction mechanism directly couples two terminal alkynes by a cupric salt. There have been reports of cupric salts such as Cu(OAc)₂ that are capable of undergoing this mechanism to produce a catalytically active Cu(I) species.⁶¹

2.3.4 Dynamic Mechanical Analyses

It is well known that the Cu(I)-catalyzed process increases the relative abundance of the 1,4-regioisomer compared to the thermal process.¹ A major hypothesis of this research is that the regularity afforded to the crosslinked network by inclusion of exclusively 1,4-triazole linkages will lead to measurable increases in bulk mechanical properties such as compression moduli and thermal properties such as T_g. The effect of the relative abundance of regioisomers was probed using dynamic mechanical analysis, specifically by monitoring α -, β -, and γ -relaxations.

Analysis of these relaxations provides insight into the mechanisms for deformation of the matrix. Since these relaxations are both frequency and temperature dependent and follow an Arrhenius-type relationship, Equation 2.1 can be used to determine the E_a.⁶² In this equation, f is the frequency used for a given temperature sweep (either 0.1, 1, 10, or 100 Hz); f₀ is the reference frequency of 1 Hz; T is the temperature at peak maximum for the relaxation under consideration (α -, β -, or γ -relaxation) at the frequency f; T₀ is the temperature at peak maximum for the relaxation under consideration at the reference frequency f₀, and R is the universal gas constant.

$$\ln \frac{f}{f_0} = -\frac{E_a}{R} \left[\frac{1}{T} - \frac{1}{T_0} \right] \quad (2.1)$$

The results of this analysis are tabulated in Table 2.3. In epoxy-amine networks, the γ -relaxation is associated with motions requiring the least amount of energy, such as crankshaft motions⁶² or motions associated to methylene units.⁵⁰ To our knowledge, assignments have not been made for specific relaxations in azide-alkyne networks. However, these networks were designed from epoxy-amine starting materials and do share similar structural features such as methylene linkages and ether bonds, capable of crankshaft motions, and we thus tentatively attribute the γ -relaxation to the same phenomenon. As can be seen in Table 2.3, the E_a for the γ -relaxation was lowest across the board (12.7 kJ/mol to 15.6 kJ/mol) and showed very little dependence on either the central linkage or the presence or absence of catalyst. This further confirmed our hypothesis that the structures responsible for γ -relaxations in our systems are like those in epoxy-amine systems, because these linkages were left unchanged in our networks.

Table 2.3 Activation Energies of Thermal Transitions for Each System

Crosslinker	E_a γ -relaxation (kJ/mol)	E_a β -relaxation (kJ/mol)	E_a α -relaxation (kJ/mol)
TPDPE	12.7	40.0	124.9
TPDPE – CuCl ₂ [PMDETA]	15.6	62.1	112.1
TPMDA	15.3	---	169.4
TPMDA – CuCl ₂ [PMDETA]	13.7	18.8	134.1

The β -relaxation in epoxy-amine networks has been most commonly attributed to the hydroxy-propyl ether linkage.^{50,62} In addition, Starkweather⁶³ attributed β -relaxations in poly(vinylcarbazole) and other thermoplastic polymers to cooperative motions of larger molecular segments specifically containing ring structures and hydroxyl groups. Like traditional epoxy-amine systems, our system has the hydroxy propyl ether linkage.

In addition, the hydroxyl group can hydrogen bond to the triazole ring as shown from the dashed line in Figure 2.12.

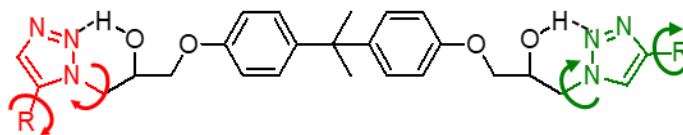


Figure 2.12 Generic structure of crosslinked matrix with both 1,4- and 1,5-regioisomer present. Green structures represent probable ring flips; whereas red structures represent unlikely ring flips. Dashed lines represent hydrogen bonding between triazole linkage and hydroxyl from hydroxy propyl ether linkage.

This theorized long range cooperative motion is further confirmed when comparing the E_a of the β -relaxation for catalyzed and uncatalyzed systems. For TPDPE, the activation energy increased approximately 20 kJ/mol when catalyst was used to cure the network; whereas with TPMDA the β -relaxation was not observed in most cases for the uncatalyzed system but became present when catalyst was added to the system, resulting in a larger presence of the 1,4-regioisomer.

The α -relaxation (T_g) is most typically associated with long-range segmental motions and is most affected by the rigidity of chains.⁵⁰ As shown in Figure 2.13, the copper-catalyzed systems exhibited a marked increase in T_g ; this was attributed to the regularity of the 1,4-regioisomer which would allow for better packing compared to a mixture of two different regioisomers. Another contribution that could effect this change is the conformation of the 1,4-regioisomer that allows for an easier mode of torsional strain release around the triazole linkage (see Figure 2.12).

Figure 2.13 shows plots of tan delta vs. temperature recorded at 1 Hz for TPDPE and TPMDA systems, with and without Cu(II). The T_g 's of the various systems, defined as the temperature of the peak maximum of each curve, are tabulated in Table 2.4. As

predicted, the T_g 's were slightly higher for the catalyzed systems. With TPDPE, T_g increased by 10 °C in the presence of catalyst, but with TPMDA the increase was approximately 20 °C. It is hypothesized that the greater increase of T_g for the latter system is due to increased exothermicity of that reaction. The $\tan \delta$ peak for catalyzed TPMDA system was broad and bimodal. This usually indicates a lack of heterogeneity in the matrix. This likely resulted from the fact that the melting point of this crosslinker is slightly above the initial curing temperature of 50°C used for the catalyzed systems. Bimodality for this system cannot be attributed to the involvement of sub- T_g relaxations, because those characteristic relaxations occur at much lower temperatures. The inset of Figure 2.13 reveals these relaxations to be located around -60 °C (γ) and 40 °C (β).

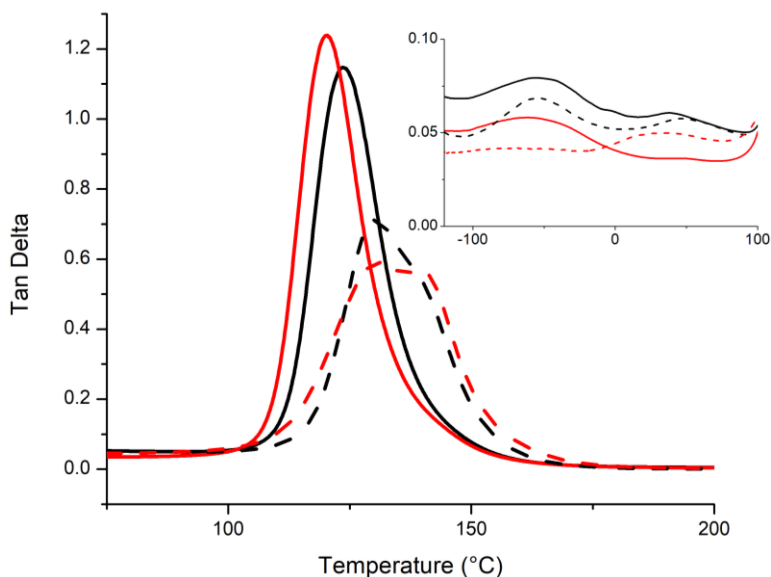


Figure 2.13 Tan delta vs. temperature curve recorded at 1 Hz of DAHP-BPA cured with neat TPDPE (black solid), catalyzed TPDPE (black dashed), neat TPMDA (red solid), and catalyzed TPMDA (red dashed). Inset shows sub- T_g relaxations.

The storage modulus was plotted versus temperature in Figure 2.14. At low temperature, the uncatalyzed systems displayed the higher storage moduli; whereas at

high temperature, the trend reversed, and the catalyzed systems had the higher storage modulus. The inset of Figure 2.14 shows the storage moduli in the rubbery region, and this was used to calculate the number-average molecular weight between cross-links (M_c) according to the theory of rubber elasticity (Equation 2.2).⁶⁴ In Equation 2.2, ν_e is the rubbery cross-link density; E' is the storage modulus measured at 40 °C above the T_g ; T is the absolute temperature at which the experimental modulus was determined, and R is the universal gas constant. Using ν_e , M_c was calculated using Equation 2.3, where ρ is the physical density of the network. The values for density, T_g , rubbery storage modulus, rubbery cross-link density, and number-average molecular weight between cross-links are found in Table 2.4 for all cured samples. All samples were expected to display approximately the same ν_e , E' , and M_c since a common resin was used and the molecular weights of TPMDA and TPDPE differ by only 2 g/mol. In general, this expectation was confirmed by the data. The uncatalyzed TPMDA system displayed a moderately higher M_c compared to the other networks, suggesting perhaps a slightly lower degree of cure for that system.

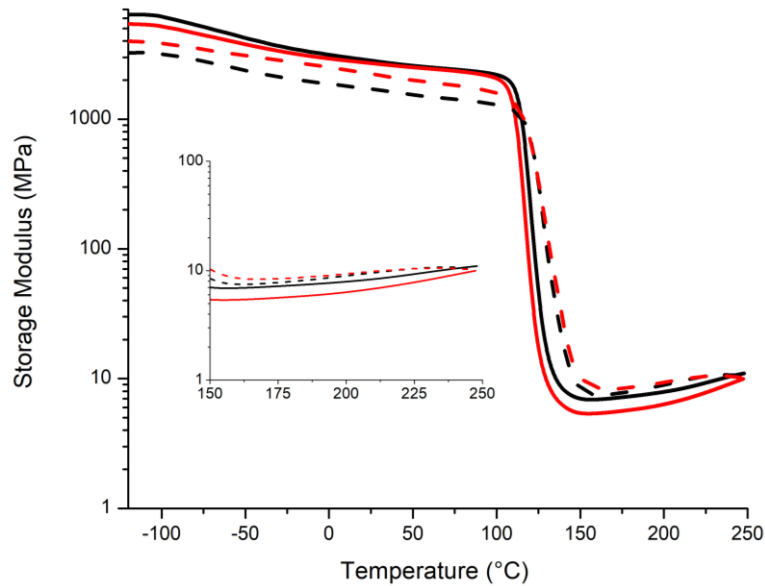


Figure 2.14 Storage modulus vs. temperature curve recorded at 1 Hz of DAHP-BPA cured with neat TPDPE (black solid), catalyzed TPDPE (black dashed), neat TPMDA (red solid), and catalyzed TPMDA (red dashed). Inset shows curved in rubbery region and was used to calculate v_e and M_c .

$$v_e = \frac{E_r}{3RT} \quad (2.2)$$

$$M_c = \frac{\rho}{v_e} \quad (2.3)$$

Table 2.4 Crosslink Density Calculations from Rubbery Storage Modulus Measured at 1 Hz

Crosslinker	ρ_{avg}^i (g/cm ³)	T_g (°C)	$E_r'_{T_g+40}$ (MPa)	v_e	M_c
TPDPE	1.23	123.4	7.0	2.1	585
TPDPE – CuCl ₂ [PMDETA]	1.21	133.1	7.6	2.1	576
TPMDA	1.20	120.3	5.4	1.6	750
TPMDA – CuCl ₂ [PMDETA]	1.05	139.7	8.5	2.3	457

ⁱ ρ_{avg} is the average density of three replicates of four specimens, as measured by Archimedes' principle.

2.3.5 Uniaxial Compression Testing

Figure 2.15 shows compressive stress-strain data the two systems under investigation, with and without Cu(II) catalyst. Three regions were identified in the

stress-strain curves of Figure 2.15: 1) reversible elastic deformation (Hookean region), which is characterized by a linear relationship between stress and strain and occurs at low strains; 2) yield stress which is the point where elastic deformation ends and irreversible plastic deformation begins (occurs between 6 and 12 % strain), and 3) plastic deformation, which is the irreversible deformation region after yield, where stress remains nearly constant with increasing strain.⁵⁰ The exception to this was catalyzed TPDPE which undergoes strain-induced strengthening. The stress-strain curves for the uncatalyzed systems were remarkably similar (Figure 2.15). The compressive moduli were very comparable (1913 MPa for TPDPE and 1615 MPa for TPMDA). In fact, the only noticeable difference between the materials was the yield onset. The difference in strain at yield for the uncatalyzed vs. the catalyzed system was statistically significant and believed to be related to the cooperative motions attributed to the β - relaxations, observed in TPDPE but not in TPMDA. Relative to catalyzed TPDPE, catalyzed TPMDA displayed a much lower Young's Modulus but a higher yield strain. This was attributed to the heterogeneous network that was first discussed with the bimodal $\tan \delta$ vs. temperature curves shown in Figure 2.13. A direct comparison between the catalyzed and uncatalyzed systems confirmed our original hypothesis that networks containing predominantly the 1,4-regioisomer would have a higher compressive modulus due to increased network packing; whereas having a mixture of both regioisomers results in compliant regions in the network that can absorb the mechanical stress exerted on the matrix, leading to a higher strain at yield (Table 2.5).

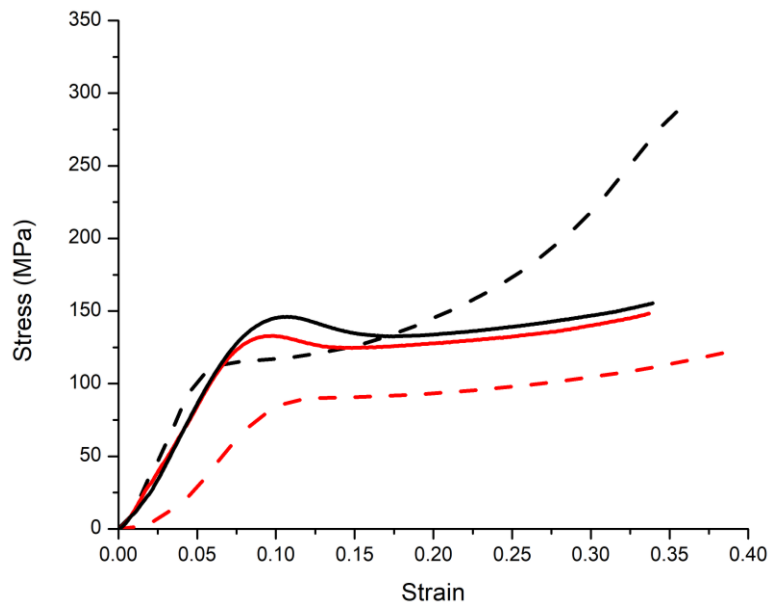


Figure 2.15 Compressive stress-strain data of the four matrices under investigation: neat TPDPE (black solid), catalyzed TPDPE (black dashed), neat TPMDA (red solid), and catalyzed TPMDA (red dashed).

Table 2.5 Uniaxial Compressive Data of all Crosslinkers Studied

Crosslinker	Strain at Yield (%)	Peak Stress (MPa)	Compressive Modulus (MPa)
TPDPE	11.13±0.38	154.5±2.7	1913.1±80.6
TPDPE – CuCl ₂ [PMDETA]	5.95±0.32	353.7±33.1	2336.8±78.5
TPMDA	9.99±0.52	130.7±7.4	1615.4±137.5
TPMDA – CuCl ₂ [PMDETA]	7.81±0.28	126.9±7.5	1366.6±90.7

2.3.6 Thermogravimetric Analyses

Thermal gravimetric analysis was performed on all networks, and the results are shown in Figure 2.16 and tabulated in Table 2.6. The T_{d5} and T_{d10} were high for all samples (> 300 °C), and the char for all samples was the same within experimental error. Two general trends were extracted from the data. The first was that the uncatalyzed systems tend to reach a higher temperature before degradation begins compared to the catalyzed systems, and the second was that the methylene linkage of TPMDA is slightly

more stable than the oxygen linkage of TPDPE. As reported by Xue *et al.*⁴⁵ the triazole system has one decomposition process when performed under nitrogen. Interestingly, these authors did not perform TGA on a catalyzed system, but in our studies they also seem to have one decomposition process. They reported, using pyrolysis/gas chromatography/mass spectrometry, that the earliest cleavages occurred between CH₂-N bonds, implying that they are the least thermally stable, with further degradations following rapidly thereafter. There is little difference in the CH₂-N bond between the 1,4- and the 1,5-regioisomer, and comparing crosslinking densities in Table 2.4 offers no obvious trend. We postulate two reasons for the higher thermal stability of the uncatalyzed networks. Either there is a slight difference in acidity in the single proton of the 1,4- vs. 1,5- triazole which could yield a more favorable degradation mechanism or the presence of copper simply catalyzes the degradation mechanism.

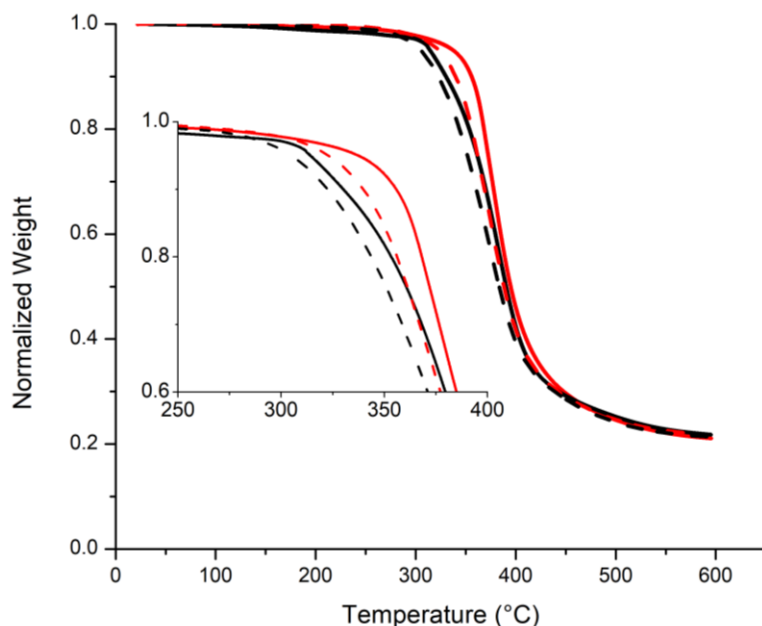


Figure 2.16 Thermal decomposition of all matrices cured with DAHP-BPA: neat TPDPE (black solid), catalyzed TPDPE (black dashed), neat TPMDA (red solid), and catalyzed TPMDA (red dashed). Inset shows the differences in degradation onset.

Table 2.6 Degradation Profile of All Matrices

Crosslinker	T _{d5%} (°C)	T _{d10%} (°C)	Char at 600 °C (%)
TPDPE	314.2±0.4	330.3±0.2	21.3±1.8
TPDPE – CuCl ₂ [PMDETA]	306.3±2.2	323.5±2.8	21.3±0.7
TPMDA	337.3±0.3	355.7±0.2	20.9±0.2
TPMDA – CuCl ₂ [PMDETA]	313.5±10.7	331.1±9.5	22.9±1.2

2.4 Conclusions and Future Work

In this chapter, we demonstrated the synthesis, formulation, and curing of high- T_g glassy azide-alkyne networks. The azidated resin was previously developed in the Storey research group by Gorman *et al.*² The aromatic tetrafunctional crosslinkers were propargylated from commercially available amines using propargyl bromide and K_2CO_3 . By varying the central linkage, many differences could be seen between crosslinkers such as physical state and cure onset. TPDPE and TPMDA were highly soluble in the DAHP-BPA resin at 70 °C; whereas TP44DDS was not. This created difficulty in preparing homogeneous networks from TP44DDS. Light microscopy was used to search for a curing temperature profile that could be used to create homogeneous DAHP-BPA/TP44DDS mixtures prior to gelation, but this effort was unsuccessful. To further understand the curing of these networks, both neat matrices and matrices containing 0.2 mol% $CuCl_2$ PMDETA (relative to azide functionality) were cured using multiple DSC heating rates (2, 5, and 10 °C/min) and analyzed using the FWO method. Surprisingly, the E_a increased with addition of $CuCl_2$ [PMDETA]. This was attributed to the catalytic curing being a compound process. Presumably the reduction of Cu(II) to Cu(I) has a high activation energy that increases the overall E_a of the reaction. Along with the increase in E_a , the Arrhenius pre-factor also increased. This increase in the pre-factor was used to

explain the increase in rate as determined by RT-FTIR spectroscopy and isothermal rheology as determined by gel point.

Sub- T_g relaxations (γ and β) as well as T_g were measured at four different frequencies, and E_a was determined using a method defined by Cukierman *et al.*⁶² Neither the central linkage nor the regioisomers seemed to have any effect on γ -relaxation. A relationship was observed between the intensity of the β -relaxation and an increase in the relative abundance of the 1,4-regioisomer caused by the presence of Cu-catalyst. This trend was most obvious with the TPMDA crosslinker, which had no observable β -relaxation when cured thermally but did show the relaxation when cured with copper. In addition, storage modulus was measured, and the theory of rubber elasticity was used to calculate molecular weight between crosslinks, which was similar in all cases except TPMDA. This was attributed to a slightly lower degree of cure. Uniaxial compression data were obtained on all cured specimens. Generally, the uncatalyzed systems behaved similarly, with exception of the yield stress. TPDPE displayed a higher yield stress, and we believe that the β -relaxations detected in TPDPE provide an alternative pathway to relieve strain as the network approaches the yield point. In addition, the copper-catalyzed TPDE system displayed a much higher compressive modulus compared to the uncatalyzed system. This supported our hypothesis that network regularity, afforded by increased packing efficiency of the single regioisomer, yields higher modulus. This trend was not seen when comparing catalyzed and uncatalyzed TPMDA, likely due to network heterogeneity of the catalyzed TPMDA, which was noticed in the $\tan\delta$ vs. temperature curve. Finally, TGA was performed on all samples and a single degradation pathway was observed, similarly to Xue *et al.*⁴⁵ In

addition, the uncatalyzed systems were more thermally stable than the catalyzed systems, and the methylene linkage was more thermally stable than the ether linkage.

Future work should include optimization of the cure profile for each crosslinker. It has been shown by increasing the curing temperature a higher T_g can be achieved. In addition, PALS and PVT studies would be ideal in order to understand the role free-volume plays in these crosslinked systems.

CHAPTER III – NON-ISOCYANATE CURED POLYURETHANES VIA AZIDE- ALKYNE CYCLOADDITION

3.1 Introduction

The desirable properties of polyurethanes are an inherent result of the unique primary and secondary structure of the urethane linkage. The linkage itself is naturally resistant to chemicals such as acids, bases, and solvents, and its capacity to serve as both a hydrogen bond donor and acceptor promotes organization of the polyurethane chains into microdomains that increase the bulk properties of the material.¹⁹ The desirability of the urethane linkage, combined with the health concerns associated with isocyanates, has generated an interest in non-isocyanate polyurethanes (NIPU), defined herein as a polyurethane produced without the presence of free isocyanate groups in the final curing step. Thus, NIPUs possess urethane linkages, but workers such as painters are not at risk of exposure to free isocyanate groups. One method to produce a NIPU is to incorporate functional groups for an alternative curing mechanism into the polymer via urethane linkages. An example is the capping of isocyanate-terminated oligomers with 2-hydroxyethyl acrylate or 2-hydroxyethyl methacrylate. The result is consumption of free isocyanates and creation of urethane linkages, with their attendant desirable properties, and at the same time, providing an alternative curing pathway, in this case UV-induced radical chain polymerization of acrylate groups.^{14,22–24}

Copper(I)-catalyzed azide-alkyne cycloaddition (CuAAC), a so-called “click” reaction, is an attractive alternative to acrylate functionalities, as a wide range of reactivity can be achieved by specifying the concentration of copper(I) catalyst, as shown in this chapter, or by altering the electron density of the alkyne through conjugation with

an electron-withdrawing group (Chapter IV). The product of CuAAC is the chemically stable 1,2,3-triazole ring. The concept of “click chemistry” was introduced by Kolb, Finn, and Sharpless¹ in 2001, as a foundational approach toward joining molecules. They recognized a small set of chemical reactions, described as “click” reactions, which are particularly useful in this regard and share certain characteristics. These reactions are modular, wide in scope, stereospecific, and high yielding, proceed under simple reaction conditions, exhibit insensitivity to oxygen and water, and generate only inoffensive byproducts that are easily removed. Click reactions achieve these required characteristics in part by possessing a high thermodynamic driving force, usually greater than 20 kcal/mol.¹

The Raju research group has recently extended the concept of organic coatings containing triazole moieties via azide-alkyne cycloaddition and published a review on the role of triazole rings in functional coatings.⁶⁶ First, Kantheti *et al.*⁶⁷ reported two novel, triazole-containing polyols that were reacted with 4,4' dicyclohexyl methane diisocyanate to produce triazole-containing polyether-based polyurethane coatings with good thermal, mechanical, and anti-corrosion properties. Kantheti and coworkers⁶⁸ then synthesized triazole-rich hyperbranched polyether polyols, which again had improved anti-corrosive and antimicrobial properties. However, in all of these instances free isocyanates were still used in the final curing step. Although the Raju research group have pioneered the incorporation of triazoles into functional coatings, their interests largely lie in properties inherent to triazole moieties. In many cases their resins still contain free isocyanates that are consumed in the final curing step.^{67,69} Irani *et al.*⁷⁰ demonstrated the utility of incorporating triazoles into epoxidized soybean oil as a potential biocide but again

utilized free isocyanate groups in the final curing step. Nair and coworkers⁷¹ did in fact demonstrate a NIPU method via azide-alkyne cycloaddition by reacting hydroxyl-terminated polybutadiene (HTPB) with excess toluene diisocyanate to produce isocyanate-terminated HTPB. This was subsequently reacted with propargyl alcohol, which produced the desired urethane functionality while allowing free alkynes to react in the final cure with azide-terminated HTPB. In doing so, they were able to demonstrate triazole-triazoline networks with superior mechanical properties and a longer pot-life. However, the application for this research was propellant binders and they did not study this system as a coating. An invention disclosed by Carter *et al.*⁷² again synthesized NIPUs via azide-alkyne cycloaddition by, for example, reacting propargyl alcohol with methylene diphenyl diisocyanate to achieve the desired urethane linkage with alkyne functionality and Grilonit F704 with sodium azide to give the azidated polyol. However, the focus of this invention was solely on synthesis of small molecules, and the inventors did not adequately address many considerations such as kinetics of cure or effect of catalyst on coating properties and color.

We have been interested in polytriazole linear systems⁷ and networks² as next-generation composite matrices for a number of years. One important finding was that the bulk azide-alkyne cycloaddition is extremely exothermic, and in order to limit autoacceleration (gel effect), a high surface area-to-volume ratio must be maintained.⁵ This process requirement naturally led to the adaptation of these systems to polymeric coatings, which have a much more favorable ratio than thick composite matrices. The goal of this chapter was to develop NIPU coatings that cure by azide-alkyne cycloaddition. This was achieved by converting the isocyanate and alcohol groups of

commercially available polyisocyanates and polyols to propargyl and azide functionalities, respectively. This chapter will discuss the synthetic strategies used to achieve these functionalities as well as the catalytic and non-catalytic curing of the new functionalities and will conclude by comparing coating properties of the azido-alkyne cured systems to the unmodified polyurethane coatings. *It is hypothesized that converting isocyanate and alcohol functionalities to alkyne and azide will cause only minor difference in final coating properties, but will, in the absence of catalysis, reduce curing kinetics.*

3.2 Experimental

3.2.1 Materials

PPG 1000 (113.2 mg KOH/g), Desmophen 650A (179 mg KOH/g), Setalux DA 870 (2.94 % hydroxyl), Desmodur 3200 (22.9% isocyanate), Desmodur 3300 (21.8 % isocyanate), and Desmodur XP2580 (19.3% isocyanate) were generously donated by Covestro. Methanesulfonyl chloride (Mes-Cl) ($\geq 99.7\%$), triethylamine (TEA) ($\geq 99.5\%$), sodium azide (ReagentPlus[®], $\geq 99.5\%$), N,N,N',N'',N''-pentamethyl-diethylenetriamine (99%), copper(II) chloride (97%), and tin(II) 2-ethylhexanoate ($\sim 95\%$) were purchased and used as received from Sigma-Aldrich. Diethyl ether (DEE) (Spectranalyzed[®]), molecular sieves (Type 4A, Grade 514, 8-12 Mesh beads, 4 Å pore size), and dichloromethane were purchased and used as received from Fisher Chemical. Propargyl alcohol (99%) was purchased from Fisher Chemical and dried further using molecular sieves. *n*-Butyl acetate (ACS reagent, $\geq 99.5\%$) was purchased from Sigma-Aldrich and further dried using molecular sieves. Dibutyltin dilaurate (98%) was purchased from

Strem Chemicals and used as received. Dupont Metal Conditioner 5717S was purchased from Ryan Automotive Supply, 1009 W. Scooba St. Hattiesburg, MS.

3.2.2 Instrumentation

Proton nuclear magnetic resonance (^1H NMR) spectra were obtained using a 600.13 MHz Varian Mercury^{plus} NMR (VNMR 6.1C) spectrometer. Typical acquisition parameters were 10 s recycle delay, 7.8 μs pulse corresponding to a 45° flip angle, and an acquisition time of 1.998 s. The number of scans acquired for each sample was 32. All ^1H chemical shifts were referenced to TMS (0 ppm). Sample solutions were prepared at a concentration of approximately 2.5% (w/v) in CDCl_3 containing 1% TMS as an internal reference, and the resulting solution was charged to a 5 mm NMR tube. Carbon nuclear magnetic resonance (^{13}C NMR) spectra were obtained using a 150.90 MHz Varian Mercuryplus NMR (VNMR 6.1C) spectrometer. Typical acquisition parameters were 1 sec recycle delay, 11 ms pulse corresponding to a 45° flip angle, and an acquisition time of 0.908 s. The number of scans acquired for each sample was 1024. All ^{13}C chemical shifts were referenced to residual chloroform (77.16 ppm). Sample solutions were prepared at a concentration of approximately 5 wt% in CDCl_3 containing 1% TMS as an internal reference, and the resulting solution was charged to a 5 mm NMR tube. The FTIR studies were conducted using a Nicolet 8700 spectrometer with a KBr beam splitter and a DTGS detector. Samples were sandwiched between two NaCl salt plates (approximate thickness: 5 mm). Flash chromatography was performed on a Teledyne Isco CombiFlash Purification System using RediSep Rf prepacked columns.

Matrix-assisted laser desorption ionization time of flight mass spectrometry (MALDI-TOF) was performed using a Bruker Microflex LRF MALDI-TOF mass

spectrometer equipped with a nitrogen laser (337 nm) possessing a 60 Hz repetition rate and a 50 mJ energy output. Samples of polyol were prepared using the dried-droplet method with trans-2-[3-(4-*tert*-Butylphenyl)-2-methyl-2-propenylidene]malononitrile (DCTB) as the matrix and sodium trifluoroacetate (NaTFA) as the cationizing agent. A representative procedure was as follows: a 20 mg/mL DCTB solution, a 10 mg/mL sample solution, and a 10 mg/mL NaTFA solution, all in THF, were prepared separately and then mixed in a volumetric ratio of matrix/sample/NaTFA of 2:1:0.1. Then, a 0.5 μ L aliquot was applied to a MALDI-TOF sample target for analysis. All spectra were obtained in the positive ion mode utilizing the reflector mode micro-channel plate detector and the sum of 900 – 1000 shots.

Isothermal real-time Fourier transform infrared spectroscopy (RT-FTIR) was measured using a Thermo Fisher Scientific Nicolet 6700 FTIR equipped with a mid-IR beam splitter and integrated with a Simplex Scientific HT-32 heated transmission cell. The Simplex software was paired to the OMNIC FTIR software native to the Nicolet 6700. Approximately 1.5 g of sample was mixed at 1:1 stoichiometry for NCO:OH or 1.5:1 for azide:alkyne for 2 min. A small aliquot was taken from the mixture and compressed between two polished NaCl plates. The plates were then inserted in the transmission cell and subsequently placed in the chamber for FTIR analysis. The sample chamber was purged with N₂ for approximately 10 min to reduce the intensity of the CO₂ peak that could overlap with the isocyanate peak. The sample was rapidly heated from room temperature to 80 °C and spectra were immediately obtained in 1 min intervals (32 scans; 4 cm⁻¹ resolution) for the duration of the run (90 min). Conversion was monitored as either the disappearance of the isocyanate stretching peak (most typically around 2271

cm⁻¹) or disappearance of the peak attributed to both azide (N=N=N stretching) and alkyne (C≡C stretching) at approximately 2100 cm⁻¹. Aliphatic C-H stretching (2755 cm⁻¹) was used as an internal standard. Baselines were taken above a two-point baseline, of the absorbance centered at 2271 cm⁻¹, associated with the NCO stretching or the absorbance centered at 2100 cm⁻¹, associated with the azide and alkyne stretches.

3.2.3 Preparation of Polyazides

Polyazides were prepared in two steps. First, the starting polyol was mesylated; then, the crude mesylated intermediate was reacted with sodium azide. The synthetic procedure was the same for each polyol except for final product isolation. The azidized polyether was isolated using diethyl ether (DEE) as the extracting solvent; whereas the azidized polyester and acrylic polymers were isolated using DCM as the extracting solvent.

Mesylation of PPG 1000, which is representative, was as follows: A 250 mL three-neck, round-bottom flask, a 125 mL pressure-equalizing addition funnel, and a mechanical stirrer were baked in an oven at 160 °C for approximately 2 h and then allowed to cool to room temperature under vacuum. The flask was fitted with the mechanical stirrer, and PPG 1000 (9.934 g; hydroxyl value supplied by manufacturer = 113.2; 20.04 mmol OH) and THF (70 mL, previously dried over CaH₂) were added directly to the flask. The mixture was then stirred to dissolve the polyol. During dissolution, a solution of Mes-Cl (4.623 g; 40.35 mmol) and 50 mL of dry THF were charged to the addition funnel and purged with N₂. Upon complete dissolution of the polyol, TEA (6.143 g; 60.71 mmol) was added to the polyol solution. The addition funnel was attached to the flask, and the final port was closed with a rubber septum. The

Mes-Cl solution was added dropwise to the polyol solution, and the reaction progressed at 0 °C overnight. The reaction mixture containing the desired product, THF, and salts, was filtered to remove the salts and concentrated *in vacuo*. The concentrated polymer was redissolved in diethyl ether (50 mL x 3) and washed with water (70 mL x 3), chemically dried with MgSO₄ and concentrated *in vacuo*. This resulted in the desired mesylate polyol (yellow oil; yield: 70.7%).

Azidation of mesylated PPG1000 was as follows: A 250 mL round-bottom flask, equipped with a magnetic stirrer, reflux condenser, and inlet and outlet ports providing continuous N₂ purge, was charged with mesylated PPG 1000 (8.138 g; 16.4 mmol OMs) and 60 mL of DMF. Upon dissolution of the polymer, NaN₃ (1.326 g; 19.7 mmol) was charged to the flask, and the mixture was subsequently heated to 95 °C with continuous stirring and allowed to react overnight. Upon completion, the reaction mixture was cooled to room temperature, filtered to remove remaining salts, and transferred to a separatory funnel using three 20 mL DEE rinses. DI water (100 mL) was added to the separatory funnel to separate the DMF from the organic layer containing the product. Upon separation, the aqueous DMF solution was extracted with fresh DEE (50 mL x 3), and the extracts were combined with the organic layer. The combined organic layer was then washed with DI water (150 mL x 3), dried over MgSO₄, filtered, and finally concentrated *in vacuo* to yield the azidated polyol (light yellow oil; yield: 66.0%).

3.2.4 Preparation of Polypropargyl Carbamates

The propargylation of all polyisocyanates followed the same general procedure. As an example, the synthesis of propargylated Desmodur N3200 was as follows: All glassware was baked overnight in an oven at 160 °C and transferred hot into a N₂-

atmosphere glovebox (MBraun Labmaster 130). Into a 250 mL 3-neck, round-bottom flask, equipped with mechanical stirrer, pressure-equalizing addition funnel, and ATR-FTIR probe with resistance temperature detector (RTD) (ReactIR Reaction Analysis System, Mettler Toledo AutoChem, Inc., 7075 Samuel Morse Dr., Columbia, MD 21046), were charged 55.160 g of Desmodur N3200 (301 mmol isocyanate), 0.60 mL of dibutyltin dilaurate (1.0 mmol), and 16 g of butyl acetate. The reaction mixture was then cooled to 0 °C using a cryostated heptane bath. Propargyl alcohol (17.012 g; 303 mmol) was charged to the addition funnel and added to the stirred reaction at a sufficiently slow rate (approximately 1 drop/s) to ensure that the temperature did not exceed 40 °C. If the temperature began to approach 40 °C, the addition of propargyl alcohol was paused until the reaction cooled to ~20 °C or below, at which point dropwise addition was resumed. Urethane conversion was determined by monitoring the left half of the area (2390 – 2281 cm^{-1}), above a two-point baseline, of the absorbance centered at 2281 cm^{-1} , associated with the NCO stretching. Although the reaction was usually completed within 90 min (>99% conversion), it was allowed to mix overnight in the chilled bath to ensure homogeneity. At this point the reaction was allowed to warm to room temperature, and the product of the reaction was ready for immediate use.

3.2.5 Synthesis of $\text{CuCl}_2[\text{PMDETA}]$ complex

The preparation of $\text{CuCl}_2[\text{PMDETA}]$ followed a procedure reported by Song *et al.*⁴¹ To a 100 mL single neck, round-bottom flask, CuCl_2 (0.993 g; 7.39 mmol) and acetonitrile (7.5 mL) were charged. PMDETA ligand (1.283 g; 7.40 mmol) was added dropwise to the stirred solution. Upon the addition, the reaction turned from brown to

turquoise. After reacting at room temperature for 24 h, the acetonitrile was removed *in vacuo* resulting in a blue powder, CuCl₂[PMDETA].

3.2.6 Real-Time Cure Kinetics as a Function of Catalyst Concentration

To a 20 mL scintillation vial, azidated Setalux DA 870 (4.697 g), CuCl₂[PMDETA] (0.0927 g) and 5 mL of DCM were charged. The three were mixed thoroughly until complete dissolution, and the DCM was removed *in vacuo*. DCM removal was verified by ¹H NMR. The resulting 2% (wt/wt) stock solution was then used as a means of introducing controlled amounts of copper catalyst to samples of neat azidated Setalux DA 870, to yield a pre-catalyzed resin with a desired catalyst concentration. Pre-catalyzed, azidated Setalux DA 870 was then hand mixed with an appropriate amount of Desmodur XP2580-PC to yield a homogenous solution at 1.5:1 (mol:mol) azide:alkyne. As an example, the 1% (wt/wt) solution will be described. To a 20 mL scintillation vial, azidated Setalux DA 870/CuCl₂[PMDETA] (0.223 g; 0.451 mmol), neat azidated Setalux DA 870 (0.237 g; 0.487 mmol), and Desmodur XP2580-PC (0.174 g; 0.636 mmol) were charged and thoroughly mixed. Immediately prior to FTIR analysis, three drops of tin(II) 2-ethylhexanoate were added to the vial and thoroughly mixed. Isothermal runs were carried out at 80 °C for 90 min and conversion was monitored as the disappearance of the peak at approximately 2100 cm⁻¹ indicative of both azide and alkyne functionalities.

3.2.7 Preparation of Coated Substrates

Azidated Setalux DA 870 (4.145 g; 8.528 mmol azide) and Desmodur XP 2580-PC (1.582 g; 5.780 mmol propargyl) were hand mixed in a scintillation vial until smooth. The mixture was dilute with *n*-butylacetate (1.18 mL) then placed in a FlakTech mixer

and allowed to mix at 1800 rpm for approximately 20 min. The mixture was drawn down at 80% solids on QD steel or aluminum (3003 H14 aluminum) panels. The panels were most often treated with acetone rinsing to remove surface contaminants. In the study using metal conditioner to improve adhesion, the metal conditioner was diluted with an equal volume of DI water and the panels were soaked in this solution for approximately 20 min. Immediately prior to use, the conditioner was removed with DI water and finally cleaned with an acetone rinse. The solvent was allowed to flash at room temperature for 2 h, and then the coating was cured in a pre-heated oven set at 100 °C for 4 h.

3.2.8 Coatings Testing

Reaction conversion was qualitatively compared using methyl ethyl ketone (MEK) double rubs using cheesecloth and a 32 oz hammer according to ASTM D5402. Flexibility was determined using a conical mandrel according to ASTM D522. Adhesion was determined using the crosshatch adhesion test by using a 25-square grid cut by a razor and grading on a 0B-5B scale based on the percent coating remaining after having been taped and quickly removed at a 180° angle. Hardness was measured using a pencil hardness test in accordance with ASTM D3363. Using a BYK-Gardner glossmeter, the coatings were tested at 20°, 60°, and 85°. The color of the panels were determined using a BYK-Gardner colorimeter based on L*, a, b* values.

Differential scanning calorimetry (DSC) was performed using a TA Instruments Q200. For this purpose, coatings were prepared, mixed, and drawn down as described in *Preparation of Cured Substrates* except that the substrate was PE film. The coating, which had little adhesion to the film was peeled off and punched to give circular samples (d = 0.25 in) of the film. Stacks of five such samples (total ~5 mg) were placed in a

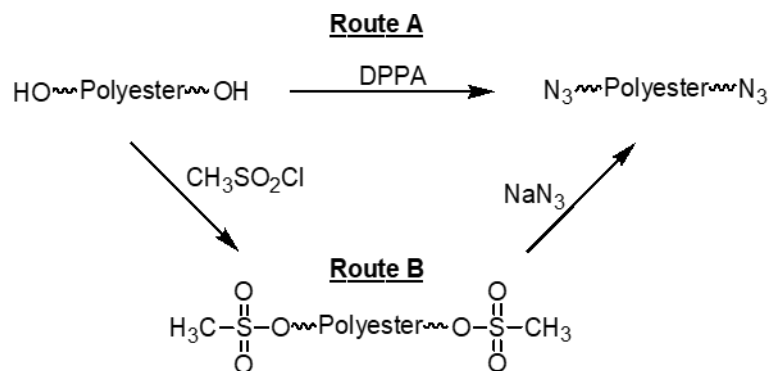
hermetically sealed pan. A heat/cool/heat cycle was performed on each stack starting at room temperature and ending at 100 °C at a rate of 10 °C/min. T_g of the cured material was determined from the second heating cycle, and TA Universal Analysis software was used to determine the midpoint of the T_g inflection as the reported value.

3.3 Results and Discussion

3.3.1 Polyazide Synthesis

Non-isocyanate polyurethane coatings were created by reaction of a propargylated polyurethane resin component with an azidated crosslinker component created from one of three different types of commercially available polyols: polyether, polyester, and polyacrylate. A major challenge was to develop an azidation process that would be commercially viable. PPG 1000 (polyether) is very nearly a linear, difunctional (telechelic) polymer; due to this well-defined nature, it proved to be an appropriate model for initial experiments. End-group modification experiments were monitored using MALDI-TOF, which is able to reveal subtle changes in the end-group of the polymer at a wide range of degrees of polymerization. A synthetic strategy using diphenyl phosphoryl azide (Scheme 3.1; Route A) to directly convert alcohol groups to azides was briefly explored but quickly abandoned due to the difficulty of removing the phosphonium salt by-product, low conversion, and high cost. Subsequently, a two-step process was adopted (Scheme 3.1; Route B) involving first, conversion of the alcohol (pKa of conjugate acid: ~15.7) to a better leaving group such as methane sulfonate (pKa of conjugate acid: -2.6), and second, addition of the desired azido functionality via nucleophilic substitution.

Scheme 3.1 Two synthetic strategies for achieving polyazide component. Route A: direct azidation using diphenyl phosphoryl azide (DPPA). Route B: two-step method involving 1) conversion of alcohol moieties to a mesylate leaving group, and 2) nucleophilic substitution using NaN₃.



Conversion of the hydroxyl group to a more suitable leaving group was first attempted using thionyl chloride (pKa of conjugate acid: -7). This route resulted in complete chlorination as indicated by MALDI-TOF (Figure 3.1 and Figure 3.2). The predicted residual mass for the chlorinated PPG 1000 was 309.15, which matched well with the experimental value of 309.87 Da (0.23% error), indicating conversion to the desired chlorinated end groups. However, the resulting polymer was undesirably dark (burnt orange), and the subsequent azidation proved to be difficult.

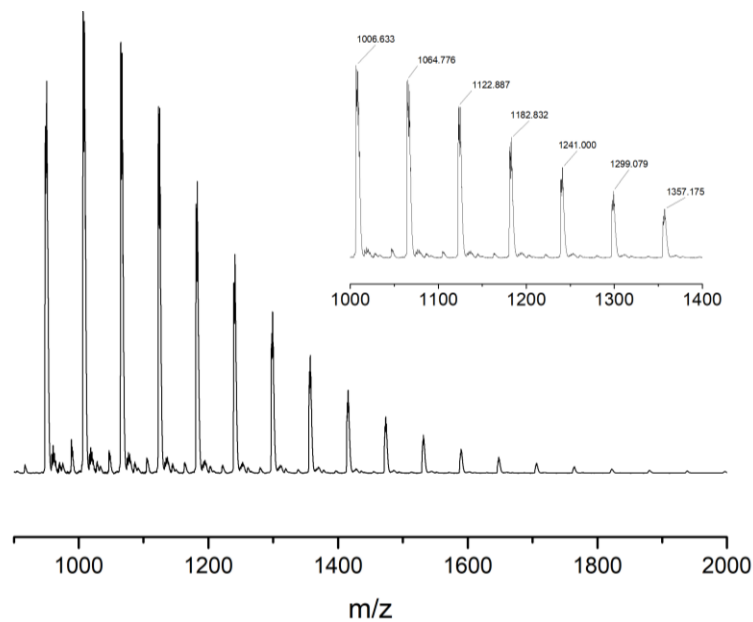


Figure 3.1 MALDI-TOF mass spectrum of chlorinated PPG 1000.

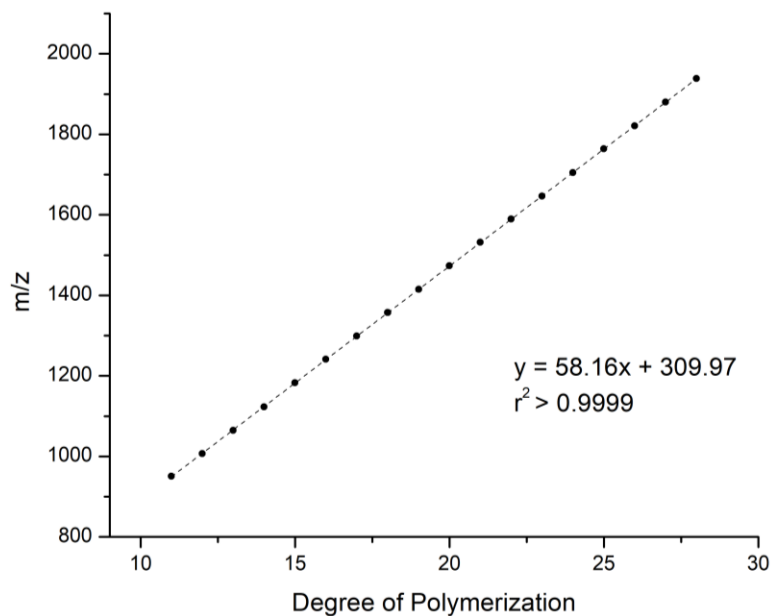


Figure 3.2 Linear regression of MALDI-TOF spectrum of chlorinated PPG 1000.

End-group modification with *p*-toluenesulfonyl chloride was then pursued. In initial trials, only moderate conversion at room temperature was achieved as indicated by three distributions in MALDI-TOF (Figure 3.3). In addition, column chromatography was required to remove residual *p*-toluenesulfonyl chloride. Comparing the resulting

residual masses from the linear regression of each distribution in Figure 3.3 (Figure 3.4) to the theoretical residual masses indicated that the three distributions corresponded to the unmodified, mono-tosylated and di-tosylated PPG 1000 (Table 3.1). Although it was believed that quantitative conversion could be achieved by increasing time and/or temperature, the purification requirement (column chromatography) was unattractive in terms of a commercial process, and therefore use of a different leaving group was explored.

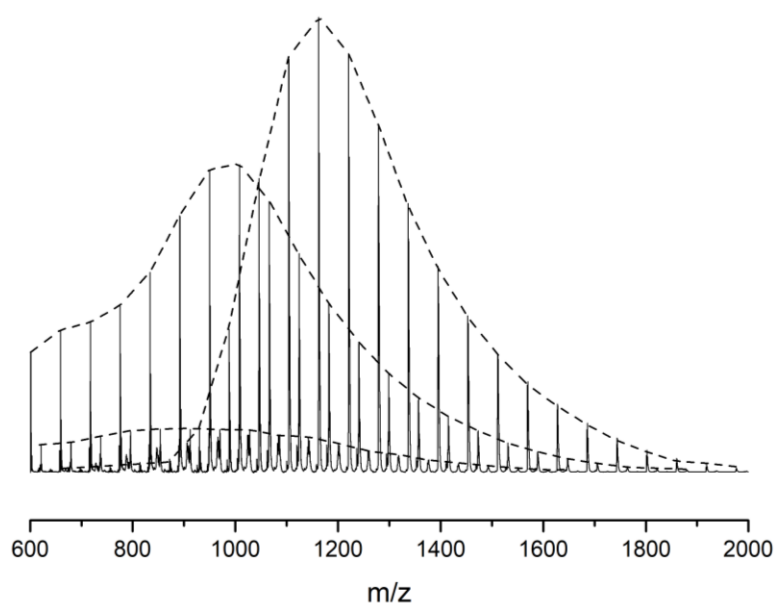


Figure 3.3 MALDI-TOF mass spectrum of partially tosylated PPG 1000 showing three sets of end group functionalities.

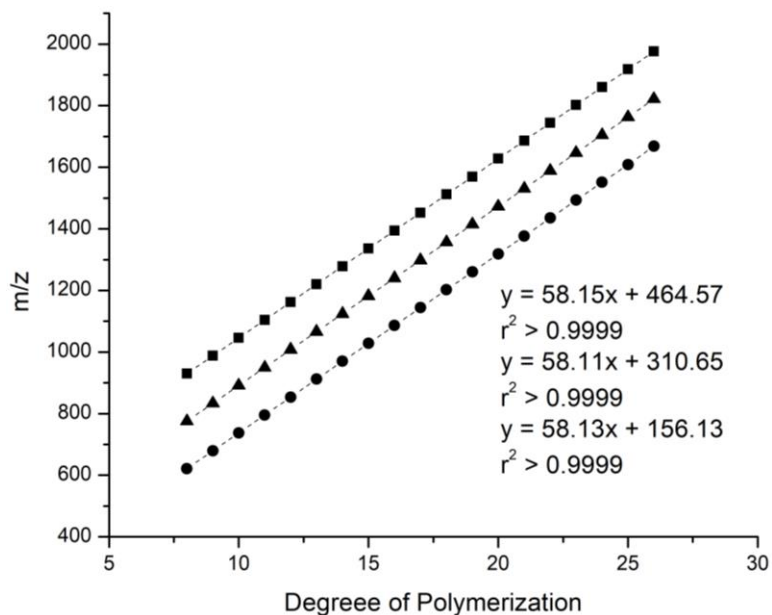


Figure 3.4 Linear regression of each MALDI-TOF spectrum of Figure 3: HO-PPG1000-OH (circle), TosO-PPG1000-OH (triangle), and TosO-PPG1000-OTos (square).

Table 3.1 Results from MALD-TOF of Partially Tosylated PPG 1000

Distribution		Experimental Mass (Da)	Theoretical Mass (Da)	%error ⁱ
HO-PPG1000-OH	Repeating Unit	58.13	58.09	0.07
	Residual Mass ⁱⁱ	156.13	157.08	0.61
HO-PPG1000-OTos	Repeating Unit	58.11	58.09	0.03
	Residual Mass ⁱⁱ	310.65	311.09	0.14
TosO-PPG1000-OTos	Repeating Unit	58.15	58.09	0.10
	Residual Mass ⁱⁱ	464.57	465.10	0.11

ⁱ calculated as the absolute value of the difference between experimental and theoretical values divided by the theoretical value

ⁱⁱ includes dipropylene glycol initiator and Na cationizing agent.

By using a chemical analogue of *p*-toluenesulfonyl chloride, methanesulfonyl chloride (a liquid), it was hypothesized that purification would no longer require chromatography and the reaction could be driven to completion. In addition, it is well-

known that purification using *p*-toluenesulfonyl chloride and quantitative conversion can be problematic.⁷³ This is usually overcome by using a slight excess of the tosyl chloride and purification with column chromatography or other purification methods. Whereas methanesulfonyl chloride and methanesulfonic acid can be quantitatively removed by washing with water. Upon using methanesulfonyl chloride complete conversion was achieved at room temperature, and complete azidation was easily achieved by reaction overnight at elevated temperatures (95 °C) in DMF. The MALDI-TOF spectra of PPG 1000, the methanesulfonyl intermediate, and the azidated product are shown in Figure 3.5. Mesylation of both terminal hydroxyl groups of PPG 1000 is predicted to increase the molecular weight of each homologue by 156 Da; exactly this shift was observed between the spectra of PPG 1000 and the methanesulfonyl intermediate. Replacement of CH₃SO₃ with N₃ at both termini is predicted to decrease the molecular weight of each homologue by 106 Da, and this also was observed. These shifts, along with the fact that the overall shape of the distribution as well as the distance between peaks remain unchanged in the three spectra, indicated selective end-group modification.

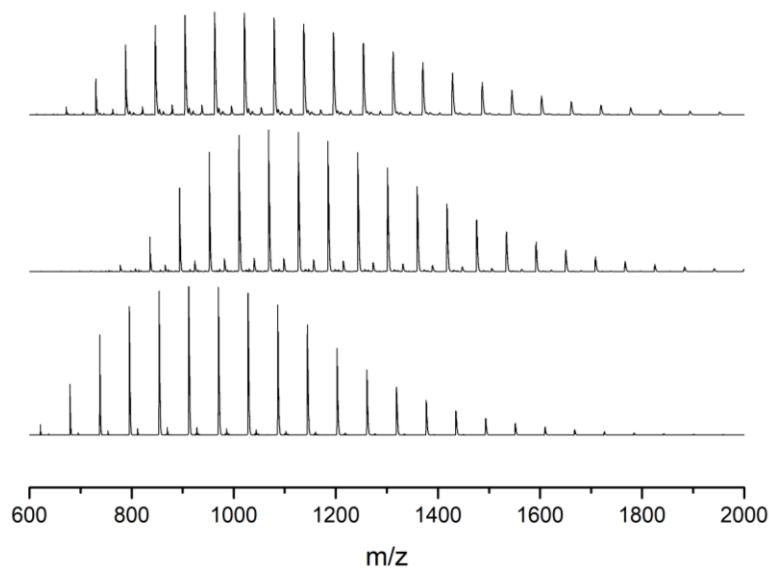


Figure 3.5 MALDI-TOF spectra of PPG 1000 (bottom), its methanesulfonyl intermediate (middle), and its final, azidated derivative (top).

Linear regression of a plot of m/z vs. degree of polymerization (Figure 3.6) quantified the change in end-group mass and confirmed that the mass of the repeating unit remains unchanged through the modifications. Table 3.2 compares the experimental masses as determined by the linear regression to the theoretical masses of the polymers. The values matched extremely well (all values had less than 0.5 % error) indicating that desired end-group modifications were achieved.

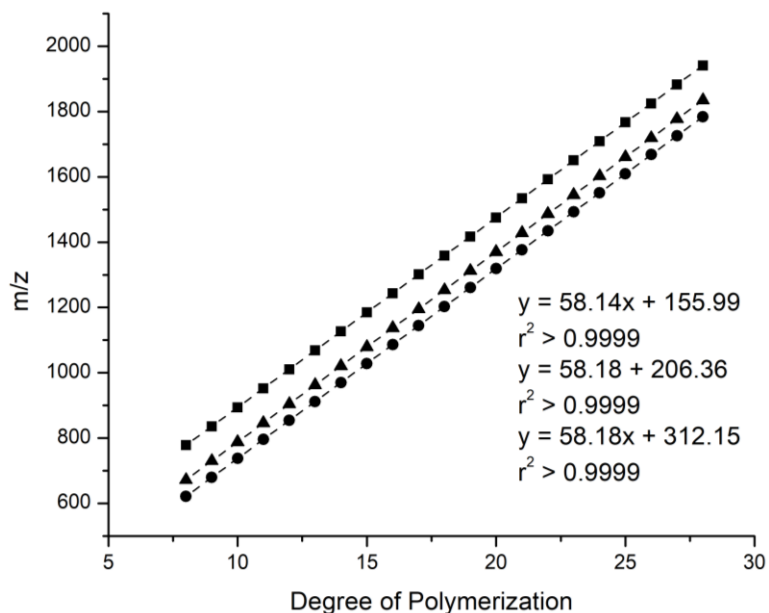


Figure 3.6 Linear Regression of MALDI-TOF spectra for neat (circle), mesylated (square) and azidated (triangle) PPG 1000.

Table 3.2 Results from MALD-TOF of End-Group Modified PPG 1000

Distribution		Experimental Mass (Da)	Theoretical Mass ⁱⁱ (Da)	%error ⁱ
HO-PPG1000-OH	Repeating Unit	58.14	58.09	0.09
	Residual Mass ⁱⁱ	155.99	157.08	0.70
MsO-PPG1000-OMs	Repeating Unit	58.18	58.09	0.15
	Residual Mass ⁱⁱ	312.15	313.04	0.28
N ₃ -PPG1000-N ₃	Repeating Unit	58.18	58.09	0.15
	Residual Mass ⁱⁱ	206.36	207.10	0.36

ⁱ calculated as the absolute value of the difference between experimental and theoretical values divided by the theoretical value

ⁱⁱ includes dipropylene glycol initiator and Na cationizing agent

Once complete mesylation and azidation were achieved and confirmed by MALDI-TOF, simpler and more robust methods were sought to monitor reaction progress. As an alternative method, ¹³C NMR spectroscopy was used to confirm the end

group modification. Upon mesylation of PPG 1000, two peaks indicative of the carbon atoms adjacent to the terminal hydroxyl groups, located at 65.35 and 67.08 ppm, shifted upfield to become a single peak at 38.39 ppm, and upon azidation the latter peak shifted downfield to 57.08 ppm (Figure 3.7). The observation of two end-group peaks in the received polyol has been tentatively attributed to hydrogen-bonded and non-hydrogen-bonded species that occur in the unmodified polyols but which become identical upon end-group modification.

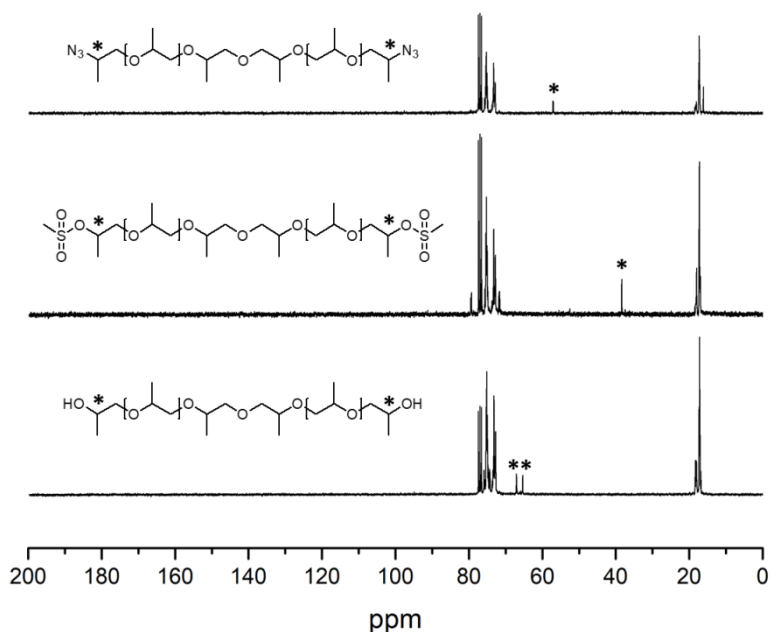


Figure 3.7 ^{13}C NMR spectrum (150 MHz, CDCl_3 , 23 °C) of PPG 1000 (bottom), its methanesulfonyl intermediate (middle), and its final, azidated derivative (top).

The two-step synthetic strategy (Scheme 3.1; Route B) was also applied to the polyester polyol by again converting alcohol moieties to methanesulfonates and subsequently replacing the methanesulfonates with azide functionalities using $\text{S}_{\text{N}}2$ reaction conditions. MALDI-TOF was again chosen to characterize the neat and mesylated polyester (Figure 3.8). The spectrum shows two distributions. One is of

higher intensity, with the most intense peak located at 607.607 m/z and subsequent peaks gradually decreasing in intensity (major distribution); while the other distribution has a relatively lower intensity with the most intense peak occurring at 900.017 m/z (minor distribution). As expected, the peaks for the major and minor distributions shifted to higher molecular weight upon mesylation. However, the spacing between the major and minor distributions was reduced upon mesylation (~134 Da before mesylation and ~26 Da after mesylation), indicating that mesylation also occurred on the repeating unit.

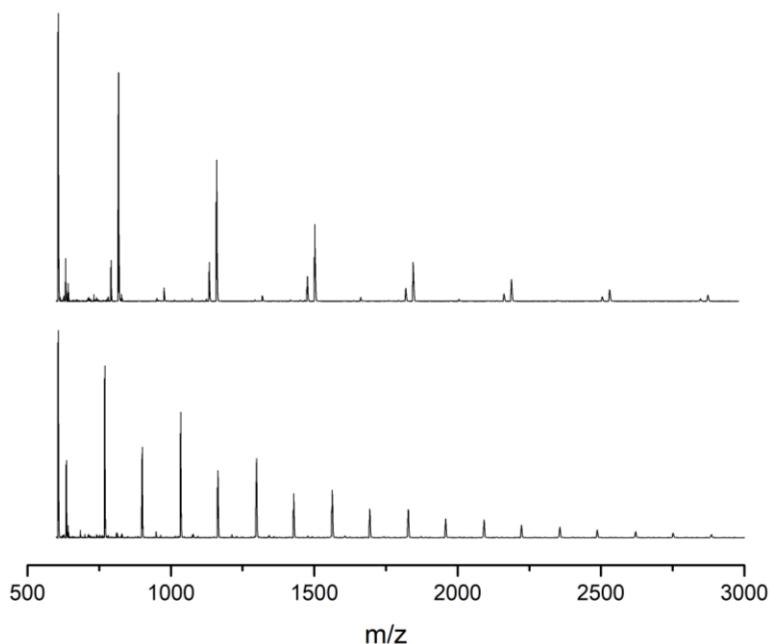


Figure 3.8 MALDI-TOF spectra of neat (lower) and mesylated (upper) Desmophen 650A.

The overall shift to higher molecular weights and difference in spacing between distributions can better be observed in the plots of m/z v. degree of polymerization (Figure 3.9) for the major and minor distributions of the MALDI-TOF spectra. Comparing the y-intercepts for the mesylated and neat distributions showed substantial increases in molecular weight, which indicated mesylation of the end-groups of the

polymer chain. In addition, comparing the slopes for the starting distributions to the slopes of the respective mesylated distributions also indicated mesylation of hydroxyl functionalities contained within the repeating units.

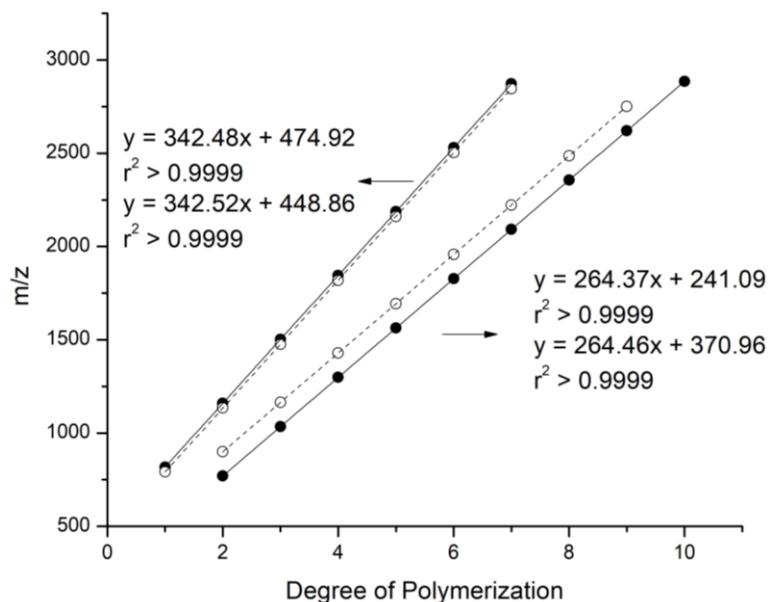


Figure 3.9 Linear regression of neat and mesylated Desmophen 650A. Minor distributions, defined as the less intense peaks in Figure 3.8, are open circles; major distributions are closed circles.

To determine the number of hydroxyls in both the residual mass and repeating unit, the difference in mass before and after mesylation was calculated (Table 3.3). For example, the residual mass of the major distribution before mesylation was 241.09 Da, and after mesylation it increased to 474.92 Da for a difference of 233.83 Da. The effective increase in mass by adding a single methanesulfonate is approximately 78 Da. Therefore, the increase in the residual mass of the major distribution is caused by the addition of three terminal methanesulfonate functionalities, indicating that in the neat sample there are precisely three terminal hydroxyl units. The same can be inferred for the repeating units and residual masses for both the major and minor distributions, and

the results are shown in Table 3.3. From these data, along with knowledge of the exact masses of the repeating unit and end groups, the structures for both the major and minor distributions could be determined. For the major distribution, the data suggest that the degree of polymerization is an odd number, and that the repeating unit consists of phthalic acid and trimethylolpropane with one free hydroxyl group; the end groups consist of odd trimethylol propane structural units with (on average) three free hydroxyls. For the minor distribution, the data suggest that the degree of polymerization is an even number, and that the repeating unit again consists of phthalic acid and trimethylolpropane with one free hydroxyl group; in this case, the end groups consist of one free carboxylic acid group and one free hydroxyl group.

Table 3.3 Linear Regression of MALDI-TOF Spectra for Both Major and Minor Distributions (Neat and Mesylated)

		Major Distribution		Minor Distribution	
		Repeating Unit	Residual Mass ⁱ	Repeating Unit	Residual Mass ⁱ
Mass (Da)	Neat	264.37	241.09	264.46	370.96
	Mesylated	342.48	474.92	342.52	448.86
Difference		78.11	233.83	78.06	77.90
Number of OH		1	3	1	1

ⁱ includes Ag cationizing agent

Once desired products were confirmed by NMR spectroscopy and MALDI-TOF, the polymers were analyzed by FTIR spectroscopy. This method was important for the commercial application of this project. Due to cost, FTIR spectrometers are far more common in industry than either of the other instruments. In addition, FTIR allows for the easy identification of all alcohol groups that are present in the neat material (OH stretching occurs $\sim 3400\text{ cm}^{-1}$) and azide ($\sim 2100\text{ cm}^{-1}$) functionalities that are present in the polyazide (Figure 3.10).

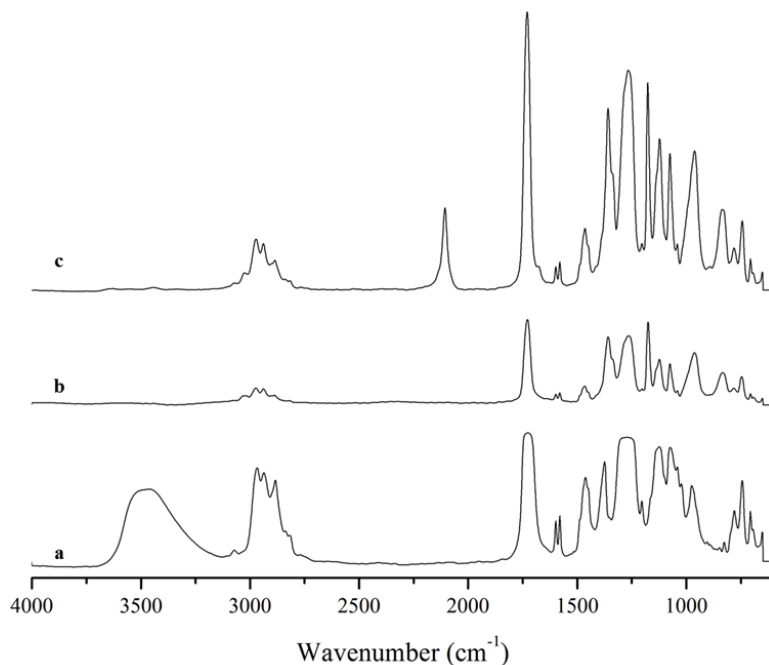


Figure 3.10 FTIR of neat (a), mesylated (b), and azidated polyester (c).

As can be seen in Figure 3.10, a strong, broad peak centered at approximately 3450 cm^{-1} indicative of O-H stretching is present in the spectrum of the neat polyester but completely absent in that of the mesylated polyester, indicating complete reaction. Upon azidation of the polymer, a strong, narrow peak forms at approximately 2150 cm^{-1} , which is inherent to N=N=N stretching.

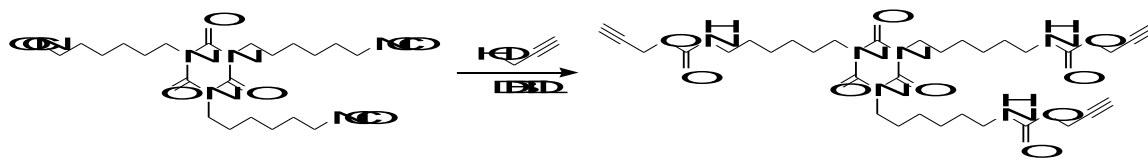
This synthetic strategy and analyses have been easily applied to three major types of polyols, polyester, acrylic, and polyether, which indicates high modularity of the process. In addition, scale-up was demonstrated by successful application of the process to 2 kg of the starting acrylic polyol.

3.3.2 Polyalkyne Synthesis

Synthesis and product analysis of the polyalkyne proved to be much more straightforward than that of the polyazide. Scheme 3.2 outlines a representative synthesis

involving an isocyanurate-based polyisocyanate and propargyl alcohol. The synthesis has also been easily extended to biuret and allophanate polyisocyanates as well as the monomeric isocyanate, hexyl isocyanate. In this chapter, propargyl alcohol was the predominant hydroxy-functional alkyne due to its relatively low reactivity with azides at room temperature, and commercial availability. However, Chapter V and Chapter VI involve other hydroxy- and amine-functional alkynes to tailor properties such as viscosity and reactivity.

Scheme 3.2 Propargylation of an isocyanurate-based polyisocyanate



Initial experiments involved using triethylamine rather than DBTDL as the catalyst and taking no special precautions to isolate the reaction from adventitious water. Not surprisingly, this resulted in low conversion and gelation (Figure 3.11 left). As a result, the process was modified to maintain dry conditions by continuously flushing the system with N₂. In addition, the catalyst was switched to DBTDL as triethylamine is known to yellow aliphatic urethanes (Figure 3.11 right).

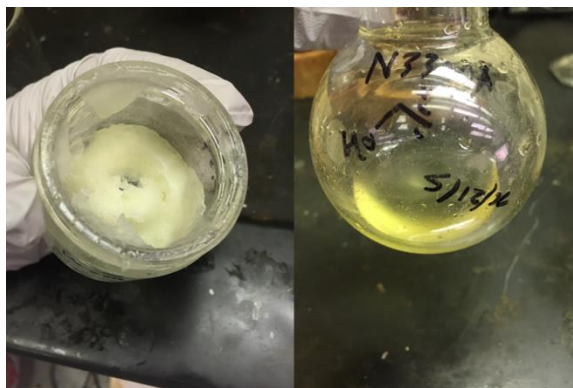


Figure 3.11 Propargylation of Desmodur N3300A: initial process (left) and water-free process (right).

Reaction progress was monitored by FTIR spectroscopy by integrating the peak located at 2274 cm^{-1} attributed to $\text{N}=\text{C}=\text{O}$ stretching, over a two-point baseline, and using the peak at 2390 cm^{-1} attributed to CH_2 stretching as an internal standard. Figure 3.12 shows a representative example of as-received Desmodur XP2580 and its propargyl carbamate (PC) derivative, Desmodur XP2580-PC, in which conversion to the carbamate was $>99.9\%$.

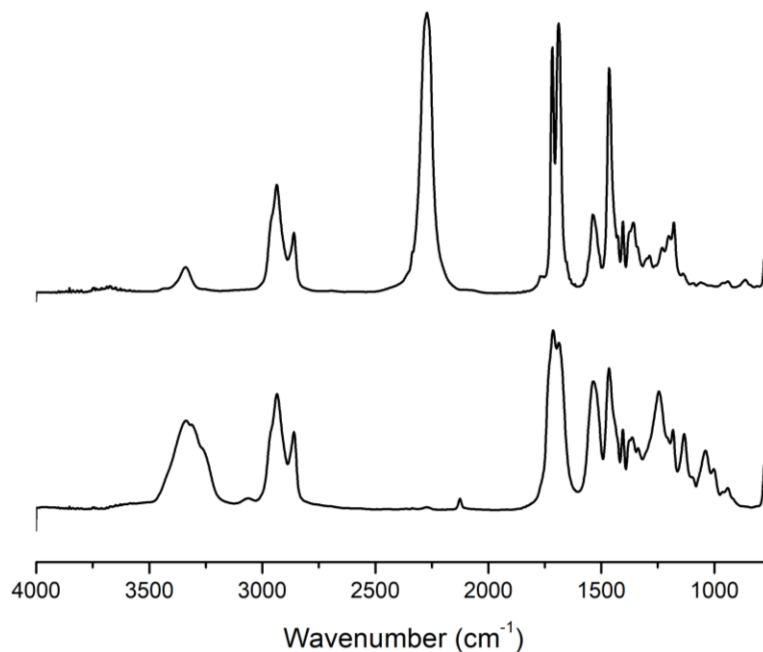


Figure 3.12 FTIR of as received (top) and propargylated Desmodur XP2580 (bottom).

This process has successfully been used to propargylate Desmodur N3300 (isocyanurate), Desmodur N3200 (biuret), and Desmodur XP2580 (allophanate). Although some yellowing has been observed with all propargyl carbamates, it was found that yellowing can be dramatically reduced by maintaining the reaction temperature ≤ 40 °C.

Reaction of the HDI-based resins such as Desmodur N3330 or N3200 with propargyl alcohol causes a dramatic increase in viscosity, attributed to extensive hydrogen bonding among carbamate groups. Although viscosity can be reduced by addition of a hydrogen bond donor/acceptor solvent such as isopropanol, we have shown that viscosity increase upon propargyl carbamate formation varies greatly with choice of precursor resin. The cause as well as techniques used to overcome this increase in viscosity will be further discussed in Chapter VI.

3.3.3 Coating Formulation and Curing

Coatings with satisfactory appearance properties and excellent resistance properties were produced from the modified resins. Of the various azide-alkyne combinations possible from the synthesized materials (*vide supra*), some were compatible and some were not, as outlined in Table 3.4. In general, the most broadly compatible propargyl carbamate resin was that derived from the allophanate resin, XP2580-PC. Some of the possible combinations in Table 3.4, including Desmodur N 3300 with PPG 1000 or Desmophen 650A, are not recommended by the supplier in terms of compatibility, so it is unsurprising that the modified materials are incompatible as well. However, Desmophen 650A and Desmodur N 3200 are compatible before

modification but appear to be less compatible after modification to azide and alkyne derivatives, respectively.

Table 3.4 Compatibility of Synthesized Azide and Alkyne Resins

	Desmodur N3300-PC	Desmodur N3200- PC	Desmodur XP2580- PC
azidated PPG 1000	-	-	+
azidated Desmophen 650	-	+/-	+
azidated Setalux DA 870	+	+	+

Azide-modified resins derived from acrylic polyols seem to display the greatest compatibility with the propargyl carbamate resins. The very best combination observed was XP2580 propargyl carbamate (XP2580-PC) and the azidated acrylic, Setalux D A 870. In fact, Setalux D A 870-azide was observed to be so perfectly miscible with XP2580-PC that the two are easily hand-stirred together with absolutely no turbidity (transient or permanent) visible to the naked eye. Furthermore, to date the best coatings have been obtained from XP2580-PC/Setalux D A 870-Azide combination.

Figure 3.13 shows the isothermal reaction kinetics (80 °C) of all azidated polyols with Desmodur XP2580-PC as well as the corresponding combinations of unmodified precursors. In every case, the polyisocyanate/polyol precursor (urethane-forming) system exhibited faster kinetics than the corresponding polyalkyne/polyazide (triazole-forming) system. In both cases (urethane-forming and triazole-forming) the backbone chemistry of the polyol (acrylic, polyester, etc.) dramatically effected cure conversion at 1.5 h (~65% for azidated Setalux DA 870 vs. ~10% for azidated PPG 1000). Of the triazole-forming pairs, azidated Setalux DA 870 and Desmodur XP2580-PC showed the highest

conversion (~65% after 1.5 h) and resulted in aesthetically pleasing coatings with a smooth, tack-free finish upon cooling.

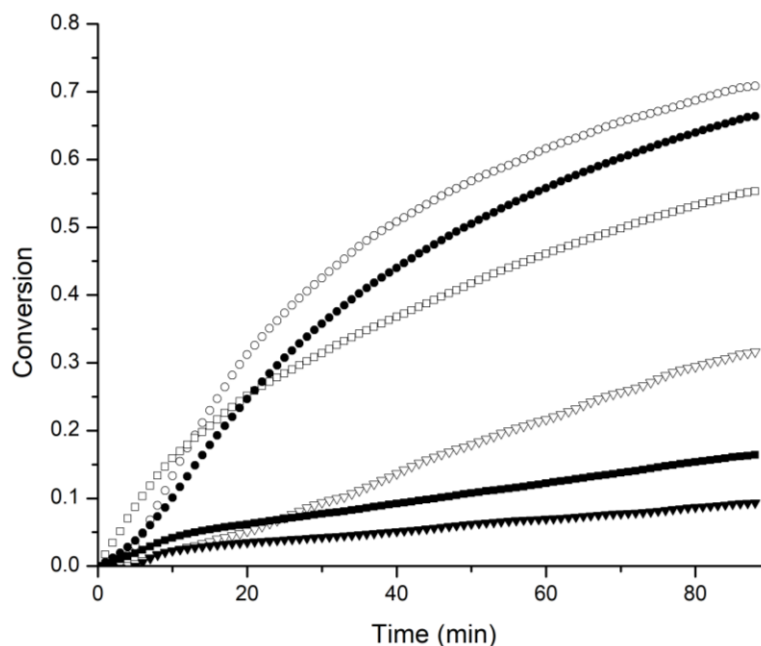


Figure 3.13 Curing kinetics at 80 °C of Desmodur XP2580 cured with Setalux DA 870 (open circle), Desmophen 650A (open square), and PPG 1000 (open triangle), and Desmodur XP2580-PC cured with: azidated Setalux DA 870 (solid circle), azidated Desmophen 650A (solid square), and azidated PPG 1000 (solid triangle).

As a compliment to Figure 3.13, Figure 3.14 shows the isothermal curing kinetics (80 °C) of the various proparyglated polyisocyanates cured with azidated Setalux DA 870. Again, the urethane-forming material showed more rapid curing kinetics than the triazole-forming material, and the backbone chemistry of polyisocyanate resin dramatically effected cure conversion after 1.5 h, which varied from 20% with Desmodur N3300-PC to 65% with Desmodur XP2580.

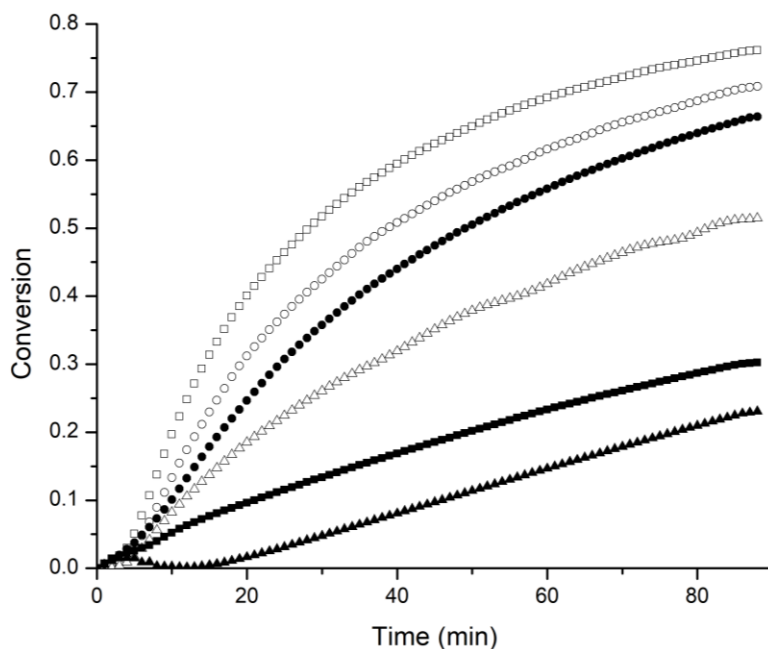


Figure 3.14 Curing kinetics at 80 °C of Setalux DA 870 cured with Desmodur XP2580 (open circle), Desmodur N3200A (open square), and Desmodur N3300A (open triangle), and azidated Setalux DA 870 cured with: Desmodur XP2580-PC (solid circle), Desmodur N3200A-PC (solid square), and Desmodur N3300A-PC (solid triangle).

It is possible to accelerate the cure of propargyl carbamate coatings by direct addition of Cu(I) catalyst, addition of a Cu(II) catalyst precursor and a reducing agent, and/or by using mixtures of propiolate ester carbamates² (discussed in Chapter V) and propargyl carbamates. Although direct addition of Cu(I) catalyst would be simplest,^{36-38,74} most research groups add a Cu(II) source and a reducing agent^{33,39,40} due to the poor solubility of most Cu(I) salts. CuCl₂[PMDETA] was shown to be soluble in similar azide-alkyne systems and so was chosen for this study.⁴¹ Figure 3.15 shows that the observed curing kinetics were greatly effected by adding Cu(II)[PMDETA]/stannous octanoate. As an initial observation, curing kinetics for the uncatalyzed triazole-forming reaction (closed circles) were slightly lower than those of the urethane-forming control reaction. By adding 1 wt% Cu(II) (relative to azide) a dramatic increase in curing

kinetics was observed, such that high conversion was rapidly achieved (>95% conversion in 10 min); none of the other systems, including the unmodified isocyanate-alcohol reaction (black triangle), exceeded 70% conversion within the 1.5 h timeframe of the experiment. Increasing the Cu(II) to 2 wt% did not increase the rate of the reaction, suggesting a saturation limit. The data suggest that this limit is somewhere between 0.4 - 1 wt% (relative to polyazide), but this analysis was complicated by observation of an induction period at lower Cu(II) concentrations. It should be noted that using the least amount of Cu(II) that still results in a quickly catalyzed system is most desired, since Cu(II) could cause discoloration in the final coating. Interestingly, adding CuCl₂[PMDETA] (open triangle) but omitting the reducing agent appears to cause an inhibition effect.

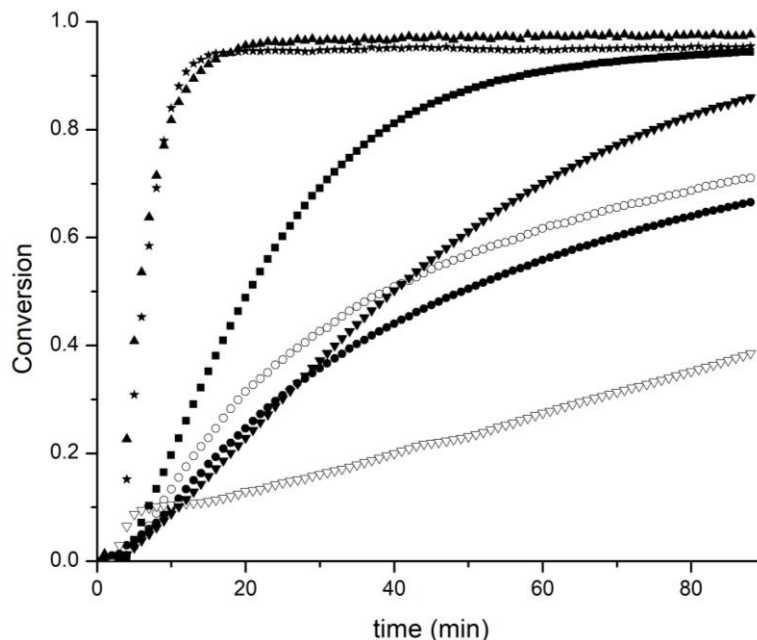


Figure 3.15 RT-FTIR isothermal cure kinetics (80 °C) of azidated Setalux DA 870 and Desmodur XP2580-PC with various Cu(II)[PMDETA] loadings: 0 (closed circle), 0.2 (closed down triangle), 0.4, (closed square), 1.0 (closed star), and 2.0% (w/w) (closed up triangle). Two drops of stannous octanoate were added to 1 g of these formulations immediately prior to analysis. In addition two controls are present: 2% (w/w) Cu(II)[PMDETA] without stannous octanoate (open down triangle) and as received resin (open circle) Weight % values are relative to polyazide.

3.3.4 Physical Properties of Neat and Modified Resins

Figure 3.16 shows a representative clear coating from the XP2580-PC/Setalux D A 870-Azide combination (right) compared to a control panel prepared from the XP2580/Setalux D A 879 polyisocyanate/polyol precursors (left). Table 3.5 lists various film properties. The coatings were drawn down on steel panels at 100% solids and cured at 80°C for 4 h. This temperature was chosen as it properly cures the modified coating without yellowing (temperatures at or above 120 °C have been shown to degrade the polyol and cause yellowing). The curing profile was as follows: a 2 h room temperature solvent flash was followed by inserting the panels in an oven preset to 80 °C. A panel removed from the oven after 2.5 h at 80 °C showed that a tack-free surface had been

achieved at this point. Conversion (as determined by MEK double rubs) was lower (130 rubs) for the sample removed after 2.5 h compared to the samples that cured for 4 h (200+ rubs).

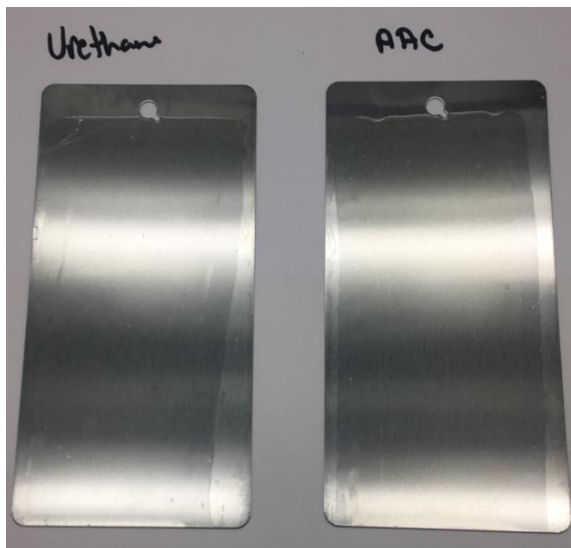


Figure 3.16 Coatings prepared from propargylated Desmodur XP2580 and azidated Setalux DA 870 (right) compared to as-received precursor resins (left), drawn down on steel panels and cured at 80 °C for 4 h.

Table 3.5 Performance Properties of Propargylated Desmodur XP2580/azidated Setalux DA 870 Coating Compared to a Control Coating Using As-Received Precursor Resins

	Propargylated Desmodur XP2580/azidated Setalux DA 870	Desmodur XP2580/ Setalux DA 870
Color (L/A/B)	36.11/11.96/-14.39	38.97/-12.19/9.21
Color (ΔE)		34.12
Gloss 20	124.83	123.43
Gloss 60	118.13	117.27
Gloss 85	103.80	105.70
Pencil Hardness	Pass @ 2H	Pass @ 2H
MEK Double Rub	200+, 200+	200+, 200+
T _g (°C)	45.8	40.8

Adhesion to QD steel substrates was much lower for the azide-alkyne system compared to the polyisocyanate-polyol precursor system. Therefore, a study was conducted to determine if various cleaning and/or pretreatment techniques could be used

to improve adhesion on steel. The results are outlined in Table 3.6. Simple acetone or MEK/toluene rinses were not enough to improve adhesion. When cleaned in the same manner as the acetone-rinsed samples and subsequently treated with a phosphoric acid (PA) metal conditioner, a substantial increase in adhesion properties was observed. The PA treated sample achieved the same results as the urethane cured sample for both cross-hatch adhesion and conical mandrel testing procedures. The impact testing results were not as good as the precursor system but were substantially improved when compared to the other treatment methods. Currently, it is believed that the decrease in impact testing could be due, at least in part, to increased brittleness imposed by the triazole linkage. Aluminum panels were tested and behaved similarly to the steel substrates. As in the case with steel, aluminum had poor adhesion unless pretreated with the metal conditioner but after treatment, the aluminum sample behaved equally as well or better than the steel substrates.

Table 3.6 Adhesion Properties of Propargylated Desmodur XP2580/azidated Setalux DA 870 Coating Using Various Cleaning Methods Compared to a Control Using As-Received Precursor Resins Cleaned with Acetone

Curing Type Cleaning Method	Urethane	Azide-Alkyne		
	Acetone	Acetone	MEK/Toluene	Phosphoric Acid Conditioner
Cross-hatch	3B, 3B	0B, 0B	0B, 0B	3B, 3B
Forward Impact	Pass @ 140 lb	Pass @ 40 lb	Pass @ 15 lb	Pass @ 80 lb
Reverse Impact	Pass @ 120 lb	Pass @ 30 lb	Pass @ 5 lb	Pass @ 80 lb
Conical Mandrel	Pass	Fail	Fail	Pass

3.4 Conclusions and Future Work

This chapter reports the synthesis, formulation, and curing of a non-isocyanate polyurethane (NIPU) coating system based on azide-alkyne cycloaddition and derived from commercial polyisocyanate and polyol resins. The synthesis of azidated polyols was achieved through a robust two-step process, in which the hydroxyl groups of the polyol were first converted to mesylate groups. In a second step, NaN_3 was used to displace the methane sulfonate under $\text{S}_{\text{N}}2$ conditions. Propargylated carbamate derivatives of commercially available polyisocyanate resins were achieved by reacting the resin with propargyl alcohol at 0°C using DBTDL as a catalyst. Propargylation of the isocyanates resulted in a dramatic increase in viscosity. This issue is addressed in Chapter VI. Curing kinetics were also monitored and shown to be easily and dramatically increased by adding small amounts ($< 1\text{ wt}\%$) of Cu(II) catalyst precursor plus a reducing agent. Coatings of azidated Setalux DA 870 and Desmodur XP2580-PC were drawn down on steel and aluminum substrates. The final properties of the triazole-forming NIPU coating system were compared to those of the polyurethane precursor system. Properties such as T_g , hardness, and conversion (as tested by MEK double rubs) were similar for both systems. However, adhesion properties of the modified systems were significantly lower. Adhesion was improved when the metal substrate was pre-treated with a phosphoric acid based metal conditioner.

Future work should include determining the difference in polarity between the polyisocyanate vs. propargylated carbamates. In some cases, due to an apparent increase in polarity as well as high viscosity, the modified components tend to phase-separate resulting in coatings of poor quality. This may be overcome by using a good solvent for

both the polyazide and polyalkyne and accelerating the cure using catalyst. It would also be of interest to determine an Arrhenius relationship for all pairs of polyazides and polyalkynes. It is hypothesized that the pairs that exhibited low conversion (for example, azidated PPG 1000 with Desmodur XP2580-PC) would show a dramatically lower pre-exponential term but relatively similar E_a as compared to the pairs that showed higher conversion. This result would indicate that the materials are likely phase separating.

CHAPTER IV – REDUCED TEMPERATURE NON-ISOCYANATE
POLYURETHANE COATINGS VIA CATALYST-FREE AZIDO-ALKYNE
CYCLOADDITION

4.1 Introduction

The CuAAC-cured, NIPU coatings of the previous chapter were achieved by modifying both components of a conventional two-component (2K) polyurethane coating system. First, a polyisocyanate resin, namely Desmodur XP2580, was reacted with propargyl alcohol to introduce propargyl functionalities via urethane linkages. Separately, polyazides were created from commercially available polyols *via* a mesylated intermediate. Reaction of this propargyl carbamate NIPU with a polyazide prepared from Setalux DA 870 produced aesthetically pleasing coatings with desirable thermal and mechanical properties, which in most cases met or exceeded the properties of the unmodified polyurethane coating. However, the curing rate of these modified coatings, in the absence of a catalyst, was found to be too sluggish to be a practical NIPU. In the previous chapter, we showed that the rate of the azide-alkyne cycloaddition could be dramatically increased by the incorporation of a Cu(I) source. Although this was done by *in situ* reduction of Cu(II) using a chemical reducing agent,^{33,39,40} specifically tin(II) 2-ethylhexanoate, other means could have been employed including direct addition of copper(I)^{27,36-38} or reduction of copper(II) to copper(I) using UV light.^{75,76} However, incorporation of Cu(I) produced undesirable coloration of the films.

Previously, our group has developed an azide-alkyne curing system for out-of-autoclave composites.² In doing so, Gorman *et al.* were able to show that activation energy of propiolate functionalities were on average about 10 kJ/mol lower than that of

propargyl functionalities when reacted with a model azide. Borrowing from this idea, we sought to incorporate propiolate functionalities into a NIPU system. Two general methods were attempted and will be discussed in this chapter. The first was the direct propiolation of the isocyanate using propiolic acid to form an amide linkage upon the removal of CO₂.^{77,78} The second was the synthesis of 2-hydroxyethylpropiolate (2-HEP), a monomer previously reported in the literature but not well-characterized,⁷⁹ and its subsequent reaction with the isocyanate. This latter method would yield the desired urethane linkages, and accelerated curing kinetics with an azide, without the need of catalyst. This chapter discusses the methods of achieving the desired propiolate-based, reduced-temperature-cure NIPU, with a special emphasis on the synthesis, isolation, and characterization of 2-HEP. It then compares the cure kinetics of the propargyl- and propiolate-based systems to the as-received control, and finally compares the properties of each cured coating system on steel.

4.2 Experimental

4.2.1 Materials

Setalux DA 870 and Desmodur XP2580 were generously donated by Covestro. Triethylamine (TEA; ≥99.5%), *n*-butyl acetate (ACS reagent; ≥99.5%), tetrabutylammonium bromide (ACS reagent; ≥98.0%), *p*-toluenesulfonic acid monohydrate, benzene (ACS reagent; ≥99.0%), propiolic acid (95%), ethylene glycol (anhydrous; 99.8%), methanesulfonyl chloride (≥99.7%), sodium azide (NaN₃; ReagentPlus®; ≥99.5%), acetonitrile (anhydrous; 99.8%), and ethylene oxide (≥99.5%) were purchased and used as received from Sigma-Aldrich. Diethyl ether (Spectranalyzed®), *N,N*-dimethylformamide (DMF; Certified ACS), ethyl acetate

(Certified ACS), hexanes (HPLC grade), and methanol (Optima ®) were purchased and used as received from Fisher Chemical.

4.2.2 Instrumentation

Proton nuclear magnetic resonance (^1H NMR) spectra were obtained using either a 300 MHz Varian Mercury^{plus} NMR (VNMR 6.1C) spectrometer or a 600.13 MHz Bruker Ascend (TopSpin 3.5) spectrometer. Typical acquisition parameters were 10 s recycle delay, 7.8 μs pulse corresponding to a 45 degree flip angle, and an acquisition time of 1.998 s. The number of scans acquired for each sample was 32. All ^1H chemical shifts were referenced to TMS (0 ppm). Sample solutions were prepared at a concentration of approximately 2.5% (w/v) in CDCl_3 containing 1% TMS as an internal reference, and the resulting solution was charged to a 5 mm NMR tube. Carbon nuclear magnetic resonance (^{13}C NMR) spectra were obtained at 150.90 MHz using Bruker Ascend (TopSpin 3.5) spectrometer spectrometer. Typical acquisition parameters were 1 s recycle delay, 11 ms pulse corresponding to a 45 degree flip angle, and an acquisition time of 0.908 s. The number of scans acquired for each sample was 1024. All ^{13}C chemical shifts were referenced to residual chloroform (77.16 ppm). Sample solutions were prepared at a concentration of approximately 5% (w/v) in CDCl_3 containing 1% TMS as an internal reference, and the resulting solution was charged to a 5 mm NMR tube.

FTIR analyses were conducted using a Nicolet 8700 spectrometer with a KBr beam splitter and a DTGS detector. Samples were sandwiched between two NaCl salt plates (approximate thickness: 10 mm). Flash chromatography was performed on a Teledyne Isco CombiFlash Purification System using RediSep Rf prepacked columns.

Isothermal Real-time Fourier Transform Infrared Spectroscopy (RT-FTIR) was performed using a Thermo Fisher Scientific Nicolet 6700 FTIR equipped with a mid-IR beam splitter and integrated with a Simplex Scientific HT-32 Heated Transmission cell. The Simplex software was paired to the OMNIC FTIR software native to the Nicolet 6700. Approximately 1.5 g of sample was hand mixed at 1:1 stoichiometry for NCO:OH and 1.15:1 for azide:alkyne for 2 min and spun using a FlakTech mixer and allowed to mix at 1800 rpm for approximately 10 min. A small aliquot was taken from the mixture and squished between two polished NaCl plates. The plates were then inserted in the Transmission Cell and subsequently placed in the chamber for FTIR analysis. The sample chamber was purged with N₂ for approximately 10 min to reduce the presence of a CO₂ peak that could overlap with the isocyanate peak. The sample was rapidly heated from room temperature to the desired temperature and spectra were immediately obtained in 1 min intervals (32 scans; 4 cm⁻¹ resolution) for the duration of the run (60 min). Conversion was monitored as either the disappearance of the isocyanate stretching peak (most typically around 2271 cm⁻¹) or disappearance of the peak attributed to both azide (N=N=N stretching) and alkyne (C≡C stretching) at approximately 2100 cm⁻¹. Aliphatic C-H stretching (2755 cm⁻¹) was used as an internal standard. Baselines were taken as the straight line between the base of the desired peaks.

4.2.3 Synthesis of Azidated Setalux DA 870

The synthesis of azidated Setalux DA 870 was performed in two steps and was modeled after the *Polyazide Synthesis* found in the previous chapter. First, the polyol was mesylated, and then the isolated product was azidated using NaN₃ under S_N2 conditions. A representative procedure was as follows: a 3-neck 250 mL round bottom

flask, a 25 mL pressure equalizing addition funnel, and a mechanical stirrer were baked in an oven at 160 °C for approximately 2 h and allowed to cool to room temperature *in vacuo*. The flask was fitted with the mechanical stirrer, and Setalux DA 870 (20.054 g; 91.4 %solids; 31.8 mmol hydroxyl) and acetonitrile (40 mL) were added directly to the flask. The mixture was then lowered into an ice bath (0 °C) and stirred to dissolve the polyol. During dissolution, a solution created by dissolving Mes-Cl (5.514 g; 48.1 mmol) into 15 mL of acetonitrile was charged to the addition funnel, and the entire system was continuously purged with N₂. Upon complete dissolution of the polyol, TEA (5.514 g; 54.5 mmol) was added to the polyol solution. The addition funnel was attached to the flask, and the final port was closed with a rubber septum. The Mes-Cl solution was added dropwise to the polyol solution, and the reaction progressed at 0 °C overnight. The reaction mixture containing the desired product, acetonitrile, and salts, was filtered to remove the salts and concentrated *in vacuo*. The concentrated resin was dissolved in ethyl acetate (50 mL) and washed with DI water (50 mL x 3) to remove residual salts, dried chemically with MgSO₄ and concentrated *in vacuo* resulting in a yellow oil (14.043 g; % yield: 61.7%) that was immediately prepared for azidation.

Azidation of mesylated Setalux DA 870 was carried out as follows: to a 3-neck 250 mL round-bottom flask equipped with a mechanical stirrer, reflux condenser, and inlet and outlet ports providing continuous N₂ purge, were charged mesylated Setalux DA 870 (14.043 g; 22.00 mmol OMs) and 110 mL of DMF:acetonitrile (1:10) cosolvent mixture. Upon dissolution of the polymer, NaN₃ (2.17 g; 33.4 mmol) was charged to the flask, and the mixture was subsequently heated to 95 °C with continuous stirring and allowed to react for 48 h. Upon completion, the reaction mixture was cooled to room

temperature, filtered to remove remaining salts, and concentrated *in vacuo* to remove most of solvent. The concentrated solution was transferred to a separatory funnel using ethyl acetate rinses (30 mL x 3). DI water (100 mL) was added to the separatory funnel to separate the DMF/acetonitrile from the organic layer containing the product. Upon separation, the aqueous solution containing some DMF and trace acetonitrile was extracted with fresh ethyl acetate (50 mL x 3), and the extracts were combined with the organic layer. The combined organic layer was then washed with DI water (200 mL x 3), dried over MgSO₄, filtered, and finally concentrated *in vacuo* to yield the azidated polyol (light yellow oil; yield: 10.337 g; 78.7%).

4.2.4 Direct Amidation of Desmodur XP2580

Within a 100 mL 3-neck round-bottom reaction flask, Desmodur XP2580 (6.348 g; 34.61 mmol NCO) was dissolved in 20 mL of DMF using magnetic stirring. Triethylamine (6.999 g; 69.17 mmol) and propiolic acid (3.717 g; 53.06 mmol) were dissolved in 50 mL of DMF. The propiolic acid/TEA solution was added dropwise (1 drop/s) to the reaction flask at room temperature using a pressure-equalizing addition funnel equipped with a constant N₂ purge, and the mixture was allowed to react overnight. The next day, the reaction appeared to gel and the material was not soluble in any common organic solvents.

4.2.5 Synthesis of 2-HEP via Ethoxylation

A modification of the procedure from Miller et al.⁷⁹ was used to synthesize 2-hydroxyethylpropiolate. All glassware were heated overnight at 170 °C and then transferred to a N₂-atmosphere glovebox (MBraun Labmaster 130). Propiolic acid (PA; 10.712 g; 138 mmol) was weighed into a 3-neck, 100 mL round-bottom flask. Diethyl

ether (50 mL) and tetraethylammonium bromide (TEAB; 0.265 g) were then charged to the flask, and the resulting mixture was cooled to -5 °C. Condensed ethylene oxide (EO; 9.6 mL; 0.20 mol) was slowly added to the continuously stirred mixture over 30 min while monitoring the temperature of the reaction to avoid exotherm. Upon complete addition of EO the reaction was warmed to 10 °C and allowed to react at that temperature overnight. The reaction was then brought to room temperature and additional EO (6.5 mL; 0.14 mol) was charged to the flask over a 20-minute period and allowed to react for 2 h. The second addition of EO produced no noticeable exotherm. The light brown mixture was concentrated in vacuo to produce a dark brown oil, which was purified using flash chromatography (50:50 hexanes/ethyl acetate spiked with 5% MeOH as eluent) to yield the desired, slightly yellow product (Yield: 3%). FT-IR (KBr plate): 3400 (strong, broad), 3274 (medium, sharp), 2959 (medium), 2884 (medium), 2119 (strong, sharp), 1715 (strong), 1453 (medium), 1370 (medium), 1245 (strong) cm^{-1} . ^1H NMR (600 MHz, CDCl_3): δ = 4.32 (2H, t, J = 0.01 Hz, $\text{COO-CH}_2\text{-CH}_2$), 3.87 (2H, t, J = 0.01 Hz, $\text{CH}_2\text{-CH}_2\text{-OH}$), 3.01 (1H, s, $\text{H-C}\equiv\text{C}$), 2.75 (1H, s, -OH). ^{13}C NMR (150 MHz, CDCl_3): δ = 152.71 (C=O), 75.53 (H-C \equiv C), 74.29 (H-C \equiv C), 67.48 (COO-CH $_2$ -CH $_2$), 60.26 (CH $_2$ -CH $_2$ -OH).

4.2.6 Synthesis of 2-HEP via Fischer Esterification using H_2SO_4 catalyst

A procedure developed by Duran et al.⁴⁷ was adapted to synthesize 2-HEP. All glassware were heated for 2 h at 170 °C and cooled in vacuo. Into a 500 mL round-bottom flask, propiolic acid (9.646 g; 95%; 131 mmol), dry toluene (300 mL), and ethylene glycol (42.763 g; 689 mmol) were charged. One drop of sulfuric acid was added to the mixture, and magnetic stirring was begun. A Dean-Stark apparatus was

attached to the flask, and the reaction was brought to reflux and allowed to continue refluxing for 48 h. Upon cooling and cessation of stirring, a dark brown oil settled to the bottom of the flask below the clear liquid. The brown oil was isolated using a separatory funnel and concentrated *in vacuo*. Flash chromatography (50:50 hexanes/ethyl acetate spiked with 5% MeOH as eluent) yielded the desired 2-HEP (1.438 g; 9.62 % yield).

4.2.7 Synthesis of 2-HEP via Fischer Esterification using *p*-Toluenesulfonic Acid Catalyst

A procedure developed by Gorman *et al.*² was adapted to synthesize 2-HEP. All glassware were heated for 2 h at 170 °C and cooled *in vacuo*. Benzene (400 mL) was dried by azeotropic distillation for 1 h prior to use. Ethylene glycol (55.580 g; 895 mmol) was charged to a 1 L round-bottom flask equipped with a magnetic stirrer and dried under high vacuum at 75 °C for 1 h. Propiolic acid (12.345 g; 95%; 167.42 mmol), the previously dried benzene, and *p*-toluenesulfonic acid mono-hydrate (0.813 g; 4.274 mmol) were charged to the 1 L round-bottom flask containing ethylene glycol. A Dean-Stark trap and condenser was added to the flask, and the system was continuously purged with N₂. The stirred mixture was heated to reflux using a heating mantle, upon which the water of condensation began to collect in the trap. The mixture was allowed to react for 24 h at which point no additional water was being collected (3.8 mL; theoretical: 3.02 mL). The mixture was cooled to room temperature and concentrated *in vacuo* yielding a slightly brown oil. The oil was purified using flash chromatography using a gradient elution (hexanes to ethyl acetate/hexanes (50:50)). The structure of the resulting yellow oil was verified by 600 MHz ¹H NMR and was found to be 2-HEP (10.80 g; 53.7 % yield).

4.2.8 FTIR Kinetic Study

All resin pairs were mixed and cured in the same manner. As received Setalux DA 870 was mixed with as received Desmodur XP 2580 at 1:1 (OH:NCO) stoichiometry. Azidated Setalux DA 870 was mixed with either Desmodur XP2580-PC (propargyl-based) or Desmodur XP2580-2HEPC (propiolate-based) with a slight excess of azide at 1.15:1 (N₃:propargyl). The procedure used for the representative resin pair, azidated Setalux DA 870 and Desmodur XP 2580-PC, was as follows. Azidated Setalux DA 870 (0.8850 g; 91.4 %solids; 576.27 g polymer/mol N₃; 1.664 mmol azide) and Desmodur XP 2580-PC (0.3132 g; 19.3% NCO; 1.439 mmol propargyl) were hand mixed in a scintillation vial until smooth. The mixture was then placed in a FlakTech mixer and allowed to mix at 1800 rpm for approximately 20 min. A small aliquot was sandwiched between two salt plates. Isothermal runs were performed at ten degree increments from 60 to 90 °C for 60 min. Spectra were collected in 1 min increments and each spectrum was an average of 32 scans at 4 cm⁻¹ resolution. For the azide/alkyne resin pairs, conversion was monitored as the disappearance of the peak at approximately 2100 cm⁻¹ attributed to both azide and alkyne stretching. For the unmodified resin pairs, conversion was monitored using the peak attributed to NCO stretching, usually observed around 2271 cm⁻¹.

The rate constant was calculated for each resin pair at 60, 70, 80, and 90 °C by plotting the inverse of concentration vs. time, which typically gave a line with $r^2 > 0.98$. The one exception was the propargyl system at 60 °C, which only had a linear regime from 20 to 60 min. The rate constant (k) was taken as the slope of this line and subsequently used to find E_a via the Arrhenius relationship (Equation 4.1), where A' is

the Arrhenius pre-exponential factor, T is absolute temperature, and R is the ideal gas constant (8.3145 J/mol-K).

$$k = A' e^{\frac{-E_a}{RT}} \quad (4.1)$$

4.2.9 Coating Curing

All resin pairs were mixed and cured similarly to FTIR kinetic study, but with two major differences: the total scale was ~15 g and the resin pairs were diluted with *n*-butyl acetate at 20 wt% of the total mass to reduce viscosity. After hand stirring, each mixture was placed in a FlakTech mixer and mixed at 1800 rpm for approximately 20 min. The resulting solution was drawn down on either QD steel panels or CHEMFILM® ECTFE fluoropolymer films. The panels were then transferred to a programmable oven and subjected to the “standard cure profile” consisting of a solvent flash at 30 °C for 2 h, a temperature ramp at 1 °C to 100 °C, and a final cure at 100 °C for 4 h.

4.2.10 Coating Physical Testing

Reaction conversion was qualitatively compared using methyl ethyl ketone (MEK) double rubs using cheesecloth and a 32 oz hammer according to ASTM D5402. Flexibility was determined using a conical mandrel according to ASTM D522. Adhesion was determined using the crosshatch adhesion test (ASTM D3359). Hardness was measured using a pencil hardness test in accordance with ASTM D3363. Using a BYK-Gardner glossmeter, the coatings were tested at 20°, 60°, and 85°. The color of the panels was determined using a BYK-Gardner colorimeter based on L*, a, b* values.

Differential scanning calorimetry (DSC) was performed using a TA Instruments Q200. For this purpose, coatings were prepared, mixed, and drawn down on CHEMFILM® ECTFE fluoropolymer film as described in *Coating Curing*. The

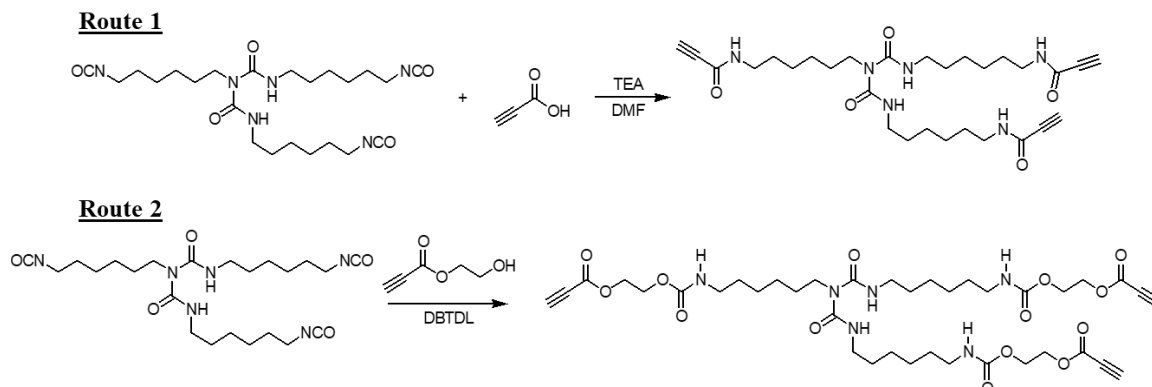
coating, which had little adhesion to the film, was peeled off and punched to give a disk of the film that fit within a DSC pan (d = 0.25 in). Stacks of five disks (~5 mg) were placed in a hermetically sealable pan. The pan was sealed and a heat/cool/heat cycle was performed on the sample starting at room temperature and ending at 100 °C at a rate of 10 °C/min. T_g of the cured material was determined from the second heating cycle, and TA Universal Analysis software was used to determine the midpoint of the T_g inflection as the reported value.

4.3 Results and Discussion

The goal of this work was to fit a commercial polyisocyanate resin with electrophilic propiolate moieties, which have been shown to provide rapid, uncatalyzed reaction with azides at room temperature. Two general methods to synthesize propiolate-functional resins were explored. The first was the direct reaction of a polyisocyanate resin, for example Desmodur N3200A, with propiolic acid in the presence of base to yield a propiolamide (Scheme 4.1, Route 1).^{77,78} The other was to synthesize 2-hydroxyethyl propiolate (2-HEP), an atom-efficient monomer comprised of a primary alcohol moiety that would easily add to an isocyanate. Reaction of 2-HEP with a polyisocyanate resin would result in a carbamate linkage and the target electrophilic alkyne (Scheme 4.2, Route 2). Below, the direct azidation of Desmodur N3200A and a few techniques to synthesize 2-HEP are discussed as well as the benefits and/or drawbacks of each synthetic strategy.

Scheme 4.1 Two Routes to yield propiolate HDI-based resin. Route 1 involves the direct reaction of propiolic acid with an isocyanate to produce an amide linkage and

CO₂. Route 2 involves first synthesizing 2-HEP and subsequent reaction with an isocyanate in the presence of DBTDL catalyst to produce a carbamate linkage.



4.3.1 Direct Amidation of Desmodur N3200A

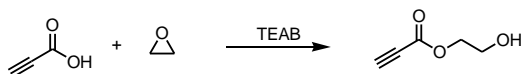
A straightforward approach to the desired functionality was the direct reaction of an isocyanate with propiolic acid to form an amide linkage (Scheme 4.1, Route 1). This can be done in the presence of a tertiary amine such as triethylamine as shown by Blagbrough *et al.*⁷⁷ or by reaction with the carboxylate salt as shown by Sasaki *et al.*⁷⁸ Both of these methods were attempted to amidate Desmodur N3200A and both yielded a product that appeared to be an organogel that was not soluble in common organic solvents (acetone, DMF, DCM, and THF). This gel was presumably a result of the formation of additional isocyanurate linkages and was not characterized further.

4.3.2 Synthesis of 2-HEP via Ring-Opening of Ethylene Oxide

The sole example of the synthesis of 2-HEP in the literature is a patent granted in 1963 to Miller and Butler, who used propiolic acid to ring-open liquid ethylene oxide in the presence of tetraethylammonium bromide (Scheme 4.2).⁷⁹ They were able to isolate the product by vacuum distillation and used boiling point, elemental analysis, and infrared spectroscopy to verify its identity. Using a modification of the procedure of Miller and Butler, a reaction was performed in a glovebox equipped with a cooling bath.

Chilled ethylene oxide liquid was added dropwise via Pasteur pipette to a stirred solution of propiolic acid and TEAB in diethyl ether contained within a reaction flask cooled to -5 °C. The reaction temperature was then slowly raised to 10 °C and allowed to react overnight. The next morning, pH test paper showed the red mixture to be still very acidic, so the reaction was brought to room temperature and additional ethylene oxide was added and allowed to react for approximately 2 h. An aliquot was removed and dried *in vacuo*.

Scheme 4.2 Synthesis of 2-HEP via ring-opening of ethylene oxide using propiolic acid.



¹H NMR was used to identify the contents of the aliquot, and the resulting spectrum is shown in Figure 4.1. Noticeably, peaks **a'** and **b'** indicative of propiolic acid starting material are present indicating little conversion of the acid to the desired ester. This issue was likely due to moisture from the propiolic acid as it was the only reagent or surface for which extra precaution was not taken to ensure removal of water. Further evidence supporting this hypothesis is the large peak at 3.60 ppm labeled **EG**, which is indicative of diethylether. Although there were many issues with this synthetic strategy as discussed, some of the desired product was identified as well, as indicated by peaks **b** and **c**.

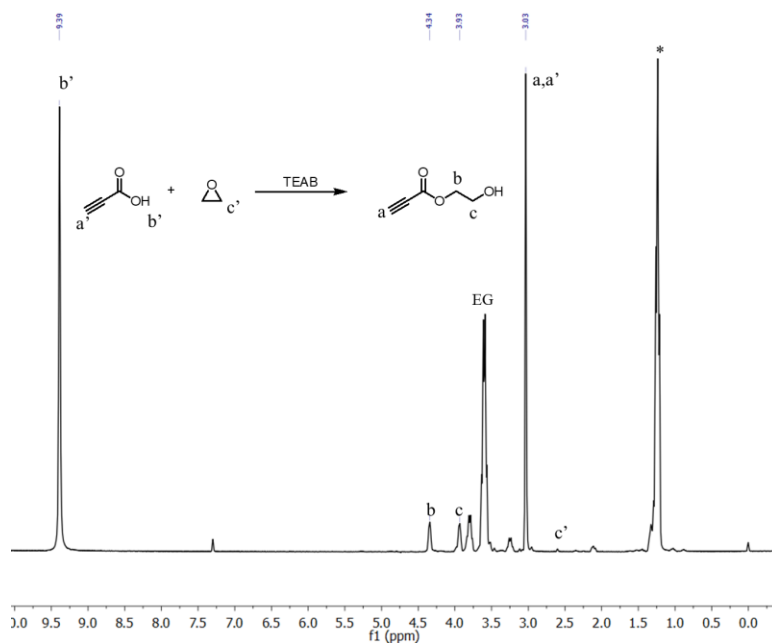


Figure 4.1 ^1H NMR spectrum (300 MHz, CDCl_3 , 23 °C) of 2-HEP synthesized by ring-opening of ethylene oxide using propiolic acid. Peaks labeled with (*) and EG are indicative of diethylether solvent.

The procedure reported by Miller *et al.*⁷⁹ indicates that the product was isolated via vacuum distillation (66-68 °C/0.5 mm Hg). The reaction and distillation were repeated approximately five times, but no product was obtained until well over 100 °C in any of the instances. In each case, the product was analyzed by potassium permanganate reduction, and in each case the test indicated the absence of an alkyne. ^1H NMR was used as a secondary method, and in agreement with the chemical analysis, showed the absence of the acetylenic proton. Continued heating of the still pot caused the crude oil to discolor (dark brown) and then eventually to undergo sudden degradation, resulting in a dark charred material.

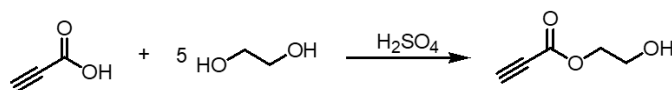
After the multiple failed attempts at distillation, the product was eventually isolated using column chromatography using a ternary mixture of ethyl acetate hexanes and methanol (47.5:47.5:5) as the eluent; however the overall yield was only

approximately 2%. As a result of the difficult reaction conditions, overall low yield, and expensive starting materials, other methods were pursued to synthesize the desired product.

4.3.3 Synthesis and Characterization of 2-HEP via Fischer Esterification

A common method to prepare propiolic esters is Fischer Esterification (Scheme 4.3).^{2,47} This reaction was initially carried out in refluxing toluene using a Dean-Stark apparatus to remove the water of condensation by azeotropic distillation. The reaction was catalyzed with sulfuric acid and allowed to react overnight. After cooling to room temperature, it was quickly noticed that there was a dark brown oil at the bottom of the flask that appeared to be the desired product. After further drying to remove trace toluene, this oil was analyzed by ¹H NMR to confirm the structure of the desired product (Figure 4.2). The peaks at 3.83 and 3.97 ppm likely signify a mono-esterified ethylene glycol, like in the desired product. However, the expected acetylenic proton, which has a known chemical shift of 3.08 ppm in propiolic acid and 3.00 in propiolic esters of oligomeric ethylene glycol² was completely absent, and peaks upfield of that region appeared indicating the presence of sp³ hybridized protons. In addition, a small amount of the isolated product was subjected to oxidation by KMnO₄, which also indicated negative for alkyne.

Scheme 4.3 Fischer esterification of 2-HEP.



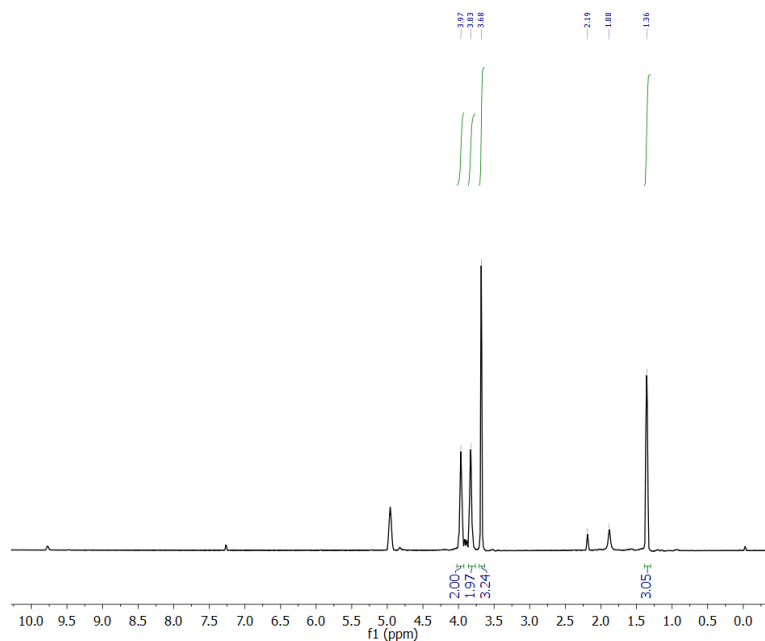


Figure 4.2 ^1H NMR spectrum (300 MHz, CDCl_3 , 23 °C) of 2-HEP synthesized by Fischer Esterification using 5:1:0.02 (ethylene glycol:propionic acid: H_2SO_4).

It was hypothesized that the failure to create the propiolic ester, counter to the results of Gorman² and Duran,⁴⁷ was caused by excessively high H_2SO_4 catalyst concentration. Therefore, the reaction was repeated using 1 drop or approximately 0.7 mol% of catalyst. The resulting ^1H NMR spectrum (Figure 4.3) shows a mixture of products. However, the peak indicative of the acetylenic proton in propiolic esters is indeed present (Figure 4.3, peak a). In addition, two additional peaks found near the predicted range for the ethylene unit of 2-HEP were tentatively assigned as **b** and **c**. Although it appeared that the ester was formed, there is still evidence of sp^3 hybridized protons likely due to the reduction of the alkyne.

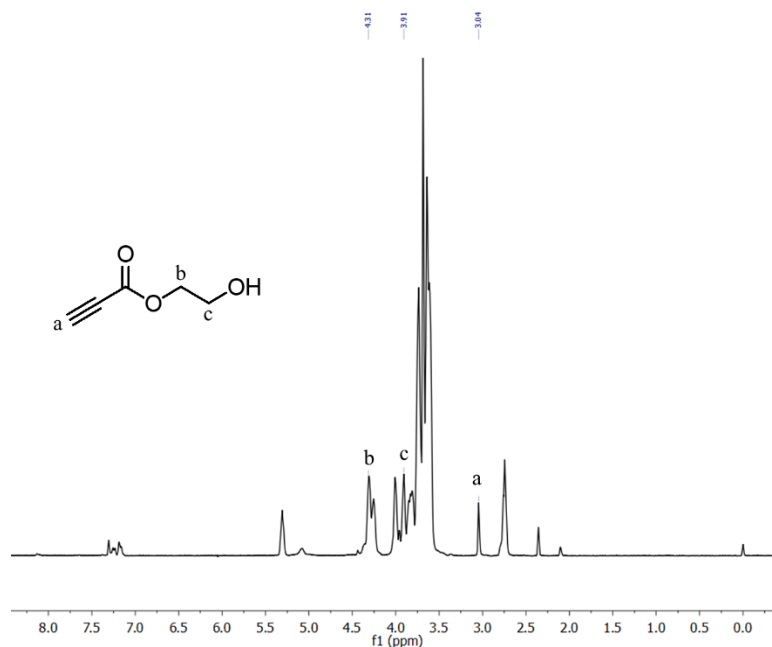


Figure 4.3 of 2-HEP synthesized by Fischer Esterification using 5:1:0.007 (ethylene glycol:propionic acid:H₂SO₄).

As shown in Figure 4.3, the crude product remained contaminated with unreacted ethylene glycol, which is revealed by the intense multiplet at approximately 3.76 ppm. To separate the desired product from ethylene glycol, the crude mixture was dissolved in an organic solvent, and the resulting solution was washed with water and brine; however, upon concentration of the organic layer it was realized that the product, even with the propiolate endcap, had partitioned into the aqueous layer instead of remaining in the organic solvent. This same result occurred with several different organic solvents including ethyl acetate, dichloromethane, and diethyl ether. Repeated attempts were made to isolate 2-HEP via vacuum distillation as well. Even at high vacuum (below 1 Torr), the product had a propensity to suddenly degrade before distillation.

As observed in the synthesis of 2-HEP from ring-opening of ethylene oxide, column chromatography could be used to isolate the desired product, but again only a

small yield was obtained (< 10 %). Although this was not enough material to react with the commercial isocyanates to create the catalyst-free low temperature cure carbamate, it was enough material to confirm the structure via other methods. Figure 4.4 shows the 600 MHz ^1H NMR of 2-HEP. As expected, there are two triplets and two singlet peaks indicative of the four sets of unique protons in 2-HEP. Peaks **a** and **b** were confirmed using similar structures reported by Gorman *et al.*² and peaks **c** and **d** were confirmed using ^1H NMR prediction software.

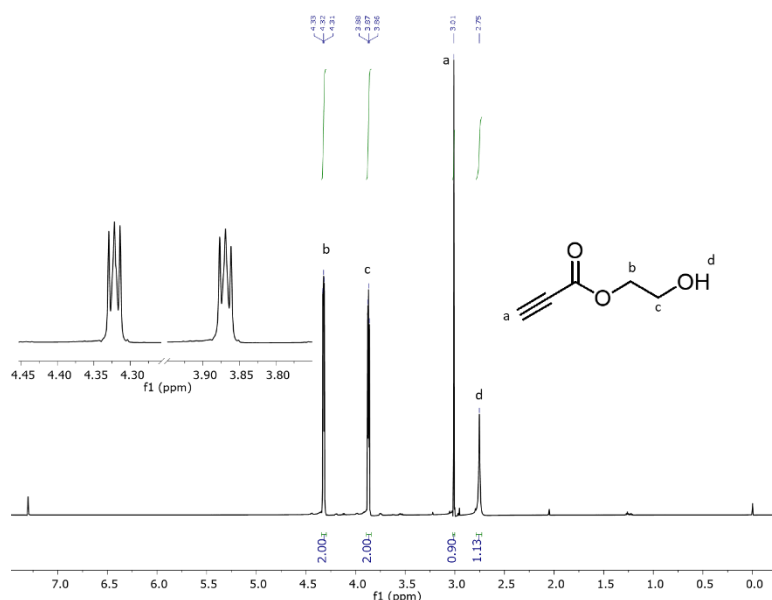


Figure 4.4 ^1H NMR spectrum (600 MHz, CDCl_3 , 23 °C) of 2-HEP. Inset shows splitting of peaks **b** and **c**.

The product (2-HEP) was further characterized by ^{13}C NMR spectroscopy (Figure 4.5). As expected, five unique carbon atoms were detected. Again similar structures reported by Gorman *et al.*² were used to confirm the identity of peaks **A**, **B**, **C**, and **D**. Peak **E** was confirmed using ^{13}C NMR prediction software (predicted value within 1 ppm).

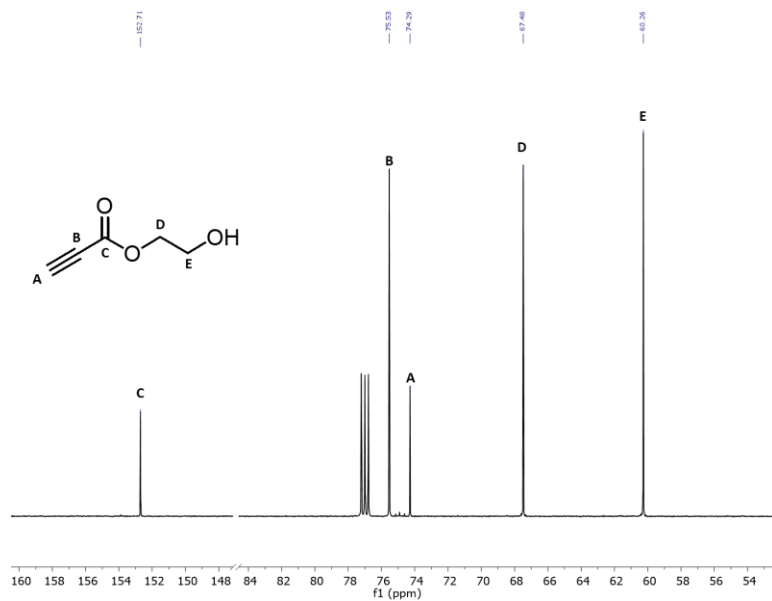


Figure 4.5 ¹³C NMR spectrum (150 MHz, CDCl₃, 23 °C) of 2-HEP.

HSQC spectroscopy was used to further confirm the ¹H and ¹³C NMR assignments, specifically the methylene protons, as shown in Figure 4.6. A significant correlation between the acetylenic proton and both carbons of the triple bond was also detected.

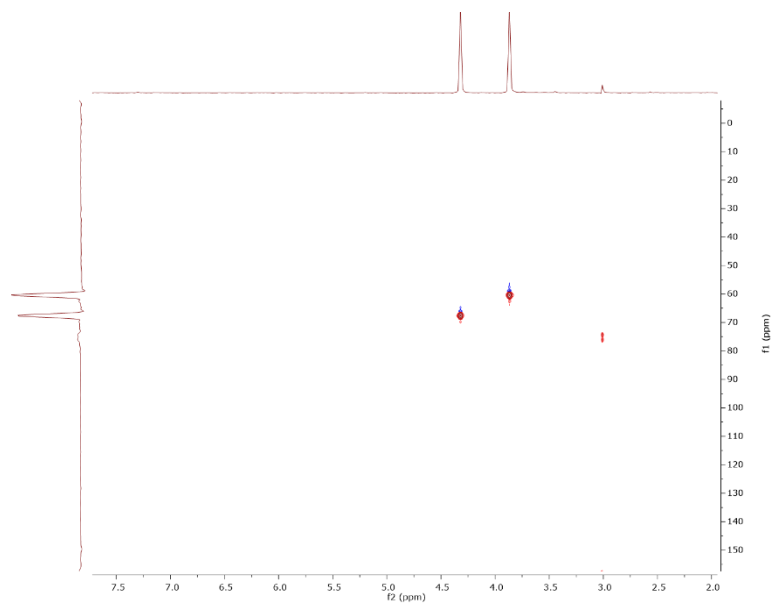


Figure 4.6 HSQC NMR spectrum (CDCl₃, 23 °C) of 2-HEP.

In addition, gas chromatography-mass spectrometry was used to verify the purity and identity of the product. As shown in Figure 4.7, a single peak was detected, indicating a single product.

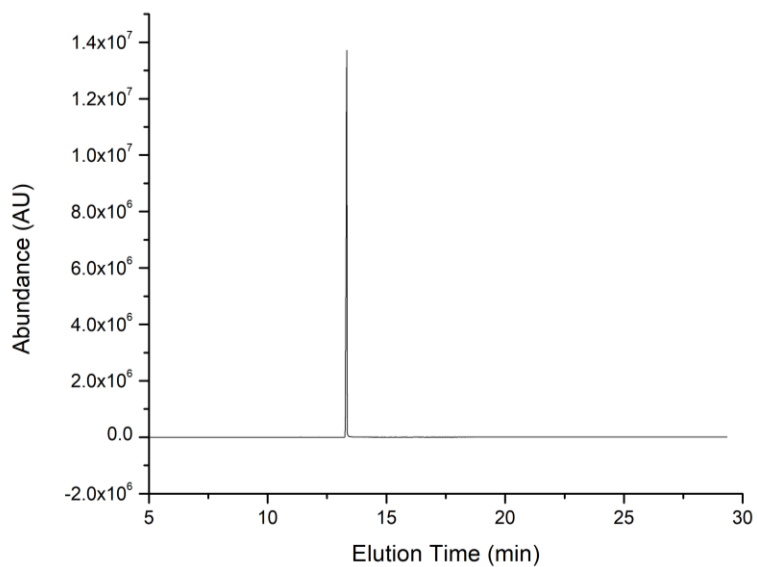


Figure 4.7 Gas chromatograph of 2-HEP.

The single peak was subsequently analyzed using mass spectrometry and the resulting spectrum is shown in Figure 4.8. Surprisingly, the molecular ion peak (m/z : 114.03) was not present, which was initially troublesome. However, this phenomenon is common for all alcohols.⁸⁰ Some prominent masses are identified in Figure 4.8. The signal at m/z 84.05 corresponds to the loss of formaldehyde, which is a common degradation product of primary alcohols. The signal at m/z 70.95 corresponds to a protonated propionic acid, indicating degradation of the ester linkage. The base peak, located at m/z 52.85 is indicative of the loss of water from the protonated propionic acid. Finally, the peak located at m/z 43.85 is indicative of loss of ethylene oxide from parent ion.

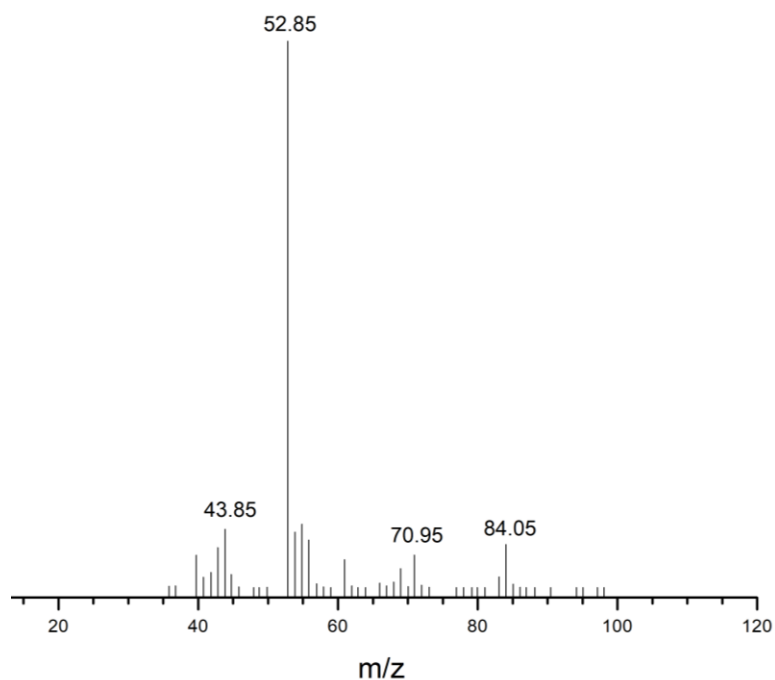


Figure 4.8 Mass spectrum of peak in Figure 4.7.

Finally, the oil was analyzed using FTIR spectroscopy (Figure 4.9). Miller *et al.*⁷⁹ analyzed their material using FTIR and the same peaks were present. For example, OH

stretching centered at 3400 cm^{-1} , $\text{C}\equiv\text{CH}$ stretching at 2100 cm^{-1} , $\text{C}=\text{O}$ stretching at 1700 cm^{-1} , and $\text{C}-\text{O}$ stretching at 1240 cm^{-1} are all present.

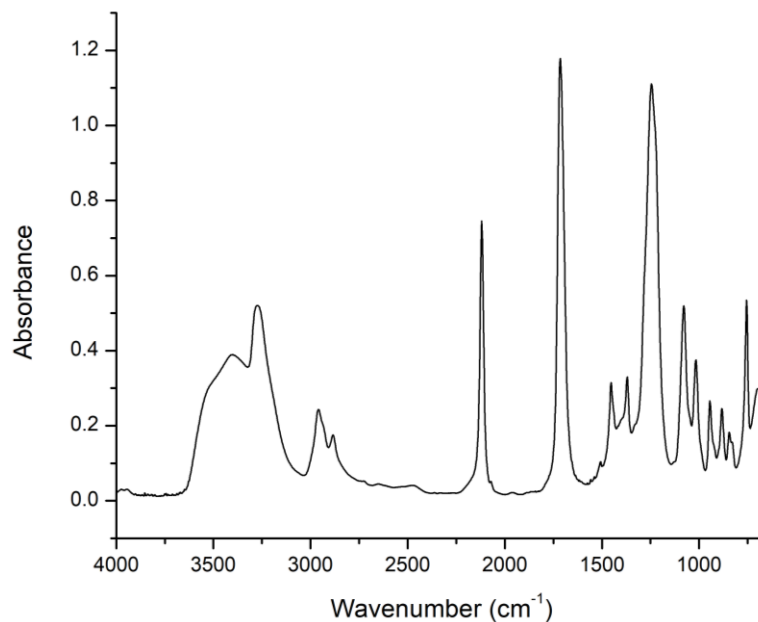


Figure 4.9 FTIR spectrum of 2-HEP.

After confirming the structure via the six techniques, the focus shifted to increasing the overall yield of the product. This led to revisiting the Fischer Esterification, as it was a facile and inexpensive method to synthesize 2-HEP. In general, the methods provided by Gorman² and Duran⁴⁷ were similar. However, Gorman used *p*-toluenesulfonic acid mono-hydrate, which is more soluble in organic media compared to the sulfuric acid catalyst used by Duran. Presumably due to greater solubility, Gorman was able to use a relatively high catalyst concentration of approximately 2.5 mol% (relative to propiolic acid); whereas Duran used only one drop of H_2SO_4 in 2.8 g of propiolic acid (approximately 0.6 mol% of H_2SO_4 relative to propiolic acid). In the synthetic pathway previously used to synthesize 2-HEP, the Duran method was followed (*vide supra*). It was hypothesized that the Gorman method would result in higher

conversion to 2-HEP as it allows a significantly higher effective catalyst concentration relative to propiolic acid. Thus, the Gorman method was closely followed. After refluxing the mixture for 24 h, the solvent was removed *in vacuo*, and then column chromatography was performed using a gradient elution of hexanes (100%) to hexanes:ethyl acetate (50:50). This resulted in a reasonable yield (10.80 g; 53.7%) of the desired 2-HEP. The ^1H NMR spectrum of the product, shown in Figure 4.10, indicates relatively high purity.

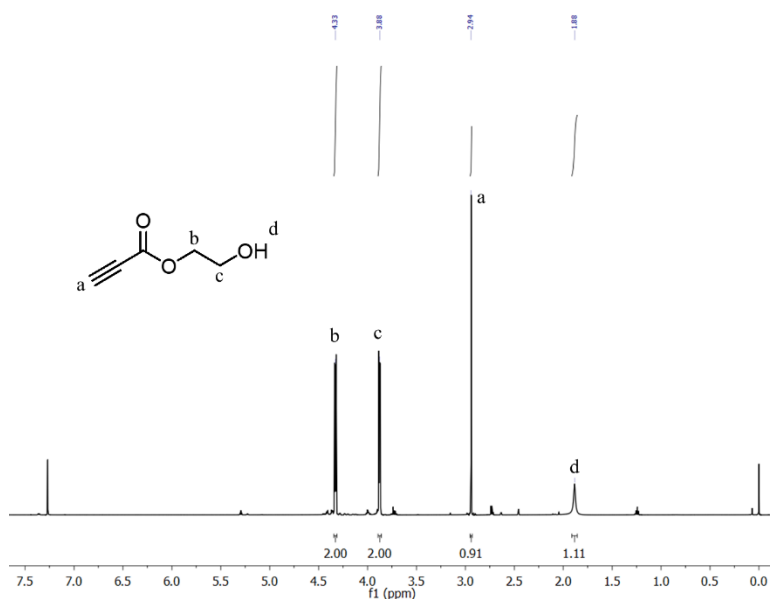


Figure 4.10 ^1H NMR spectrum (600 MHz, CDCl_3 , 23 $^\circ\text{C}$) of 2-HEP synthesized by Fischer Esterification using 5:1:0.02 (ethylene glycol:propionic acid:p-toluenesulfonic acid monohydrate) after purification.

4.3.4 Synthesis of Desmodur XP2580-2HEPC

After synthesizing an appreciable amount of 2-HEP, it was then desired to make the urethane as shown in Scheme 4.1, Route 2. Figure 4.11 shows the ^{13}C NMR spectrum of Desmodur XP2580 before and after reaction with 2-HEP. As indicated in the figure, the conversion to the desired urethane was quantitative as shown by the complete disappearance of the signal at 121.95 ppm indicative of the free isocyanate and

the appearance of signals at 74.32 indicative of the terminal carbon of the alkyne and 75.41 ppm belonging to the quaternary carbon of the alkyne. In addition, signals at 64.30 and 61.88 ppm indicative of the two methylene carbons of the 2-HEP moiety are also present post-propiolation.

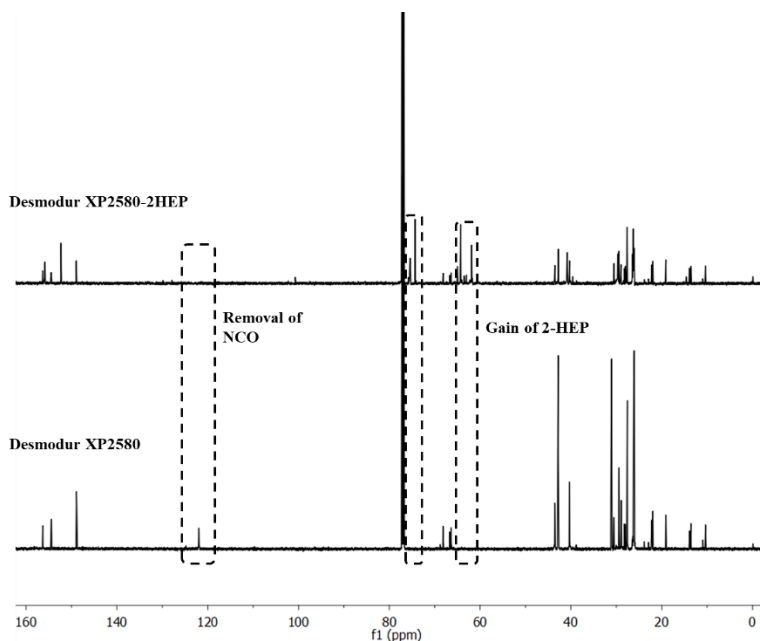


Figure 4.11 ¹³C NMR spectrum (150 MHz, CDCl₃, 23 °C) of Desmodur XP2580 as received and after propiolation.

4.3.5 Synthesis of azidated Setalux DA 870

The polyazide component was synthesized in two steps by first mesylating the hydroxyl moieties of Setalux DA 870 and then displacing the methane sulfonate under S_N2 conditions. The progress of the mesylation reaction was easily tracked using FTIR spectroscopy by following the disappearance of the broad peak centered around 3500 cm⁻¹ attributed to -OH stretching.

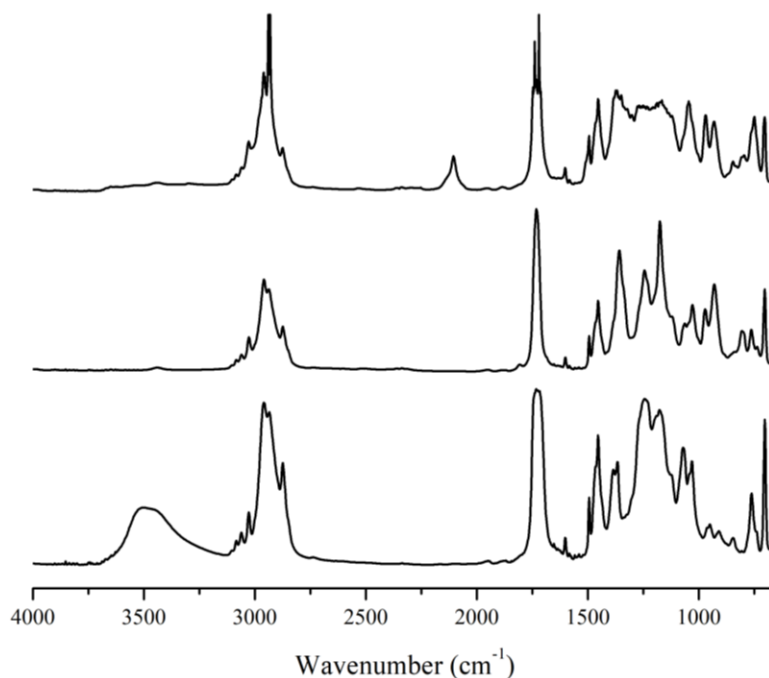


Figure 4.12 FTIR spectra of as-received Setalux DA 870 (bottom), mesylated Setalux DA 870 (middle), and azidated Setalux DA 870 (top).

Upon successful mesylation, the polymer was subjected to azidation under SN2 conditions using NaN₃ and a solvent blend of DMF and acetonitrile. Initially the reaction was carried out in 100% DMF; however, isolation of the desired resin required water washes that resulted in difficult emulsions with 100% DMF. It was determined that drastically reducing the concentration of DMF in the reaction mixture before the water washes could eliminate the emulsion; however, removal of the DMF proved to be problematic due to its high boiling point. Acetonitrile, a polar aprotic solvent but with a lower boiling point was then tried, but it was found that the azidation was sluggish. Ultimately it was discovered that a solvent blend of DMF:acetonitrile (1:10) provided suitable reaction kinetics and easy isolation of the product by first removing most of the solvents in vacuo, followed by further purification with water washes. Progress of azidation was monitored using FTIR spectroscopy (Figure 4.12), and then reaction

conversion was verified using ^1H NMR by following the disappearance of the single set of protons in the methanesulfonate.

4.3.6 Kinetic Studies

Figure 4.13 shows the isothermal kinetics of cure of the as received Setalux DA 870 cured with Desmodur XP2580, along with two modified resins Desmodur XP2580-PC (propargyl-based) and Desmodur XP2580-2HEPC (propiolate-based), each cured with azidated Setalux DA 870, within a range of temperatures from 60 to 90 °C in 10 °C increments. As expected, the conversion rapidly increased as temperature increased. For example, Desmodur XP2580-2HEPC achieved approximately 36% conversion after 1 h at 60 °C and achieved approximately 82% conversion at 90 °C over the same period. Azidated Setalux DA 870 cured with Desmodur XP2580-PC was consistently the slowest progressing reaction. The propiolate-based system had significantly faster curing kinetics, as expected. In fact, the kinetics were remarkably similar to the as received material. This observation can most clearly be seen in the kinetics performed at 90 °C where there is an almost complete overlap of the kinetic values through the isothermal cure.

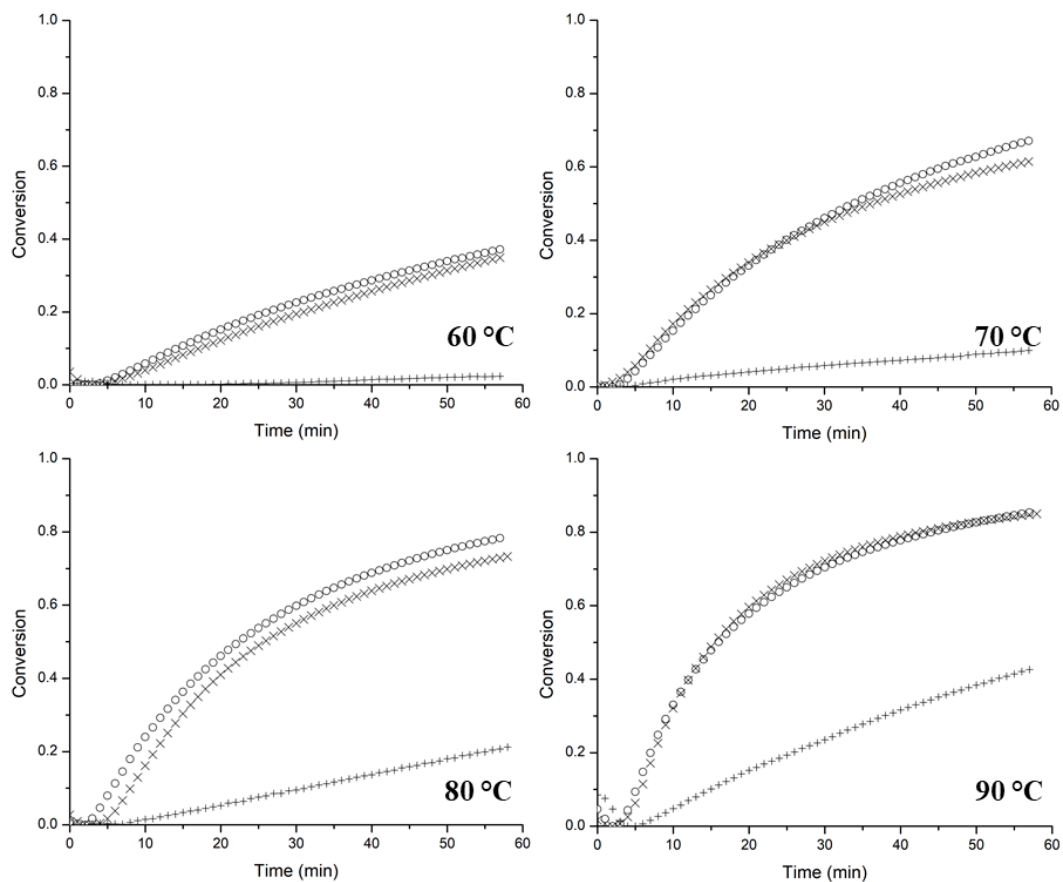


Figure 4.13 Isothermal curing kinetics at various temperatures of: as received Setalux DA 870 and Desmodur XP2580 (○), Az-Setalux DA 870 and Desmodur XP2580-PC (+), and Az-Setalux DA 870 and Desmodur XP2580-2HEPC (×).

The data in Figure 4.13 were used to calculate rate constants, k , using the integral form of the second-order rate equation, Equation 4.2, where $[A]_t$ is the concentration of reactants at time t , $[A]_0$ is the initial concentration of reactants and k is the rate constant.

$$\frac{1}{[A]_t} = kt + \frac{1}{[A]_0} \quad (4.2)$$

By plotting $[A]_t^{-1}$ vs. time, the rate constant was obtained as the slope of the line obtained through linear regression. As an example, the propiolate system isothermally cured at 70 °C is shown below (Figure 4.14). The calculated rate constants at the predetermined temperatures are displayed in Table 4.1. In most cases, this method gave a

line with $r^2 > 0.98$. The one exception was the propargyl system at 60 °C, which only had a linear regime from 20 to 60 min.

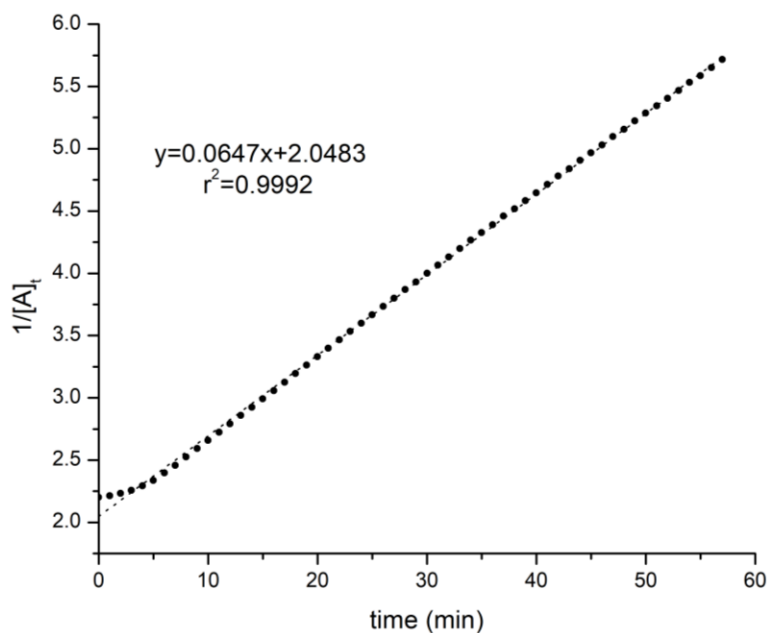


Figure 4.14 Determination of k for Az-Setalux DA870 and Desmodur XP2580-2HEPC at 70 °C.

Table 4.1 Calculated Rate Constants (k) for Each Resin Pair at Specified Temperatures

Temperature (°C)	Setalux DA 870 and Desmodur XP2580	Az-Setalux DA 870 and Desmodur XP2580-2HEPC	Az-Setalux DA 870 and Desmodur XP2580-PC
60	.016	0.022	0.003
70	.052	0.065	0.009
80	.085	0.120	0.032
90	0.141	0.246	0.087

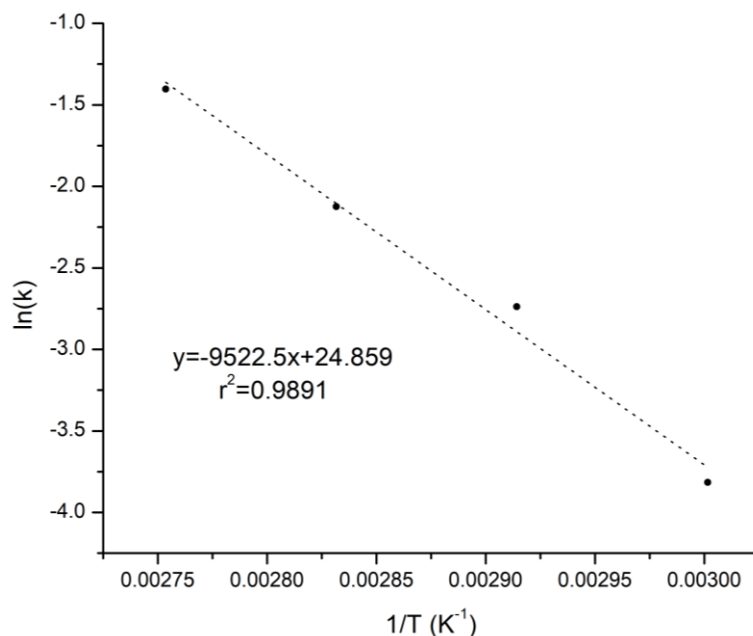


Figure 4.15 Arrhenius relationship of Az-Setalux DA870 and Desmodur XP2580-2HEPC.

Activation energy (E_a) was calculated using the Arrhenius relationship by plotting the natural log of k vs. the inverse of the absolute temperature as shown in Figure 4.15. The results are displayed in Table 4.3. In all cases the correlation coefficient was measured to be greater than 0.93. As expected, the measured activation energy was far greater for the propargyl system (110.1 kJ/mol) than either the as received (70.6 kJ/mol) or the propiolate system (79.2 kJ/mol). The reduction in E_a for the propiolic system to near the as received resin pair gives credence that the propiolate system is a good candidate for a NIPU system.

Table 4.2 Activation Energy (E_a) Calculated by the Arrhenius Relationship of Each Resin Pair

Resin Pair	E_a (kJ/mol)
Setalux DA 870 and Desmodur XP2580	69.4
Az-Setalux DA 870 and Desmodur XP2580-2HEPC	79.2
Az-Setalux DA 870 and Desmodur XP2580-PC	110.1

As a more practical method to measure the bulk conversion, MEK double rubs were chosen and the results are shown in Figure 4.16. The resin was drawn down on steel panels, and the panels were removed at various points during the cure profile (*vide supra*). The first set of samples, measured after the 2 h room temperature solvent flash, resulted in the fewest number of rubs to failure. As the temperature was increased (and time at elevated temperature), the number of double rubs before failure increased as well. Again, the propargyl system appeared to have the slowest rate of cure throughout the entire cure profile. The propiolate system did have a statistically significant faster conversion that was more apparent as the cure profile progressed. The system with the quickest cure, as indicated by double rubs, was that of the as received system. The maximum number of double rubs applied to any system was 300, at which point the test was halted. This point was achieved for the neat system after a 1 h isotherm at 100 °C. The propiolate and propargyl cured systems showed a slower rate of approach to this point as the cure progressed. Although the propiolate cured system did usually show greater resistance at a given temperature compared to propargyl, this difference was not as great as expected and is attributed to the ester linkage of 2-HEP, which may be particularly susceptible to MEK. In addition, although commercially acceptable, it is known that double rubs do not always correlate well to conversion, especially when high conversion is achieved.⁸¹

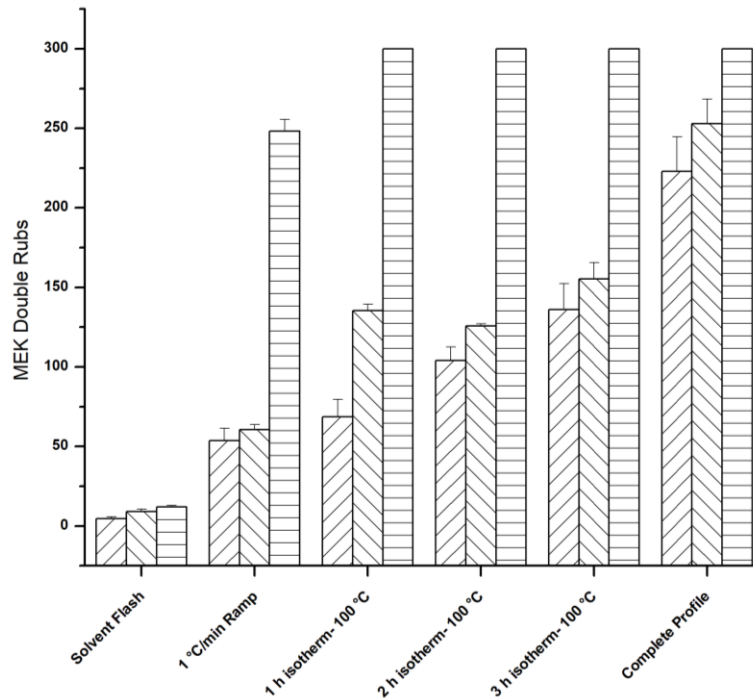


Figure 4.16 MEK double rubs, after pre-determined time points during the standard cure profile, of: Setalux DA870 and Desmodur XP2580 (horizontal lines), Az-Setalux DA870 and Desmodur XP2580-PC (forward slash), and Az-Setalux DA870 and Desmodur XP2580-2HEPC (backward slash).

4.3.7 Physical Properties of Neat and Modified Resins

A major goal of this project was to use 2-HEP to increase the kinetics of cure of the azide-alkyne NIPU while maintaining (or exceeding) all other properties inherent to the propargyl-cured system. The first part of this goal was achieved as indicated by FTIR spectroscopy and then verified at a different size-scale using MEK double rubs. Table 4.3 compares properties of the propiolate cured system to the propargyl cured system and to an unmodified control. In all cases, the coatings were drawn down on steel panels at 80% solids in butyl acetate and cured in an oven at a prescribed curing profile. The color difference (ΔE) between the propiolate cured system and the as-received resin was relatively high (26.61) and was attributed to the tendency for the resin to yellow upon mesylation and azidation. However, the ΔE between the propargyl cured system and the

propiolate cured system was extremely small (1.06) indicating a miniscule color difference between the propargyl and propiolate system. This is a very exciting result when coupled with the FTIR study, as it shows the ability to increase the kinetics of the azide-alkyne reaction without having detrimental effects to color, which would be the case if a metal catalyst were added. Gloss was similar for the propargyl and propiolate systems with the biggest difference occurring at 20 °. Pencil hardness and T_g both increased going from the as-received resins to the triazole-cured system and was attributed to the aromaticity of the triazole linkage.

Table 4.3 Performance Properties of Desmodur XP2580-2HEPC/azidated Setalux DA 870 Coating Compared to Desmodur XP2580-PC and As-Received Precursor Resins.

	Desmodur XP2580/ Setalux DA 870	Desmodur XP2580-2HEPC/azidated Setalux DA 870	Desmodur XP2580-PC/azidated Setalux DA 870
Color (L/A/B)	38.97/-12.19/9.21	37.68/-16.90/-16.95	37.81/-17.95/-16.91
Color ⁱ (ΔE)		26.61	
Color ⁱⁱ (ΔE)			1.06
Gloss 20	123.4	110.5	120.2
Gloss 60	117.3	152.0	155.0
Gloss 85	105.7	96.4	91.7
Pencil Hardness	Pass @ 2H	Pass @ 9H	Pass @ 9H
T _g (°C) ⁱⁱⁱ	40.8	41.7	45.8

ⁱ Desmodur XP2580-2HEPC/azidated Setalux DA 870 compared to Desmodur XP2580-PC/azidated Setalux DA870.

ⁱⁱ Desmodur XP2580-2HEPC/azidated Setalux DA 870 compared to Desmodur XP2580/Setalux DA 870.

ⁱⁱⁱ Designated as the midpoint of the inflection as measured by DSC.

4.4 Conclusions and Future Work

The overall goals of this chapter were to first synthesize, isolate, and characterize 2-HEP, and then to use 2-HEP to create a novel NIPU with accelerated curing kinetics but with few physical properties differences compared to the propargyl cured system studied in the previous chapter. These goals were achieved. A novel method was used to synthesize 2-HEP, and the isolated material was characterized using ¹H, ¹³C, and HSQC

NMR, GC-MS, and FTIR. Previously, this useful molecule was only characterized by FTIR, elemental analysis and boiling point. After a synthetic strategy yielded an appreciable amount of 2-HEP, it was reacted with Desmodur XP2580 to yield a polyurethane functionalized with an activated alkyne. RT-FTIR was used to characterize the curing kinetics of this NIPU when mixed with azidated Setalux 870, which showed a marked increase in kinetics relative to the propargyl system. In fact, the kinetics were accelerated so greatly that they closely mirror that of the as-received resins. MEK double rubs were performed as a second and more practical way to monitor the conversion of the system, which showed that the as-received system was most resistant to MEK. The propiolate and propargyl cured systems showed a slower rate of resistance as the cure progressed. Although the propiolate cured system did usually show greater MEK resistance at a given temperature compared to propargyl, this difference was not as great as expected and is attributed to the ester linkage of 2-HEP, which may be particularly susceptible to MEK. As expected, there was a marked difference in color between the as-received system compared to the propiolate cured system. However, the color of the propiolate and propargyl cured systems were nearly identical, which shows the ability to increase the kinetics of cure without sacrificing color of the system. The hardness of the coating increased in the NIPUs due to the incorporation of the triazole rings. Finally, the T_g showed an interesting trend in the fact that it increased by 5 °C when comparing the propargyl cured to the as-received system. However, the T_g of the propiolate system was similar to that of the as-received system, which can be attributed to the CH_2 spacer and ester linkage.

There are a number of ways to further this research. One immediate interest would be to incorporate various amounts of Desmodur XP2580-PC to Desmodur XP2580-2HEPC to determine if the kinetics can be tailored for a slower room-temperature cure, which could extend pot-life. Another interesting approach would be to synthesize the propiolate ester using higher order ethylene glycol oligomers. This could theoretically reduce the curing temperature and also reduce the very high viscosity of the system. Finally, a new monomer, 2-hydroxyethylpropiolamide could be explored. This monomer should be easily synthesized by the carbodiimide coupling of ethanolamine and propiolic acid and could impart new properties such as an increased MEK solvent resistance or harder coatings resulting from the additional hydrogen bonding.

CHAPTER V - LOW VISCOSITY NON-ISOCYANATE POLYURETHANE
COATINGS VIA AZIDO-ALKYNE CYCLOADDITION USING MONO-
HYDROXYETHYLENE GLYCOL OLIGOMERS

5.1 Introduction

Chapters III and IV discussed the successful development of non-isocyanate polyurethane (NIPU) coatings that cure *via* azido-alkyne cycloaddition (triazole formation). In Chapter III, the synthetic strategy for a propargyl-based, triazole-forming NIP was developed. Propargyl-functional polyurethanes (propargyl carbamate resins) were synthesized by reaction of propargyl alcohol with commercial polyisocyanate resins such as Desmodur N3200A. Azide-functional co-reactants were prepared by first mesylating and subsequently azidating polyols of the polyether (PPG 1000), polyester (Desmophen 650A), and polyacrylic type (Setalux DA 870). These functional polymers were then mixed and cured *via* azide-alkyne cycloaddition. The cure was carried out either in the presence of Cu(I) to achieve quick-curing coatings with desirable properties, except for slight color resulting from the catalyst, or in the absence of Cu(I) to produce a slower curing coating with properties and color nearly identical to coatings formed from the urethane-forming precursor resins. Chapter IV outlined the development of a propiolate-based, triazole-forming NIPU, which, when cured in the absence of Cu(I), produced curing kinetics and color similar to those of the precursor resins. However, in all cases the carbamate systems exhibited a very high viscosity, which makes them impractical in traditional coating applications unless highly diluted by suitable organic solvents (VOC). Although effective, this solution introduces new issues in that these VOCs must conform to stringent legislation pushing for minimal or zero VOC.^{19,82,83}

Harkal *et al.*⁸⁴ have demonstrated the synthesis of low-viscosity NIPU coatings that cure by epoxy-amine reaction. These authors reacted hexamethylene diisocyanate (HDI) biuret with glycidol to produce glycidyl carbamate resins. When 100% of the isocyanate groups were reacted with glycidol, their resins exhibited substantial increases in viscosity. However, they showed that viscosity could be dramatically reduced by reacting a fraction of the isocyanate groups with a non-functional alcohol or ether alcohol. For example, the viscosity of their glycidyl carbamate resin was reduced by 69% when a third of the glycidol was replaced with 2-ethyl hexanol and by a remarkable 91% when a third of the glycidol was replaced by diethyleneglycol monobutylether. Harkal *et al.* concluded that, in general, ether alcohols were more efficient than alcohols for lowering the viscosity of the resins. This strategy involved covalent attachment directly into the network of molecules well-known for their plasticizing effect,^{85,86} thus eliminating VOCs. However, this strategy has been applied only to epoxy-amine NIPU coatings, and the authors neglected to determine whether the degree of polymerization of the ethylene glycol oligomer or the endcap structure was the greater contributor in viscosity reduction.

This chapter discusses the use of three ether alcohols, ethylene glycol monoethyl ether (EGME), diethylene glycol monoethyl ether (DEGME), and diethylene glycol monobutyl ether (DEGBE) to determine their effect on resin viscosity as well as coating properties, when used in the manner of Harkal *et al.* to modify the structure of the propargyl-based, triazole-forming NIPU coatings introduced in Chapter III (Scheme 5.1). These particular ether alcohols were specifically chosen to provide evidence as to

whether the ethylene glycol moiety or the endcap plays a bigger role in resin viscosity reduction as well as final coating properties.

5.2 Experimental

5.2.1 Materials

Desmodur XP2580 was generously donated by Covestro. Propargyl alcohol (99%), diethylene glycol monoethyl ether (99%; ReagentPlus®), *n*-butyl acetate (ACS reagent; ≥99.5%), and diethylene glycol monobutyl ether (≥99%) were purchased and used as received from Sigma-Aldrich. Dibutyltin dilaurate was purchased from Strem Chemicals. Ethylene glycol monoethyl ether (laboratory grade) was purchased from Fisher Chemical and used as received.

5.2.2 Instrumentation

Proton nuclear magnetic resonance (^1H NMR) spectra were obtained using a 600.13 MHz Bruker Ascend (TopSpin 3.5) NMR spectrometer. Typical acquisition parameters were 10 s recycle delay, 7.8 μs pulse corresponding to a 45° flip angle, and an acquisition time of 1.998 s. The number of scans acquired for each sample was 32. All ^1H chemical shifts were referenced to TMS (0 ppm). Sample solutions were prepared at a concentration of approximately 2.5% (w/v) in CDCl_3 containing 1% TMS as an internal reference, and the resulting solution was charged to a 5 mm NMR tube. Carbon nuclear magnetic resonance (^{13}C NMR) spectra were obtained using a frequency of 150.90 MHz. Typical acquisition parameters were 1 sec recycle delay, 11 ms pulse corresponding to a 45° flip angle, and an acquisition time of 0.908 s. The number of scans acquired for each sample was 1024. All ^{13}C chemical shifts were referenced to residual chloroform (77.16 ppm). Sample solutions were prepared at a concentration of approximately 5 wt% in

CDCl_3 containing 1% TMS as an internal reference, and the resulting solution was charged to a 5 mm NMR tube.

Isothermal viscosity was measured using a strain-controlled ARES (TA Instruments) at room temperature using cone and plate methodology. The cone had a diameter of 50.0 mm with an angle of 0.04 radians, and the frequency used was 1 rad/s. Strain sweeps were performed on all specimens. The results showed that 50% strain fell within the linear viscoelastic regime for nearly all specimens, and therefore this strain value was used for all subsequent viscosity measurements. Data were collected in 10 s intervals over a 30 min period resulting in 180 total points. The data reported are the average and standard deviation of these points.

Differential scanning calorimetry (DSC) was performed using a TA Instruments Q200. To obtain free-standing films for DSC as well as dynamic mechanical analysis, azide and alkyne components were mixed at approximately 1.3:1 (azide:alkyne) and the resulting, liquid coatings were drawn down onto CHEMFILM® ECTFE fluoropolymer films. The coatings were then cured in an oven using the “standard cure profile” described in Chapter IV. For DSC analyses, the cured coatings, which had little adhesion to the fluoropolymer substrate, were peeled off and punched to give circular samples that fit within a DSC pan. Stacks of five (~5 mg) were placed in pans that were hermetically sealed. A heat/cool/heat cycle was performed on samples starting at -50 °C, rising to a maximum of 200 °C, and returning to -50°C, at a rate of 10 °C/min . The T_g of the cured material was determined from the second heating cycle, and TA Universal Analysis software was used to determine the midpoint of the T_g inflection as the reported value.

Dynamic mechanical analysis (DMA) was performed on a TA Instruments Q800 in tension mode at a strain of 0.05% and a frequency of 1 Hz. Specimens were prepared by drawdown on CHEMFILM® ECTFE fluoropolymer films as stated above and were approximately 12.00 mm length, 5.00 mm width, and 0.1 mm thickness. The temperature was ramped at 2 °C/min from 0 °C to 100 °C in an inert environment. The data were exported to TA Universal Analysis Software, which was used for calculation of the storage modulus (E') and $\tan\delta$.

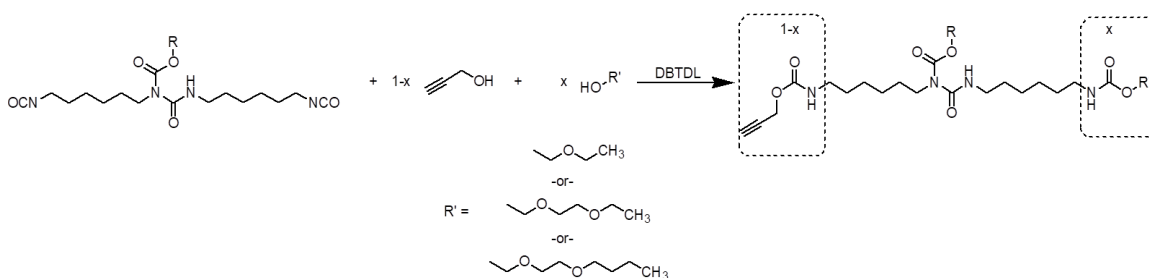
5.2.3 Synthesis

The synthesis of Azidated Setalux DA 870 can be found in Chapter IV-Reduced Temperature Non-Isocyanate Polyurethane Coatings via Catalyst-Free Azido-Alkyne Cycloaddition.

The low-viscosity non-isocyanate resins were all synthesized similarly. As an example, the synthesis of the propargyl carbamate of Desmodur XP2580 containing 33 mol% diethylene glycol monobutyl ether (67 mol% propargyl alcohol) will be described. To a 3-neck 100 mL round bottom flask equipped with mechanical stirrer, thermocouple, and addition funnel, Desmodur XP2580 (50.968g; 19.3% isocyanate; 0.234 mol isocyanate) and DBTDL (0.443 g) were charged. DEGBE (12.432 g; 76.63 mmol) was added to the addition funnel. The flask was lowered into an ice bath, and the system was allowed to equilibrate under continuous N_2 for 10 min. After the equilibration, DEGBE was added to the stirring solution at 1 drop/sec, and the temperature of the reaction was closely monitored. If the reaction temperature exceeded 30 °C, the addition of DEGBE was halted until the temperature fell below 20 °C. After complete addition of DEGBE, the reaction was allowed to progress at reduced temperature for approximately 30 min.

After this time, propargyl alcohol (8.914 g; 0.159 mol) was added to the top of the addition funnel using a syringe, and its dropwise addition (1 drop/sec) to the reaction mixture was begun. The same precautions were taken during the addition of propargyl alcohol that were taken during the addition of DEGBE. After complete addition of propargyl alcohol, the reaction was allowed to warm to room temperature, and the product was transferred to storage container for subsequent use.

Scheme 5.1 Synthesis of low-viscosity resins.



5.2.4 Preparation of Coated Substrates

All coatings were prepared similarly with a slight excess of azide (1.05:1). As an example, Azidated Setalux DA 870 cured with Desmodur XP 2580-PC will be described. Azidated Setalux DA 870 (3.8285 g; 91.4% solids; 7.200 mmol azide) and Desmodur XP 2580-PC (1.5034 g; 5.49 mmol propargyl) and butyl acetate (0.5439 g) were hand mixed in a scintillation vial until smooth. The mixture was then placed in a FlakTech mixer and allowed to mix at 1800 rpm for approximately 20 min. The mixture was drawn down on QD steel or CHEMFILM® ECTFE fluoropolymer films at 6 mil thickness. The coatings were then cured in an oven using the “standard cure profile” described in Chapter IV.

5.2.5 Coatings Testing

Reaction conversion was qualitatively compared using methyl ethyl ketone (MEK) double rubs using cheesecloth and a 32 oz hammer according to ASTM D5402.

Adhesion was determined using the crosshatch adhesion test by using a 25-square grid cut by a razor and grading on a 0B-5B scale based on the percent coating remaining after having been taped and quickly removed at a 180° angle. Hardness was measured using a pencil hardness test in accordance with ASTM D3363. Using a BYK-Gardner glossmeter, the coatings were tested at 20°, 60°, and 85°. The color of the panels was determined using a BYK-Gardner colorimeter based on L*, a, b* values.

5.3 Results and Discussion

5.3.1 Initial Viscosity Measurements

Reaction of HDI-based resins such as Desmodur N3200 or XP2580 with propargyl alcohol caused a dramatic increase in viscosity, attributed to extensive hydrogen bonding among carbamate groups. We have shown that viscosity increase upon propargyl carbamate formation varies greatly with changes in resin structure. For example, as shown in Table 5.1, Desmodur N3200 increases from 1.6 to 2200 Pa-s upon formation of the propargyl carbamate and Desmodur XP2580 increases from 0.3 to 77.9 Pa-s.

Table 5.1 Viscosity of Various Modified Resins

Resin	Viscosity (Pa-s)
Desmodur N3200 (HDI biuret trimer)	1.6
N3200 propargyl carbamate	2,200
Desmodur N3300 (HDI isocyanurate trimer)	12.8
N3300 propargyl carbamate	362
Desmodur XP2580	0.3
XP2580 propargyl carbamate	77.9

Assuming that the large viscosity increase was the result of hydrogen bonding, viscosity should be reduced by adding a hydrogen bond donor/acceptor solvent such as isopropanol or 1-propanol. As shown in Figure 5.1 for the case of Desmodur N3200

propargyl carbamate (PC), the viscosity does decrease substantially as the wt% of 1-propanol is increased, with the largest increase happening between the addition of 2 and 5 wt% of 1-propanol. This effect of reduced viscosity is attributed to disrupting polymer-polymer hydrogen bonding interactions.

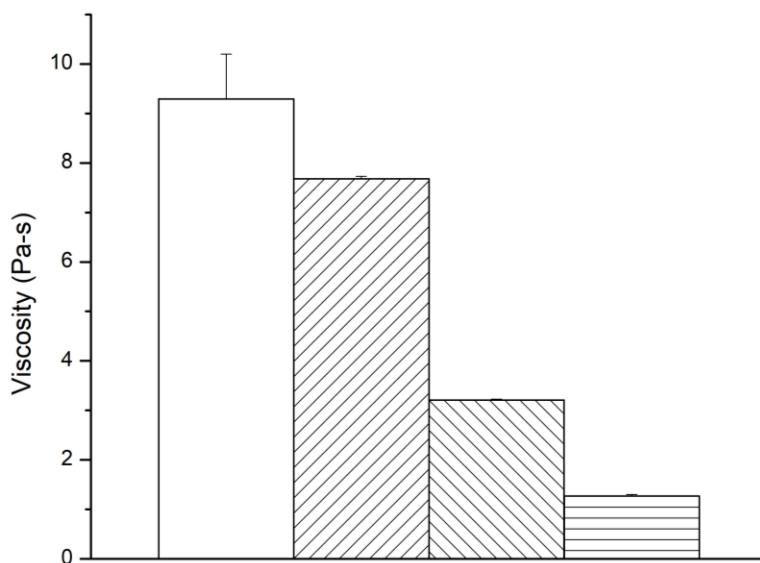


Figure 5.1 Isothermal viscosity of Desmodur N3200-PC with various amounts of 1-propanol: 0 wt% (empty), 2 wt% (forward slash), 5 wt% (back slash), and 10 wt% (horizontal slash). All systems additionally contained approximately 20 wt% n-butyl acetate.

Polyurethane coatings formulators are more familiar with the use of isopropanol as opposed to 1-propanol, since the free isocyanates in traditional polyurethanes react more slowly with the secondary alcohol vs. a primary alcohol.⁸¹ With this in mind, the experiment was repeated but using isopropanol in the second iteration. Again, the viscosity decreased as the amount of isopropanol was added with the most significant drop in viscosity occurring between 2 and 5 wt% (Figure 5.2). The results between the two sets of data agree remarkably well indicating that only the presence and not the identity of the hydrogen bond donor seems to be the dominating factor in reducing viscosity.

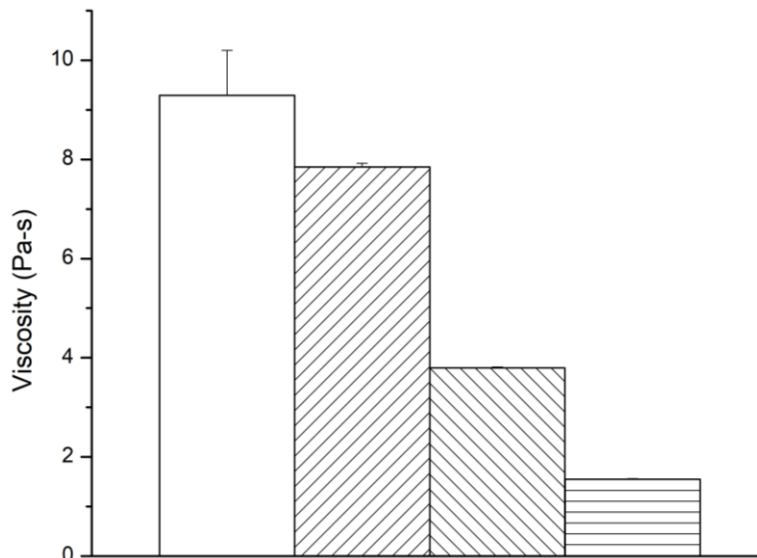


Figure 5.2 N3200-PC with various amounts of isopropanol: 0 wt% (empty), 2 wt% (forward slash), 5 wt% (back slash), and 10 wt% (horizontal slash). All systems contained approximately 20 wt% n-butyl acetate.

Addition of the propanol, although effective, had the major disadvantage of increasing VOC, and therefore we sought to decrease viscosity via a different mechanism, *i.e.* plasticization. Incorporating the plasticizer in this manner would still reduce the viscosity of the resin and have the additional benefit of limiting additional volatile organic compounds (VOCs) in the coating formulation, which as previously stated is a crucial factor in new coating formulations due to strict legislation in North American and Europe such as The Clean Air Act.

5.3.2 ^{13}C and ^1H NMR Characterization of Low Viscosity Propargyl Carbamates

Both proton and carbon NMR were used to analyze the low-viscosity resins. First ^{13}C NMR was used to determine the complete consumption of the isocyanate moiety. Figure 5.3 is an overlay of Desmodur XP2580-PC, in which the propargyl moieties have been diluted with various amounts of EGMEE. As shown in this figure, the peak at 121.95 ppm corresponding to the unreacted isocyanate is not present in any of the other

resins indicating complete consumption of isocyanate, and a new peak is present at 155.38 ppm, which is indicative of the formation of the carbamate moiety. The presence of peaks at 74.40 and 78.36 ppm are indicative of the propargyl moiety.² In addition, there are three new peaks upfield of 80 ppm corresponding to the ethylene glycol oligomer.

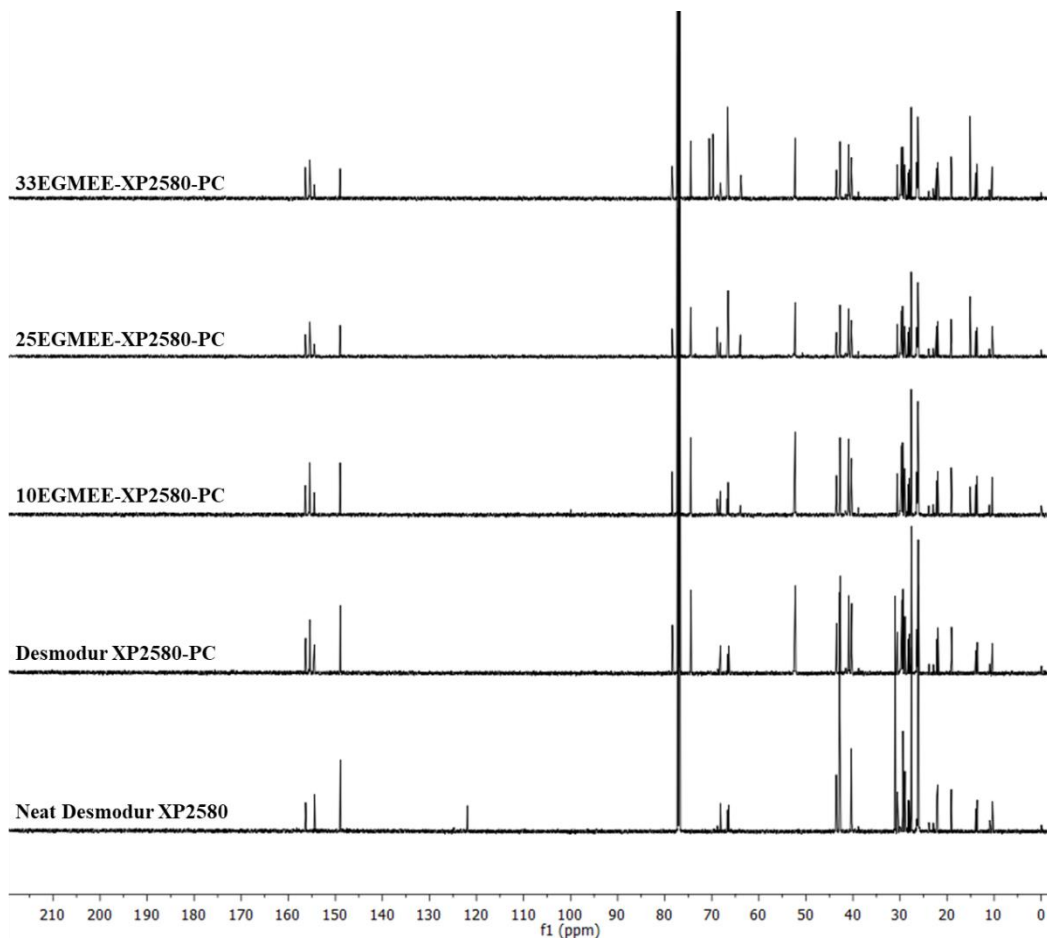


Figure 5.3 ^{13}C NMR spectrum (150 MHz, CDCl_3 , 23 °C) of EGME-modified propargyl carbamates as well as the Desmodur XP2580 precursor and Desmodur XP2580-PC.

Similar trends are present in Figure 5.4, which shows ^{13}C NMR spectra of resins modified with DEGBE. The complete disappearance of the peak at 121.95 ppm along with the appearance of the peak at 155.38 ppm indicates complete conversion from the isocyanate to a carbamate. Again, peaks are present at 74.40 and 78.36 ppm in the

modified resins indicating propargylation and finally there are multiple new peaks upfield of 80 ppm indicative of the ethylene glycol dimer.

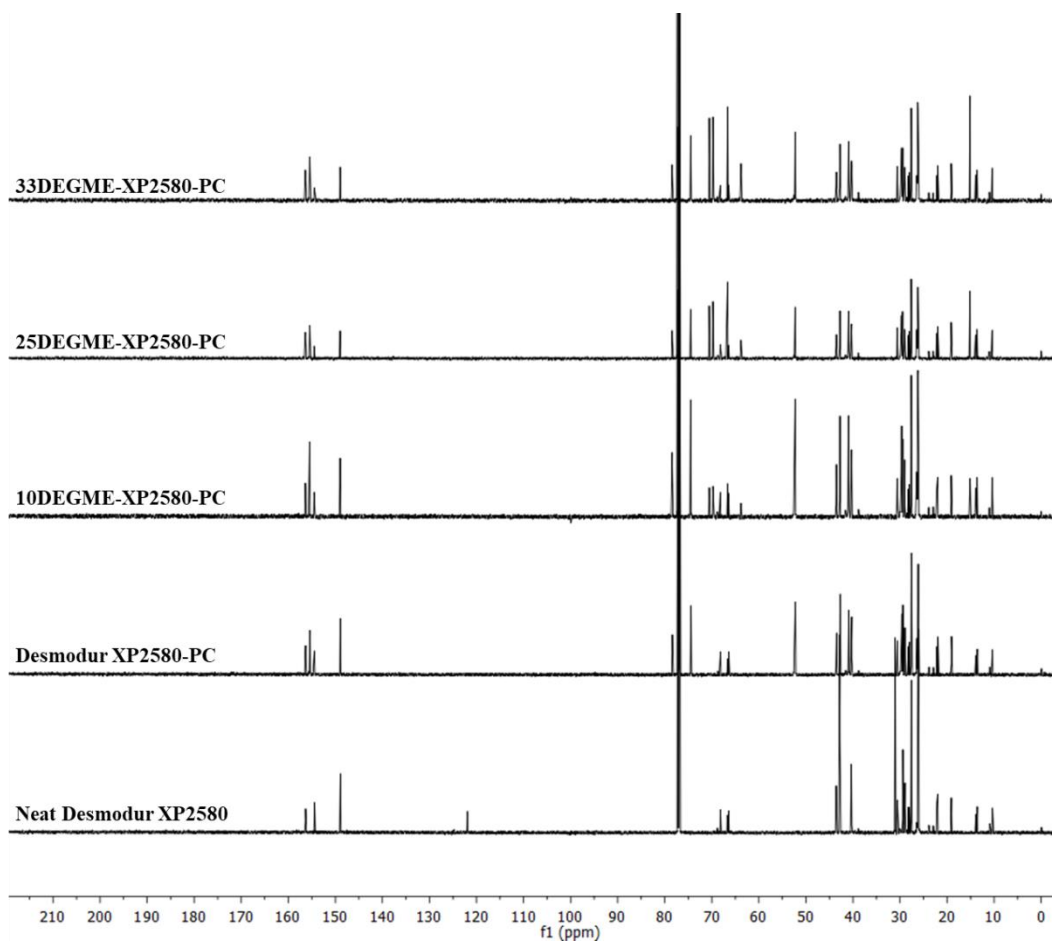


Figure 5.4 ^{13}C NMR spectrum (150 MHz, CDCl_3 , 23 °C) of DEGBE-modified propargyl carbamates as well as the Desmodur XP2580 precursor and Desmodur XP2580-PC.

Finally, the same trends can be seen in Figure 5.5, which shows ^{13}C NMR spectra of resins modified with DEGBE. Once again, the complete disappearance of the peak at 121.95 ppm along with the appearance of the peak at 155.38 ppm indicates quantitative conversion from the isocyanate to a carbamate. Likewise, peaks are again present at 74.40 and 78.36 ppm in the modified resins indicating propargylation. Again, there are many additional peaks upfield of 80 ppm, indicative of diethylene glycol butyl ether.

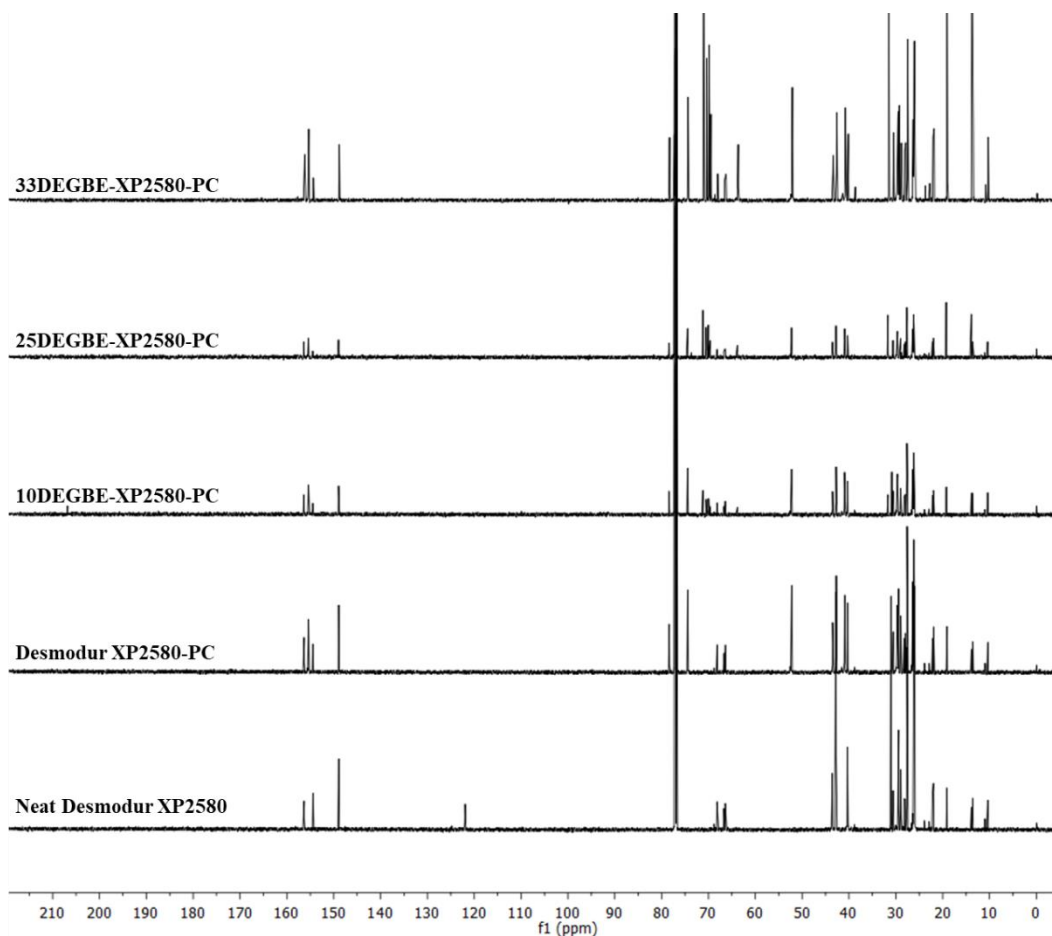


Figure 5.5 ^{13}C NMR spectrum (150 MHz, CDCl_3 , 23 °C) of DEGBE modified propargyl carbamates as well as neat Desmodur XP2580 and Desmodur XP2580-PC.

5.3.3 600 MHz ^1H NMR Characterization of Low Viscosity Propargyl Carbamates

After ^{13}C NMR evidence indicated that the isocyanate was completely converted to the respective carbamate, 600 MHz ^1H NMR was used to determine the relative ratio of reactive (propargyl) and unreactive (monohydroxy ethylene glycols) moieties which was, in turn, used in formulation of the low viscosity coatings. The subsequent figures in this section show representative spectra of each type of monohydroxy ethylene glycol used in this study. Figure 5.6 shows the ^1H NMR spectrum of 33EGME-XP2580-PC. Peaks **a** and **b** were chosen to calculate the %propargyl due to their baseline resolution and the fact that they represent the same number of protons within the molecule. As

shown in previous work (Chapter III) peak **a** was determined to be the methylene adjacent to the alkyne. Worthy of note, the shoulder slightly downfield of the main peak corresponding to **a** is present in all samples. The cause for this artifact is unknown but has been included in all integrations. Peak **b** was assigned to the protons adjacent to the terminal methyl in ethylene glycol monoethyl ether and, as predicted by the molecular structure, is a quartet. The equation for calculating %propargyl is shown in Equation 5.1 where I_a is the integration for peak **a**, and I_b is the integration for peak **b**. All integrations are divided by the number of corresponding protons they represent in a single molecule, which in all cases is two. Since the number of protons for **a** and **b** are equivalent, these values cancel. The reduced form is shown in Equation 5.1.

$$\%propargyl = \frac{I_a}{I_a + I_b} \times 100 \quad (5.1)$$

As can be seen in Table 5.2, the actual propargylation (67.3%) was nearly identical to the targeted propargylation (67%).

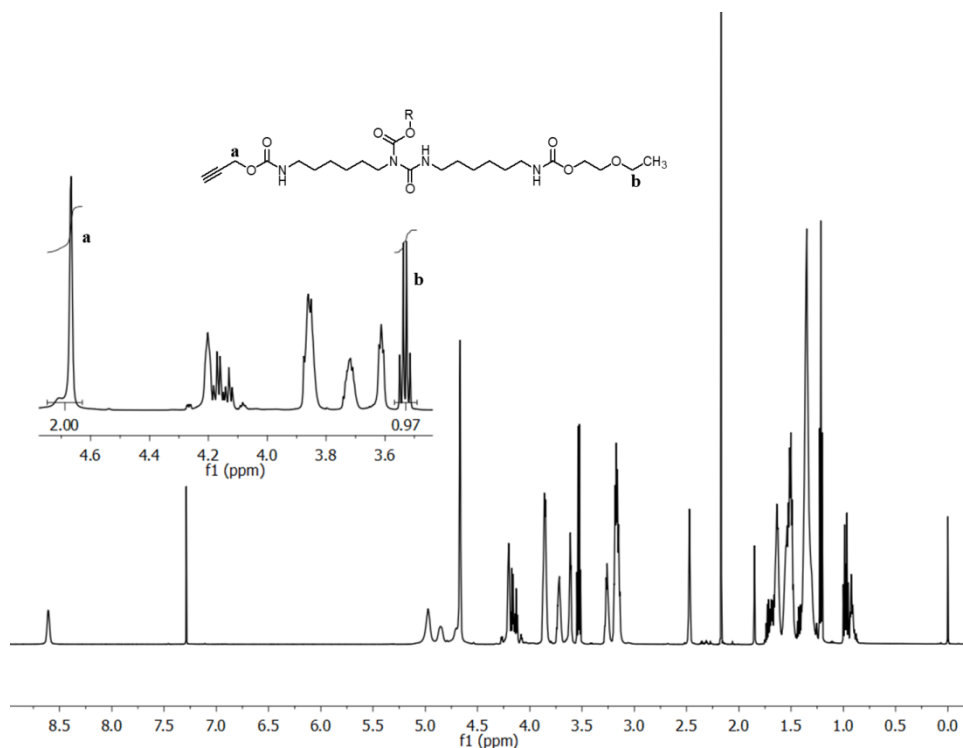


Figure 5.6 ¹H NMR spectrum (600 MHz, CDCl₃, 23 °C) of 33EGME-XP2580-PC. Inset shows region used to verify %propargyl.

Figure 5.7 depicts the 600 MHz ¹H NMR spectrum of 33DEGME-XP2580-PC. The shift corresponding to the methylene adjacent to the alkyne, **a**, has a similar shift to the corresponding protons in Figure 5.6 and again the shoulder upfield of the main peak is present. The shift corresponding to the protons adjacent to the terminal methyl in diethylene glycol monoethyl ether, **b**, again, results in a quartet, which is predicted by the molecular structure. The %propargylation calculated for 33DEGME-XP2580-PC was 66.9% as displayed in Table 5.2, which is nearly indistinguishable from the targeted propargylation.

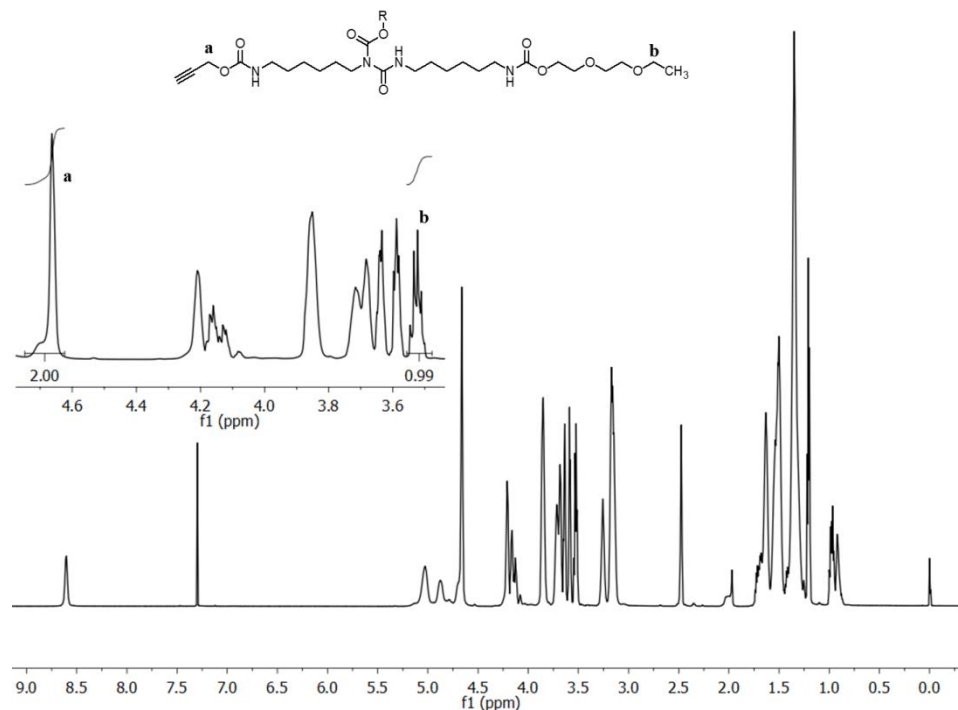


Figure 5.7 ¹H NMR spectrum (600 MHz, CDCl₃, 23 °C) of 33DEGME-XP2580-PC. Inset shows region used to verify %propargyl.

Figure 5.8 illustrates the 600 MHz ¹H NMR spectrum of 33DEGBE-XP2580-PC. The shift corresponding to the methylene adjacent to the alkyne, **a**, has a similar shift to the corresponding protons shown in Figure 5.6 and Figure 5.7, and again a shoulder slightly upfield of the predominant peak is present. The shift corresponding to the protons of the terminal butyl group adjacent to the ether moiety, **b**, results in a triplet as predicted by the molecular structure. The %propargylation calculated for 33DEGBE-XP2580-PC was 66.9% (Table 5.2), which is again nearly equivalent to the targeted propargylation of 67%.

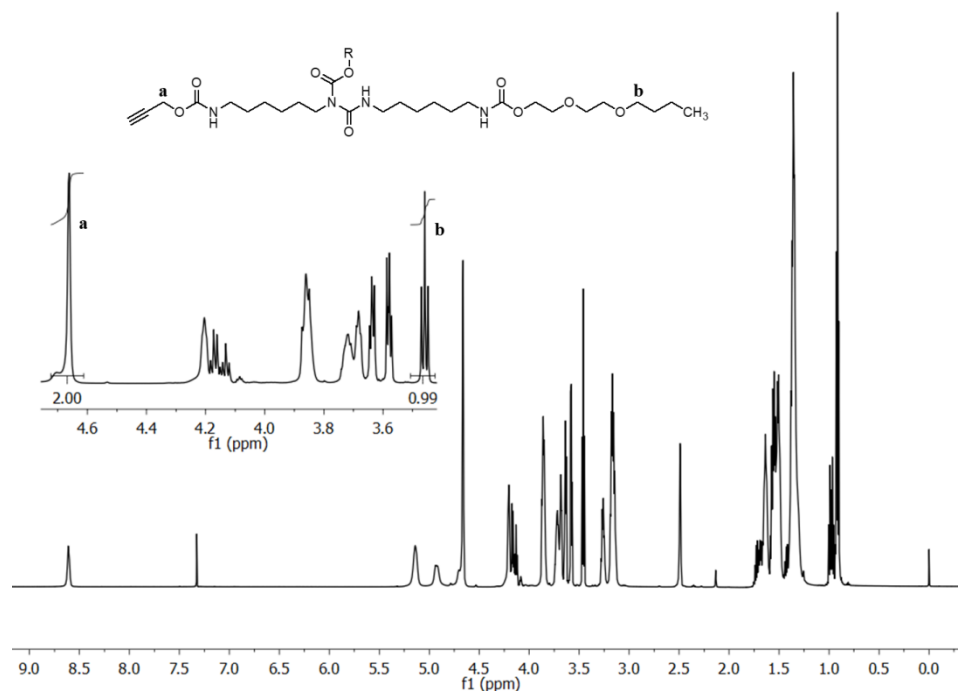


Figure 5.8 ^1H NMR spectrum (600 MHz, CDCl_3 , 23 °C) of 33DEGBE-XP2580-PC. Inset shows region used to verify %propargyl.

The targeted and actual propargylations, calculated by Equation 5.1, are shown in Table 5.2. In all cases, the actual propargylation agreed extremely well with the targeted propargylation. The largest error occurred with 25DEGBE-PC, at 1.3 %error, while for the majority of the formulations the error was less than 0.2%.

Table 5.2 Propargylation Results of Ethylene Glycol Modified Resins

Name	Targeted Propargylation (%)	Actual Propargylation ⁱ (%)
10EGME-PC	90.0	90.1
25EGME-PC	75.0	74.9
33EGME-PC	67.0	67.3
10DEGME-PC	90.0	90.1
25DEGME-PC	75.0	74.9
33DEGME-PC	67.0	66.9
10DEGBE-PC	90.0	90.5
25DEGBE-PC	75.0	76.0
33DEGBE-PC	67.0	66.9

ⁱDetermined by 600 MHz ^1H NMR.

5.3.4 Viscosity Analysis of Modified Resins

As stated previously, the propargylation of HDI-based resins such as Desmodur XP2580 resulted in a dramatic increase in viscosity, attributed to extensive hydrogen bonding among carbamate groups between chains. With this in mind, we believed it would be possible to reduce the viscosity of the system by incorporating plasticizing moieties into the system. Figure 5.9 shows the viscosity of the carbamate resins functionalized with 10 (forward slash), 25 (backward slash), and 33 (horizontal slash) mol% of either EGME, DEGME, or DEGBE (remaining carbamates are functionalized with propargyl). Each set of data also contains the 100% propargylated specie (open box) and the unmodified, precursor resin (vertical slashes). The resins functionalized with EGME and DEGME follow the same general trend. Upon incorporation of a small percentage (10%) of either EGME or DEGME, the viscosity increased significantly (146% and 124% for EGME and DEGME, respectively) relative to the 100% propargylated system. However, as the substitution percentage was increased to 25 and finally to 33%, the viscosity fell below the original viscosity for both EGME and DEGME. At 33% the viscosity was 68% and 38% of the original viscosity, for for EGME and DEGME, respectively. The initial spike in viscosity was surprising, but we theorize that there is a certain threshold of either EGME or DEGME needed to properly plasticize the resin. It is of note that Harkal *et al.*⁸⁴ did not see this initial spike. However, their study did not include ethylene glycol derivatives end-capped with ethyl moieties; although it did include DEGBE. In agreement with Harkal et al., we did not observe the spike with DEGBE. As we increased its substitution percentage in the resin, the viscosity decreased from 70% to 27% and then leveled out at 35% of the initial

viscosity, as the substitution percentage increased as 10, 25, and 33%, respectively. The initial decrease in viscosity followed by the eventual leveling was expected and follows the trend showed by Harkal *et al.*,⁸⁴ albeit on a different resin system.

EGME, DEGME, and DEGBE were strategically chosen as plasticizers as they were commercially available and allowed for the analysis of properties as a function of ethylene glycol concentration (EGME vs. DEGME) and endcap type (DEGME vs. DEGBE). As indicated by these data, both the amount and structure of the plasticizer proves to be important when reducing the viscosity of the resin. A direct comparison between EGME vs. DEGME in Figure 5.9 does not indicate that the amount of ethylene glycol plays a major role in viscosity reduction as the values are only slightly lower for the resins functionalized with DEGME. However, a direct comparison between DEGME and DEGBE in Figure 5.9 indicates a marked reduction in viscosity as the endcap is switched from ethyl to butyl. Harkal *et al.*⁸⁴ noticed substantial differences in viscosity as a function of the endcap as well and attributed it to plasticization of the alkyl chain. However, they may have incorrectly attributed the greatest factor in terms of viscosity reduction to the ethylene glycol moiety rather than endcap type or this could be an artifact resulting from the difference in resin systems. Further studies will be needed to validate this effect but these preliminary data certainly suggest that the endcap does play a more substantial role in viscosity reduction.

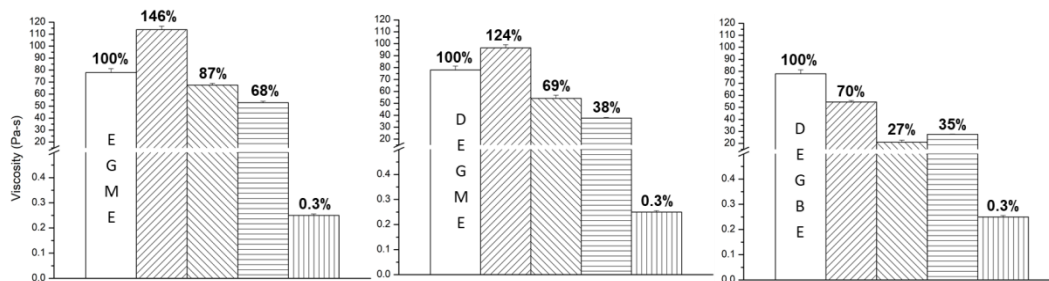


Figure 5.9 Room temperature isothermal viscosity of Desmodur XP2580 (vertical slash), Desmodur XP2580-PC (open), and various loadings of monohydroxyethylene glycols. Loadings are 10% (forward slash), 25% (backward slash), and 33% (horizontal slash). The type of monohydroxyethylene glycol is depicted in each plot. Percentages are normalized to 100% propargylated system.

5.3.5 Coating Properties

Table 5.3 compares various film properties for formulations containing EGME and for two control coatings made from the as-received resins and the 100% propargylated control resin. The coatings were drawn down on steel panels at 100% solids and cured using the “standard cure profile” initially defined in Chapter IV, which holds the panels at 30 °C for 2 h, followed by a ramp at 1 °C/min to 100 °C and a final cure at 100 °C for 4 h. The difference between the as-received (unmodified precursor) resin system and each experimental resin, with respect to color in 3-D space, was defined by ΔE . A large ΔE value indicates a large difference in color, while smaller values signify smaller differences. It is generally accepted that a value of less than one is indistinguishable to the human eye. The color difference for the networks containing any amount of EGME is significantly less than that of the fully propargylated system. This is believed to be attributed to dilution of the molar amount of propargyl moieties in a given system (100 \rightarrow 90 \rightarrow 75 \rightarrow 67). As propargyl is diluted, more of the low viscosity carbamate resin is needed to react with a given amount of Azidated Setalux DA 870, which is a major source of yellow color. Interestingly, there is a substantial gloss

difference at all angles between the precursor resin system and the 100% propargylated system. For example, the gloss measurement at 60° is 199 for the precursor coating and decreases to 118 for the 100% propargylated coating. However, it increases back above 190 for all systems containing ether alcohols. It is believed that the same logic presented above to explain the ΔE values can also be used to explain the gloss results. Finally, MEK double rubs were performed and showed a very high degree of cure for all systems.

Table 5.3 Properties of Azidated Setalux DA 870 Cured with EGME-Modified Desmodur XP2580 Compared to Desmodur XP2580-PC and Unmodified Resins

Part A	Setalux DA 870	Azidated Setalux DA 870			
Part B	Desmodur XP2580	Desmodur XP2580-PC	10EGME-PC	25EGME-PC	33EGME-PC
Color (L/A/B)	37.04/- 27.14/27.38	36.96/ -15.41/22.64	36.28/ -24.94/29.0	35.73/ -24.24/28.26	36.60/ -25.23/28.96
Color (ΔE)	---	12.65	2.87	3.30	2.51
Gloss 20	151	124.8	149	150	148
Gloss 60	199	118.1	192	194	191
Gloss 85	98.8	103.8	99	98	99
MEK Double Rub	200+, 200+	200+, 200+	200+, 200+	200+, 200+	200+, 200+

Table 5.4 lists various film properties for formulations containing DEGME and compares those formulations to two control coatings made from the as-received resins and the 100% propargyl resin. Again, the color difference for the networks containing any amount of DEGME was significantly less than the coatings derived from the fully propargylated system for the reasons explained above. The same trend as before was seen for the gloss values. The difference between the gloss values for the as-received resins and the ether alcohol modified coatings were within 10 gloss units, with the gloss

at 85° showing the closest agreement (less than 1 gloss unit difference). Finally, MEK double rubs were performed and showed a very high degree of cure for all systems.

Table 5.4 Properties of Azidated Setalux DA 870 Cured with DEGME-Modified Desmodur XP2580 Compared to Desmodur XP2580-PC and Unmodified Resins

Part A	Setalux DA 870	Azidated Setalux DA 870			
Part B	Desmodur XP2580	Desmodur XP2580-PC	10DEGME-PC	25DEGME-PC	33DEGME-PC
Color (L/A/B)	37.04/- 27.14/27.38	36.96/- 15.41/22.64	35.98/- 24.29/27.66	35.85/- 24.41/29.58	36.48/- 25.43/29.77
Color (ΔE)	---	12.65	3.05	3.70	2.99
Gloss 20	151	124.8	152	195	98.3
Gloss 60	199	118.1	195	194	189
Gloss 85	98.8	103.8	98.3	98.3	97.8
MEK Double Rub	200+, 200+	200+, 200+	200+, 200+	200+, 200+	200+, 200+

Table 5.5 lists various film properties for formulations containing DEGBE and compares those formulations to two control coatings made from the as-received resins and the 100% propargyl resins. The coatings were prepared similarly to the previous two sets of data. Once again, the color difference for the networks containing any amount of DEGME was significantly less than the coatings derived from the fully propargylated system, and as in the EGME and DEGME systems, the smallest color difference occurred for the system containing 33% DEGBE. The gloss values were a bit more scattered for the DEGBE-modified resins. However, in general the same trend holds that they agree more to the as-received resin than the fully propargylated system. Finally, MEK double rubs were performed and showed a very high degree of cure for all systems.

Table 5.5 Properties of Azidated Setalux DA 870 Cured with DEGBE-Modified Desmodur XP2580 Compared to Desmodur XP2580-PC and Unmodified Resins

Part A	Setalux DA 870	Azidated Setalux DA 870			
Part B	Desmodur XP2580	Desmodur XP2580-PC	10DEGBE-PC	25DEGBE-PC	33DEGBE-PC
Color (L/A/B)	37.04/- 27.14/27.38	36.96/- 15.41/22.64	35.90/- 24.60/28.73	36.14/- 24.64/27.66	35.77/- 24.59/28.88
Color (ΔE)	---	12.65	3.09	2.67	3.22
Gloss 20	151	124.8	145	112	131
Gloss 60	199	118.1	192	170	181
Gloss 85	98.8	103.8	97.1	88.4	94.2
MEK Double Rub	200+, 200+	200+, 200+	200+, 200+	200+, 200+	200+, 200+

Crosshatch adhesion was performed to determine the adhesion on the steel substrate (Figure 5.10). Regardless of the identity of the ether alcohol, all ether alcohol modified systems recovered the adhesion that was lost in the 100% propargylated system and achieved adhesion similar to the as-received systems. This recovered adhesion is likely due to the ether moieties being able to coordinate with the metal.

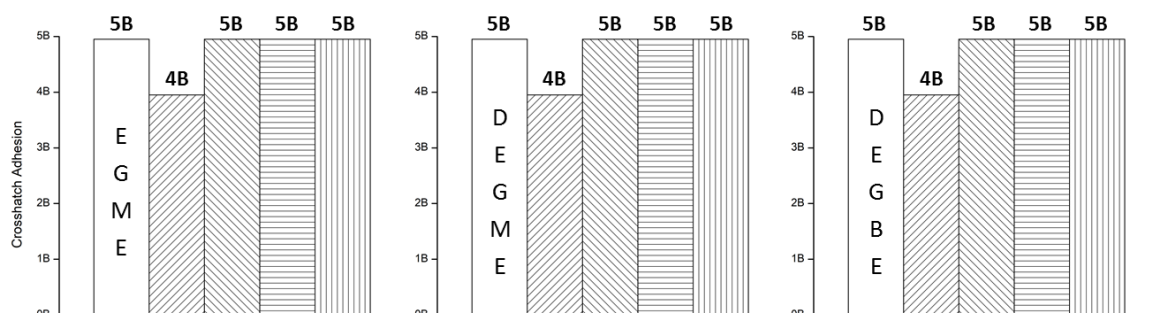


Figure 5.10 Crosshatch adhesion of as-received Setalux DA 870 cured with Desmodur XP2580 (open) and Azidated Setalux DA 870 cured with Desmodur XP2580-PC (forward slash). The final three bars are formulations containing various loadings of monohydroxyethylene glycols. Loadings are 10% (backward slash), 25% (horizontal slash), and 33% (vertical slash). The type of ethylene glycol is depicted in each plot.

Pencil hardness was performed on all coatings (Figure 5.11). The hardness of the coating seemed to follow a logical trend. As the crosslinking density decreased (from left

to right in each plot) so did the pencil hardness. In addition, there seemed to be a noticeable albeit slight dependence on the type of ether alcohol used in the study. EGME, which has the least amount of ethylene glycol, resulted in the hardest coatings while DEGME and DEGBE, which both contain twice as many ether moieties, resulted in slightly softer coatings. This difference was most pronounced in the highest loadings of the respective ether alcohols.

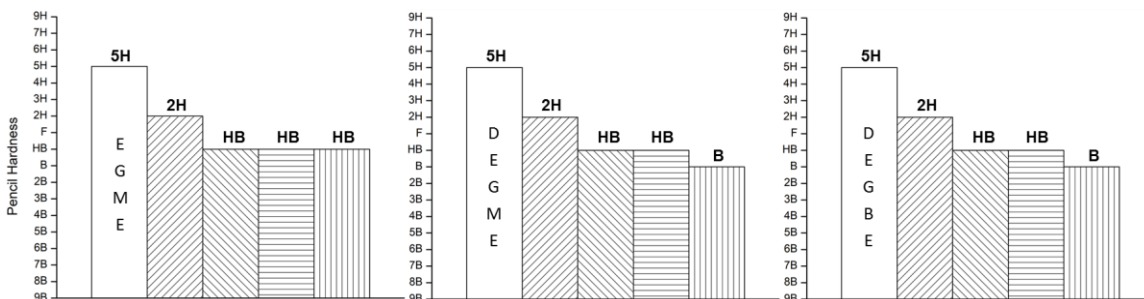


Figure 5.11 Pencil Hardness of as received Setalux DA 870 cured with Desmodur XP2580 (open) and Azidated Setalux DA 870 cured with Desmodur XP2580-PC (forward slash). The final three bars are formulations containing various loadings of monohydroxyethylene glycols. Loadings are 10% (backward slash), 25% (horizontal slash), and 33% (vertical slash). The type of ethylene glycol is depicted in each plot.

It was observed that the hardness of a given coating correlates well with its T_g . As shown in Figure 5.12, all systems showed the same trend. A slight increase in T_g (103% of the as-received T_g) was observed for the 100% propargylated system compared to the as-received coating, and the T_g steadily decreased as the molar percentage of ether alcohol increased. This decrease is largely attributed to equivalent weight and in turn crosslinking density. DEGME and DEGBE, which contain twice as many ethyl ether moieties and therefore have a higher equivalent weight, showed a more dramatic decrease in T_g (40 and 43% of the initial T_g compared to 52% for EGME) at the highest loadings.

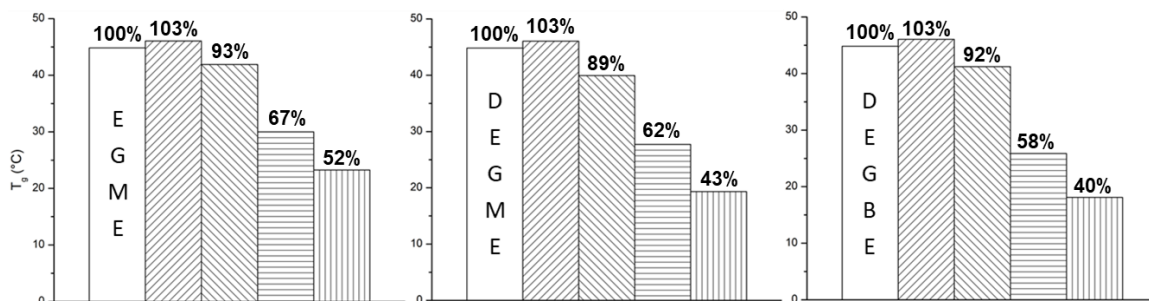


Figure 5.12 Glass transition temperature (T_g) as determined by DSC of as received Setalux DA 870 cured with Desmodur XP2580 (open) and Azidated Setalux DA 870 cured with Desmodur XP2580-PC (forward slash). The final three are formulations containing various loadings of monohydroxyethylene glycols. Loadings are 10% (backward slash), 25% (horizontal slash), and 33% (vertical slash). The type of ethylene glycol is depicted in each plot. The percentages are normalized to the as-received samples.

The storage modulus vs. temperatures plots are shown in Figure 5.13. In general, the moduli at 0 °C are close to one another with the DEGBE-modified resins showing a slightly higher modulus than the coatings containing ethyl chain ends. The major decrease in modulus associated with the glass transition occurred in the range 20-60 °C, depending on the identity of the plasticizing moiety as well as its loading level. Regardless of ether alcohol type, the temperature at which the decrease in the storage modulus occurred was highest for the sample containing the least amount of ether alcohol and decreased as the concentration of ether alcohol increased. This is a direct result of the plasticizing effect caused by inclusion of the various alcohol moieties as well as the decreasing crosslinking density of the network with increasing alcohol substitution percentage.

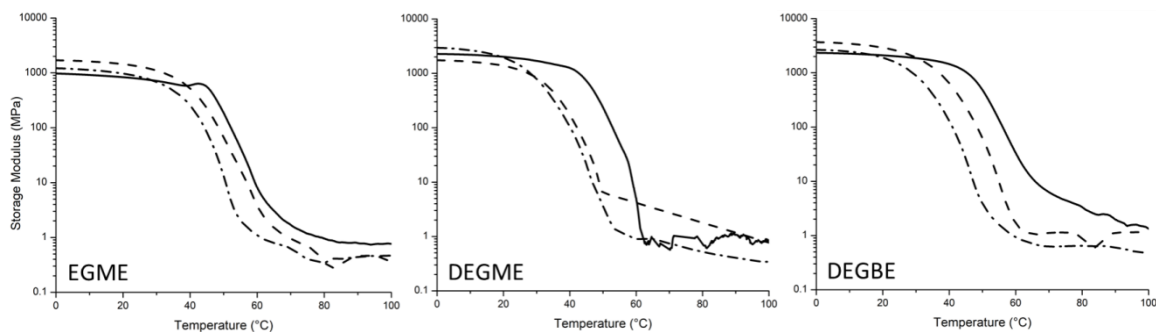


Figure 5.13 Representative storage modulus vs. temperature plots of cured coatings comprised of ether alcohol modified propargyl carbamates at three loading levels: 10% (solid), 25% (dash), and 33% (dash-dot). The type of ether alcohol is displayed in the plot.

The storage modulus at approximately 40 °C above the T_g was used to calculate the number-average molecular weight between cross-links (M_c) according to the theory of rubber elasticity (Equation 2.2).⁶⁴ Using v_e , M_c was calculated using Equation 2.3, where ρ is the physical density of the network. The values for density, T_g , rubbery storage modulus, rubbery cross-link density, and number-average molecular weight between cross-links are found in Table 5.6 for all cured samples.

The values for density, T_g , rubbery storage modulus, rubbery cross-link density, and number-average molecular weight between cross-links are found in Table 5.6 for all cured samples. It was expected that M_c would increase as the amount of ether alcohol increased (10 → 25 → 33) due to a decrease in crosslinking density. In general, this expectation was not seen in the data. It is believed to be due to noise in the rubbery storage modulus. This noise could be reduced by testing thicker samples and this test is suggested for future work.

Table 5.6 Crosslink Density Calculations from Rubbery Storage Modulus Measured at 1 Hz.

Alkyne Type	ρ_{avg}^i (g/cm ³)	T _g (°C)	E _r ' _{T_g+30} (MPa)	v _e (·10 ⁻⁵)	M _c (x10 ³)
10EGME-PC	1.31	56.3	0.76	9.1	16.6
25EGME-PC	1.11	51.5	0.99	9.3	10.5
33EGME-PC	1.15	52.4	0.45	4.5	22.8
10DEGME-PC	1.36	57.8	0.46	9.1	14.5
25DEGME-PC	1.27	46.6	0.61	9.0	19.9
33DEGME-PC	1.23	47.7	0.86	6.9	20.0
10DEGBE-PC	1.23	61.4	1.93	23	5.78
25DEGBE-PC	1.12	49.5	0.44	4.5	23.7
33DEGBE-PC	1.19	47.7	0.62	7.3	19.6

ⁱ ρ_{avg} is the average density of three replicates of four specimens, as measured by Archimedes' principle.

5.3.6 Conclusions and Future Work

The overall goal of this chapter was to synthesize low-viscosity propargyl carbamates and react them with a polyazide resin to achieve NIPU coatings that had a workable viscosity with minimal (or no) VOCs. This was achieved by partially sacrificing the functionality of the starting polyisocyanate with monofunctional ether alcohols and using the remaining functionality to create the propargyl carbamate linkage. The ether alcohol types (EGME, DEGME, and DEGBE) were strategically chosen as they varied by either ether concentration or endcap, which allowed for the understanding of which moiety played the bigger role in viscosity reduction and network properties. NMR spectroscopy (¹³C and ¹H) was used to confirm the complete conversion of isocyanate groups and targeted propargylation, respectively. Isothermal viscometry was used to determine the effect of the ether alcohol type as well as its concentration on viscosity. For EGME and DEGME, there was an initial increase in viscosity followed by a dramatic reduction, showing these ether alcohols need to overcome a threshold to properly plasticize the resin. For the case of DEGBE the viscosity steadily decreased as

DEGBE was added, which was predicted and suggested that DEGBE plasticizes the resins more efficiently than the other two ether alcohols. The color and gloss of the cured coatings were measured, and it was determined that both trended toward the gloss of the commercially available unmodified resins as the concentration of ether alcohol increased, which added an unforeseen benefit to these formulations. In addition, the crosshatch adhesion improved upon incorporating the ether alcohols into the matrix likely due to the extra ether linkages in the low-viscosity networks improving adhesion to the metal. As expected, both the T_g and the hardness of the material decreased as the amount of ether alcohol increased due to a decrease in crosslink density. DMA was utilized to understand the network properties of the cure material. In general, DEGBE modified materials showed the highest storage modulus at 0 °C and the major decrease in modulus associated with the glass transition occurred in the range 20-60 °C, depending on the identity of the plasticizing moiety as well as its loading level. DMA was also used to calculate M_c via the theory of rubber elasticity. However, these data were inconclusive due to noise in the rubbery storage modulus.

CHAPTER VI

Concluding remarks and suggested future work have been separated according to the corresponding chapters within this dissertation.

CHAPTER II – The Effect of Microstructure on Thermal and Mechanical Properties in Azide-Alkyne Matrices

In this chapter, we demonstrated the synthesis, formulation, and curing of high- T_g glassy azide-alkyne networks. The molecular architecture of these networks was controlled by the addition or omission of Cu(I) catalyst, which greatly favors the formation of the 1,4-regioisomer, and by varying the central linkage of the tetrapropargyl bis-aniline-type crosslinker as ether, methylene, or sulfone. The identity of the central linkage greatly affected the physical properties of the crosslinker; the ether was a liquid at room temperature; the methylene-linked material was a soft solid, and the sulfone-linked material was a high melting solid. The liquid crosslinker was much easier to mix than the solid ones. Therefore, it is of great interest to introduce the solid crosslinkers into the resin as oils. This may be done by heating the crosslinker above its melting point and quickly cooling it to below room temperature, possibly in the presence of a known concentration of the liquid crosslinker. In addition, future work should include optimization of a cure profile to handle all crosslinkers and catalyst loadings. The introduction of all crosslinkers as oils would greatly facilitate this goal. Also, PALS and PVT studies would be performed to understand the role of free volume in these crosslinked systems. Finally, solid-state NMR would advance this research greatly with respect to quantifying the relative abundance of the 1,4- vs. 1,5-regioisomer.

CHAPTER III – Non-Isocyanate Cured Polyurethanes via Azide-Alkyne Cycloaddition

The goal of this chapter was to develop NIPU coatings that cure by azide-alkyne cycloaddition. This was achieved by converting the isocyanate and alcohol groups of commercially available polyisocyanates and polyols to propargyl and azide functionalities, respectively. This chapter outlined the synthetic strategies used to achieve these functionalities, curing of formulated coatings in the presence and absence of catalyst, and comparison of coating properties of the azido-alkyne cured systems to the unmodified polyurethane coatings. Solubility between resin pairs dramatically changed after modification. In some cases, due presumably to a high viscosity and changes in polarity, the coating co-reactants phase-separated, which lowered the appearance and performance properties of the final coatings. Thorough understanding of the solubility parameters of these resin pairs could lead to the use of appropriate solvents which would achieve desirable coatings. Different preparation conditions for the azidated Setalux DA 870 are also desirable as currently the workup results in somewhat thermodynamically stable emulsions that are difficult to separate.

CHAPTER IV –Reduced Temperature Non-Isocyanate Polyurethane Coatings via Catalyst-Free Azide-Alkyne Cycloaddition

In this chapter, two general methods were discussed to increase the non-catalyzed kinetics of the azide-alkyne cycloaddition. The first was the direct propiolation of the isocyanate using propiolic acid to form an amide, and the second was the synthesis of 2-HEP and its subsequent reaction with free isocyanates. An area of this research that could be immediately addressed is to determine whether blends of the propargyl- and propiolate ester-functional resins can be used to tailor curing kinetics at room-temperature, which would allow customized pot-lives for specific applications. A second

area of study would to be use the synthetic technique developed with 2-HEP on higher order ethylene glycol oligomers, which could reduce viscosity of the highly viscous resins in addition to increasing the kinetics. Finally, other monomers could be designed to incorporate the propiolate functionality such as 2-hydroxyethylpropiolamide, which could impart properties such as increased MEK solvent resistance or harder coatings resulting from the additional hydrogen bonding.

CHAPTER V – Low Viscosity Non-Isocyanate Polyurethane Coatings via Azide-Alkyne Cycloaddition Using Mono-Hydroxyethylene Glycol Oligomers

The overall goal of this chapter was to synthesize low-viscosity propargyl carbamates by utilizing a fraction (one third or less) of the isocyanate functionality to attach internal plasticizing moieties consisting of a monoalkyl ether of either ethylene glycol (EG) or diethylene glycol (DEG). After conversion of the remaining isocyanates to propargyl carbamate functionalities, the resulting resin was reacted with a polyazide resin to achieve NIPU coatings that had a workable viscosity with minimal (or no) VOCs. The ether alcohols (EGME, DEGME, and DEGBE) were strategically chosen as they varied by either concentration of ether units (EG vs. DEG) or endcap type (ethyl vs. butyl). This allowed for a systematic study showing which moiety had a greater effect on viscosity of the resin as well as the cured coating. A major area of interest is to explore other functionalities that could be incorporated to decrease the viscosity of the system. The goal would be to find internally plasticizing moieties that could be introduced at a minimal concentration and would dramatically reduce the viscosity of the system. In addition, with clever design, the ethylene glycol functionality could be incorporated in the backbone as a spacer between the urethane and propargyl functionalities. This should reduce the viscosity of the system without sacrificing functionality. Finally, di-

propargylated (and higher order) PEG could be incorporated into the system to reduce its viscosity and tailor crosslink density.

REFERENCES

- (1) Kolb, H. C.; Finn, M. G.; Sharpless, K. B. Click Chemistry: Diverse Chemical Function from a Few Good Reactions. *Angew. Chemie Int. Ed.* **2001**, *40* (11), 2004–2021.
- (2) Gorman, I. E.; Willer, R. L.; Kemp, L. K.; Storey, R. F. Development of a Triazole-Cure Resin System for Composites: Evaluation of Alkyne Curatives. *Polymer (Guildf)*. **2012**, *53* (13), 2548–2558.
- (3) Huisgen, R.; Szeimies, G.; Möbius, L. 1.3-Dipolare Cycloadditionen, XXXII. Kinetik Der Additionen Organischer Azide an CC-Mehrfachbindungen. *Chem. Ber.* **1967**, *100* (8), 2494–2507.
- (4) Zhang, L.; Chen, X.; Xue, P.; Sun, H. H. Y.; Williams, I. D.; Sharpless, K. B.; Fokin, V. V.; Jia, G. Ruthenium-Catalyzed Cycloaddition of Alkynes and Organic Azides. *J. Am. Chem. Soc.* **2005**, *127* (46), 15998–15999.
- (5) Brei, M. R. Curing of Polymer Thermosets via Click Reactions, University of Southern Mississippi, 2016.
- (6) Cooke III, R. H.; Brei, M. R.; VandeWalle, D. T.; Storey, R. F. A “Drop-In” Composite Matrix via Azide-Alkyne Cycloaddition. In *The Composites and Advanced Materials Expo: CAMX*; 2017.
- (7) Brei, M. R.; Hunter Cooke, R.; Hanson, D. J.; Gray, C. T.; Storey, R. F. NMR and Mass Spectral Analysis of Step-Growth Polymers from Azide Alkyne Cycloaddition and Regioselectivity Afforded by Copper(I) and Ruthenium(II) Catalysts. *J. Macromol. Sci. Part A* **2016**, *53* (7), 413–423.
- (8) Bayer, O. Das Di-Isocyanat-Polyadditionsverfahren (Polyurethane). *Angew. Chemie* **1947**, *59* (9), 257–288.
- (9) Baur, X.; Marek, W.; Ammon, J.; Czuppon, A. B.; Marczyński, B.; Raulf-Heimsoth, M.; Roemmelt, H.; Fruhmman, G. Respiratory and Other Hazards of Isocyanates. *Int. Arch. Occup. Environ. Health* **1994**, *66* (3), 141–152.
- (10) Bello, D.; Herrick, C. A.; Smith, T. J.; Woskie, S. R.; Streicher, R. P.; Cullen, M. R.; Liu, Y.; Redlich, C. A. Skin Exposure to Isocyanates: Reasons for Concern. *Environ. Health Perspect.* **2007**, *115* (3), 328–335.
- (11) Merenyi, S. REACH: Regulation (EC) No 1907/2006: Consolidation Version (June 2012) With an Introduction and Future Prospects Regarding the Area of Chemicals Legislation. *GRIN Verlag* **2012**.
- (12) Hoa, S. V. 1. Introduction. In *Principles of the Manufacturing of Composite Materials*; DEStech Publications.
- (13) marketsandmarkets.com. Carbon Fiber Market & Carbon Fiber Reinforced Plastic (CFRP) Market by Type, Fiber size, & Region; CFRP Market by (Type, Manufacturing processes/semi-finished product, Resin, Application and Region)-Global Forecast to 2019 <http://www.marketsandmarkets.com/Market-Reports/carbon-fiber-composites-market-416.html>.
- (14) Decker, C.; Masson, F.; Schwalm, R. Weathering Resistance of Waterbased UV-Cured Polyurethane-Acrylate Coatings. *Polym. Degrad. Stab.* **2004**, *83* (2), 309–320.
- (15) Klempner, D.; Frisch, K. C. *Handbook of Polymeric Foams and Foam*

- Technology*; Hanser Publishers: Munich, 1992.
- (16) Chattopadhyay, D. K.; Raju, K. V. S. N. Structural Engineering of Polyurethane Coatings for High Performance Applications. *Prog. Polym. Sci.* **2007**, *32* (3), 352–418.
 - (17) Sato, M. The Rate of the Reaction of Isocyanates with Alcohols. II. *J. Org. Chem.* **1962**, *27* (3), 819–825.
 - (18) Delebecq, E.; Pascault, J. P.; Boutevin, B.; Ganachaud, F. On the Versatility of Urethane/Urea Bonds: Reversibility, Blocked Isocyanate, and Non-Isocyanate Polyurethane. *Chem. Rev.* **2013**, *113* (1), 80–118.
 - (19) Melchior, M.; Sonntag, M.; Kobusch, C.; Jürgens, E. Recent Developments in Aqueous Two-Component Polyurethane (2K-PUR) Coatings. *Prog. Org. Coatings* **2000**, *40* (1–4), 99–109.
 - (20) Odian, G.; John Wiley and Sons, I. *Principles of Polymerization*, 4th ed.; 2004.
 - (21) Kathalewar, M. S.; Joshi, P. B.; Sabnis, A. S.; Malshe, V. C. Non-Isocyanate Polyurethanes: From Chemistry to Applications. *RSC Adv.* **2013**, *3* (13), 4110.
 - (22) Wang, F.; Hu, J. Q.; Tu, W. P. Study on Microstructure of UV-Curable Polyurethane Acrylate Films. *Prog. Org. Coatings* **2008**, *62* (3), 245–250.
 - (23) Speckhard, T. A.; Hwang, K. K. S.; Lin, S. B.; Tsay, S. Y.; Koshiba, M.; Ding, Y. S.; Cooper, S. L. Properties of UV-curable Polyurethane Acrylates: Effect of Reactive Diluent. *J. Appl. Polym. Sci.* **1985**, *30* (2), 647–666.
 - (24) Lin, S. B.; Tsay, S. Y.; Speckhard, T. A.; Hwang, K. K. S.; Jezerc, J. J.; Cooper, S. L. Properties of UV-Cured Polyurethane Acrylates: Effect of Polyol Type and Molecular Weight. *Chem. Eng. Commun.* **1984**, *30* (3–5), 251–273.
 - (25) Huisgen, R. No Title. *Pure Appl. Chem.* **1989**, *61*, 613–628.
 - (26) Rostovtsev, V. V.; Green, L. G.; Fokin, V. V.; Sharpless, K. B. A Stepwise Huisgen Cycloaddition Process: Copper-Catalyzed Regioselective "Ligation" of Azides and Terminal Alkynes. *Angew. Chemie Int. Ed.* **2002**, *41* (14), 2596–2599.
 - (27) Tornøe, C. W.; Christensen, C.; Meldal, M. Peptidotriazoles on Solid Phase: [1,2,3]-Triazoles by Regiospecific Copper(I)-Catalyzed 1,3-Dipolar Cycloadditions of Terminal Alkynes to Azides. *J. Org. Chem.* **2002**, *67* (9), 3057–3064.
 - (28) Kolb, H. C.; Sharpless, K. B. The Growing Impact of Click Chemistry on Drug Discovery. *Drug Discov. Today* **2003**, *8* (24), 1128–1137.
 - (29) Lutz, J.-F. 1,3-Dipolar Cycloadditions of Azides and Alkynes: A Universal Ligation Tool in Polymer and Materials Science. *Angew. Chemie Int. Ed.* **2007**, *46* (7), 1018–1025.
 - (30) Binder, W. H.; Sachsenhofer, R. 'Click' Chemistry in Polymer and Materials Science. *Macromol. Rapid Commun.* **2007**, *28* (1), 15–54.
 - (31) Li Yan, J. U. Y. Z. Y.-F. Application of Azoles Synthesis in Bioconjugate Chemistry. *Chin. J. Org. Chem.* **2006**, *26* (12), 1640–1646.
 - (32) Moses, J. E.; Moorhouse, A. D. The Growing Applications of Click Chemistry. *Chem. Soc. Rev.* **2007**, *36* (8), 1249–1262.
 - (33) Himo, F.; Lovell, T.; Hilgraf, R.; Rostovtsev, V. V.; Noodleman, L.; Sharpless, K. B.; Fokin, V. V. Copper(I)-Catalyzed Synthesis of Azoles. DFT Study Predicts Unprecedented Reactivity and Intermediates. *J. Am. Chem. Soc.* **2005**, *127* (1).

- (34) Rodionov, V. O.; Fokin, V. V.; Finn, M. G. Mechanism of the Ligand-Free CuI-Catalyzed Azide–Alkyne Cycloaddition Reaction. *Angew. Chemie Int. Ed.* **2005**, *44* (15), 2210–2215.
- (35) Ahlquist, M.; Fokin, V. V. Enhanced Reactivity of Dinuclear Copper(I) Acetylides in Dipolar Cycloadditions. *Organometallics* **2007**, *26* (18), 4389–4391.
- (36) Giguere, D.; Patnam, R.; Bellefleur, M.-A.; St-Pierre, C.; Sato, S.; Roy, R. Carbohydrate Triazoles and Isoxazoles as Inhibitors of Galectins-1 and -3. *Chem. Commun.* **2006**, No. 22, 2379–2381.
- (37) Pirali, T.; Tron, G. C.; Zhu, J. One-Pot Synthesis of Macrocycles by a Tandem Three-Component Reaction and Intramolecular [3+2] Cycloaddition. *Org. Lett.* **2006**, *8* (18), 4145–4148.
- (38) Franke, R.; Doll, C.; Eichler, J. Peptide Ligation through Click Chemistry for the Generation of Assembled and Scaffolded Peptides. *Tetrahedron Lett.* **2005**, *46* (26), 4479–4482.
- (39) Gissibl, A.; Finn, M. G.; Reiser, O. Cu(II)–Aza(Bisoxazoline)-Catalyzed Asymmetric Benzoylations. *Org. Lett.* **2005**, *7* (12), 2325–2328.
- (40) Adam, G. C.; Vanderwal, C. D.; Sorensen, E. J.; Cravatt, B. F. (–)-FR182877 Is a Potent and Selective Inhibitor of Carboxylesterase-1. *Angew. Chemie Int. Ed.* **2003**, *42* (44), 5480–5484.
- (41) Song, H. B.; Baranek, A.; Bowman, C. N. Kinetics of Bulk Photo-Initiated Copper(I)-Catalyzed Azide-Alkyne Cycloaddition (CuAAC) Polymerizations. *Polym. Chem.* **2015**, 603–612.
- (42) Baranek, A.; Song, H. B.; McBride, M.; Finnegan, P.; Bowman, C. N. Thermomechanical Formation–Structure–Property Relationships in Photopolymerized Copper-Catalyzed Azide–Alkyne (CuAAC) Networks. *Macromolecules* **2016**, acs.macromol.6b00137.
- (43) Tasdelen, M. A.; Uygun, M.; Yagci, Y. Photoinduced Controlled Radical Polymerization. *Macromol. Rapid Commun.* **2011**, *32* (1), 58–62.
- (44) Sreedhar, B.; Surendra Reddy, P. Sonochemical Synthesis of 1,4-Disubstituted 1,2,3-Triazoles in Aqueous Medium. *Synth. Commun.* **2007**, *37* (5), 805–812.
- (45) Wan, L.; Luo, Y.; Xue, L.; Tian, J.; Hu, Y.; Qi, H.; Shen, X.; Huang, F.; Du, L.; Chen, X. Preparation and Properties of a Novel Polytriazole Resin. *J. Appl. Polym. Sci.* **2007**, *104*, 1038–1042.
- (46) Díaz, D. D.; Punna, S.; Holzer, P.; Mcpherson, A. K.; Sharpless, K. B.; Fokin, V. V.; Finn, M. G. Click Chemistry in Materials Synthesis. 1. Adhesive Polymers from Copper-Catalyzed Azide-Alkyne Cycloaddition. *J. Polym. Sci. Part A Polym. Chem.* **2004**, *42* (17), 4392–4403.
- (47) Wang, L.; Song, Y.; Gyanda, R.; Sakhuja, R.; Meher, N. K.; Hanci, S.; Gyanda, K.; Mathai, S.; Sabri, F.; Ciaramitaro, D. A.; et al. Preparation and Mechanical Properties of Crosslinked 1, 2, 3-Triazole-Polymers as Potential Propellant Binders. **2010**.
- (48) Ozawa, T. Kinetic Analysis of Derivative Curves in Thermal Analysis. *J. Therm. Anal.* **1970**, *2* (3), 301–324.
- (49) Sheng, X.; Mauldin, T. C.; Kessler, M. R. Kinetics of Bulk Azide/Alkyne “Click” Polymerization. *J. Polym. Sci. Part A Polym. Chem.* **2010**, *48* (18), 4093–4102.

- (50) Sindt, O.; Perez, J.; Gerard, J. F. Molecular Architecture-Mechanical Behaviour Relationships in Epoxy Networks. *Polymer (Guildf)*. **1996**, *37* (14), 2989–2997.
- (51) Tu, J.; Tucker, S. J.; Christensen, S.; Sayed, A. R.; Jarrett, W. L.; Wiggins, J. S. Phenylene Ring Motions in Isomeric Glassy Epoxy Networks and Their Contributions to Thermal and Mechanical Properties. *Macromolecules* **2015**, *48* (6), 1748–1758.
- (52) Friedman, H. L. Kinetics of Thermal Degradation of Char-Forming Plastics from Thermogravimetry. Application to a Phenolic Plastic. *J. Polym. Sci. Part C Polym. Symp.* **1964**, *6* (1), 183–195.
- (53) Anders, M.; Lo, J.; Centea, T.; Nutt, S. Development of a Process Window for Minimizing Volatile-Induced Surface Porosity in the Resin Transfer Molding of a Benzoxazine/Epoxy Blend. *SAMPE* **2016**, *52* (1), 44–55.
- (54) Patterson, M. Distortional Aryl Ketone Ether Hybrid Epoxy Matrices, University of Southern Mississippi, 2018.
- (55) Heitmann, W.; Huls, A.; Strehlke, G.; Mayer, D.; Aktiengesellschaft, H. *Ethers , Aliphatic*; WILEY-VCH Verlag GmbH, 2005.
- (56) Hartman, W. W.; Phillips, R. Diphenylmethane. *Org. Synth.* **1943**, *2*, 232.
- (57) Frazee, A. No Title, University of Southern Mississippi, 2017.
- (58) Tasdelen, M. A.; Yagci, Y. Light-Induced Copper(I)-Catalyzed Click Chemistry. *Tetrahedron Lett.* **2010**, *51* (52), 6945–6947.
- (59) Gorman, I. E.; Willer, R. L.; Storey, R. F. Isoconversional Kinetic Analysis of a Novel Triazole Resin System for Low-Temperature Cure. *Polym. Preprs.* **2010**, *51* (2), 209–210.
- (60) Eglinton, G; Galbraith, A, R. Macrocyclic Acetylenic Cornpowads. Part. *Chem. Ind.* **1956**, 737.
- (61) Liang, L.; Astruc, D. The Copper(I)-Catalyzed Alkyne-Azide Cycloaddition (CuAAC) “Click” Reaction and Its Applications. An Overview. *Coord. Chem. Rev.* **2011**, *255* (23–24), 2933–2945.
- (62) Cukierman, S.; Halary, J. L.; Monnerie, L. Dynamic Mechanical Response of Model Epoxy Networks in the Glassy State. *Polym. Eng. Sci.* **1991**, *31* (20), 1476–1482.
- (63) Starkweather, H. W. Simple and Complex Relaxations. *Macromolecules* **1981**, *14* (5), 1277–1281.
- (64) Flory, P. J. Molecular Theory of Rubber Elasticity. *Polymer (Guildf)*. **1979**, *20* (11), 1317–1320.
- (65) Buckley, C. P.; Prisacariu, C.; Martin, C. Elasticity and Inelasticity of Thermoplastic Polyurethane Elastomers: Sensitivity to Chemical and Physical Structure. *Polymer (Guildf)*. **2010**, *51* (14), 3213–3224.
- (66) Kantheti, S.; Narayan, R.; Raju, K. V. S. N. The Impact of 1,2,3-Triazoles in the Design of Functional Coatings. *RSC Adv.* **2015**, *5* (5), 3687–3708.
- (67) Kantheti, S.; Sarath, P. S.; Narayan, R.; Raju, K. V. S. N. Synthesis and Characterization of Triazole Rich Polyether Polyols Using Click Chemistry for Highly Branched Polyurethanes. *React. Funct. Polym.* **2013**, *73* (12), 1597–1605.
- (68) Kantheti, S.; Narayan, R.; Raju, K. V. S. N. Click Chemistry Engineered Hyperbranched Polyurethane-Urea for Functional Coating Applications. *Ind. Eng.*

- Chem. Res.* **2014**, *53* (20), 8357–8365.
- (69) Kantheti, S.; Narayan, R.; Raju, K. V. S. N. Development of Moisture Cure Polyurethane-Urea Coatings Using 1,2,3-Triazole Core Hyperbranched Polyesters. *J. Coatings Technol. Res.* **2013**, *10* (5), 609–619.
- (70) Bakhshi, H.; Yeganeh, H.; Mehdipour-Ataei, S.; Solouk, A.; Irani, S. Polyurethane Coatings Derived from 1,2,3-Triazole-Functionalized Soybean Oil-Based Polyols: Studying Their Physical, Mechanical, Thermal, and Biological Properties. *Macromolecules* **2013**, *46* (19), 7777–7788.
- (71) Reshmi, S.; Arunan, E.; Nair, C. P. R. Azide and Alkyne Terminated Polybutadiene Binders: Synthesis, Cross-Linking, and Propellant Studies. *Ind. Eng. Chem. Res.* **2014**, *53* (43), 16612–16620.
- (72) Carter, N.; Martin, I.; Coward, A.; Gatrell, M.; Byrne, M.; Cullen, J.; Cormack, P. Synthesis of Polyurethane Polymers via Copper Azide-Alkyne Click Chemistry for Coatings, Adhesives, Sealants and Elastomer Applications, 2015.
- (73) Lei, X.; Jalla, A.; Abou Shama, M. A.; Stafford, J. M.; Cao, B. Chromatography-Free and Eco-Friendly Synthesis of Aryl Tosylates and Mesylates. *Synth.* **2015**, *47* (17), 2578–2585.
- (74) Tornøe, C. W.; Christensen, C.; Meldal, M. Peptidotriazoles on Solid Phase: [1,2,3]-Triazoles by Regiospecific Copper(I)-Catalyzed 1,3-Dipolar Cycloadditions of Terminal Alkynes to Azides. *J. Org. Chem.* **2002**, *67* (9), 3057–3064.
- (75) Adzima, B. J.; Tao, Y.; Kloxin, C. J.; DeForest, C. A.; Anseth, K. S.; Bowman, C. N. Spatial and Temporal Control of the Alkyne–azide Cycloaddition by Photoinitiated Cu(II) Reduction. *Nat Chem* **2011**, *3* (3), 256–259.
- (76) Gong, T.; Adzima, B. J.; Baker, N. H.; Bowman, C. N. Photopolymerization Reactions Using the Photoinitiated Copper (I)-Catalyzed Azide-Alkyne Cycloaddition (CuAAC) Reaction. *Adv. Mater.* **2013**, *25* (14), 2024–2028.
- (77) Blagbrough, I. S.; Mackenzie, N. E.; Scott, a I. The Condensation Reaction between Isocyanates and Carboxylic Acids. A Practical Synthesis of Substituted Amides and Anilides. *Tetrahedron Lett.* **1986**, *27* (11), 1251–1254.
- (78) Sasaki, K.; Crich, D. Facile Amide Bond Formation from Carboxylic Acids and Isocyanates. *Org. Lett.* **2011**, *13* (9), 2256–2259.
- (79) Miller, L.; Butler, J. Esters of Acetylenic Acids and Polyhydric Alcohols. 3,082,242, 1963.
- (80) Silverstein, R. M.; Webster, F. X.; Kiemle, D. J. Mass Spectra of Some Chemical Classes. In *Spectrometric Identification of Organic Compounds*; 2005; p 22.
- (81) Wicks, Z. W.; Jones, F. N.; Pappas, S. P. Binders Based on Polyisocyanates: Polyurethanes. In *Organic Coatings*; John Wiley & Sons, Inc: Hoboken, New Jersey, 1992; pp 231–271.
- (82) Meijer, M. De. Review on the Durability of Exterior Wood Coatings with Reduced VOC-Content. **2001**, *43*, 217–225.
- (83) Rosthauser, J. W.; Nachtkamp, K. Waterborne Polyurethanes. *J. Coat. Fabr.* **1986**, *16*, 39–79.
- (84) Harkal, U. D.; Muehlberg, A. J.; Li, J.; Garrett, J. T.; Webster, D. C. The Influence of Structural Modification and Composition of Glycidyl Carbamate Resins on

- Their Viscosity and Coating Performance. *J. Coatings Technol. Res.* **2010**, 7 (5), 531–546.
- (85) Cao, N.; Yang, X.; Fu, Y. Effects of Various Plasticizers on Mechanical and Water Vapor Barrier Properties of Gelatin Films. *Food Hydrocoll.* **2009**, 23 (3), 729–735.
- (86) Vieira, M. G. A.; Da Silva, M. A.; Dos Santos, L. O.; Beppu, M. M. Natural-Based Plasticizers and Biopolymer Films: A Review. *Eur. Polym. J.* **2011**, 47 (3), 254–263.